TECHNOLOGY • RESEARCH HIGHLIGHTS • VISIONS • SCIENCE •
63

A compilation of slag foaming phenomenon research

Theoretical studies, industrial experiments and modelling

Matti Liukkonen | Karri Penttilä | Pertti Koukkari

VTT

VTT TECHNOLOGY 63

A compilation of slag foaming phenomenon research

Theoretical studies, industrial experiments and modelling

Matti Liukkonen, Karri Penttilä & Pertti Koukkari

ISBN 978-951-38-7897-9 (URL: http://www.vtt.fi/publications/index.jsp)
ISSN 2242-122X (URL: http://www.vtt.fi/publications/index.jsp)

JULKAISIJA – UTGIVARE – PUBLISHER

VTT
PL 1000 (Tekniikantie 4 A, Espoo)
02044 VTT
Puh. 020 722 111, faksi 020 722 7001

VTT
PB 1000 (Teknikvägen 4 A, Esbo)
FI-02044 VTT
Tfn +358 20 722 111, telefax +358 20 722 7001

VTT Technical Research Centre of Finland
P.O. Box 1000 (Tekniikantie 4 A, Espoo)
FI-02044 VTT, Finland
Tel. +358 20 722 111, fax +358 20 722 7001

A compilation of slag foaming phenomenon research
Theoretical studies, industrial experiments and modelling

Matti Liukkonen, Karri Penttilä & Pertti Koukkari.
Espoo 2012. VTT Technology 63. 128 p.

Abstract

A literature study was made on the foaming phenomenon in the modern electric arc furnace (EAF) stainless steelmaking process. Slag foaming has become an important feature of the EAF process. The chemical and physical conditions of the slag, which affect the foaming phenomenon of the slag-steel system, appear to be relatively complicated to control in the manufacture of stainless steel.

The foaming index is a parameter that quantifies the ability of slag to generate foam from either injected gas or gas that is generated within the slag or metal. In the case of ideal slagging, the foaming index is equal to the average foam life. The foaming index decreases with increasing viscosity and increases with decreasing viscosity. Various techniques based on dimensional analysis of the kinetic properties of the slag have been applied in order to find the relationship describing the foaming index.

In industrial experiments, the control methods of the slag foaming operations are based on the visual observation or on noise emitted by the EAF vessel. The lower Cr_2O_3 content slags and large initial FeO content slags are more foaming. The foaming is also observed to promote chromium recovery. The foaming index for the slags is observed to be relatively similar, due to the similarities between viscosity, density and surface energy values, although their compositions are quite different. The foamy slag provides protection for the melt against nitrogen pick-up. The foaming capability of slags can be enhanced by the addition of appropriate materials such as limestone and calcium nitrate.

In the modelling studies, the aim is to understand and predict foaming in EAF steelmaking. The slag foaming caused by slag-graphite reaction is dependent mainly on the CO-gas evolution rate. Decarburisation and slag formation models consider the rate phenomena for decarburisation and the carbon-FeO reaction in the slag, and the mass balance for each phase with the melting behaviour of pig iron scrap and fluxes. A recent thermodynamic model of the EAF process for stainless steel calculates the evolution of temperature and the composition of slag and metal phases with time. In the slag foaming in the EAF model the potential foaming is very high when using high amounts of input materials. The actual foam is limited by the height at which the slag is flushed out or by the volume of slag. At the end of the process the foam decays due to lower CO-gas generation.

Keywords Electric arc furnace, EAF, stainless steel, slag foaming, gas generation, foam index, foam life, foaming, surface energy, viscosity, interface, basicity, temperature, gas velocity, bubble size, dimensional analysis, carbon, CO-gas, $CaO\text{-}SiO_2\text{-}FeO$, Cr_2O_3, modelling, reconciliation, mass balance, reaction rate, kinetics, dynamics, Fact, Fortran, Chemapp

Contents

List of symbols

A	Area [m^2]
B	Degree of surface coverage
Bi	Biot number
C	Mass fraction
Ca	Capillary number
D	Diameter [m]
D	Diffusivity [m^2/s]
Fr	Froude number
g	Gravity (9.81 [m^2/s])
h	Heat transfer coefficient [J/m^2-K]
h	Height [m]
j	Superficial gas velocity [m/s]
j	Volumetric gas flow per unit area [m^3/m^2-s]
L	Length [m]
k	Mass transfer coefficient [kg/m^2-s]
k	Reaction rate constant [1/s]
K	Proportionality coefficient []
M	Molar mass [kg/mol]
Mo	Morton number
p	Partial pressure [Pa]
P	Pressure [Pa]
Q	Volume flow [m^3/s]

r	Radius [m/s]
R	Gas constant (8.314159 [J/mol-K])
Re	Reynolds number
t	Time [s]
T	Temperature [K]
x	Mole fraction
v	Rate of evolution of gas [m^3/m^2-s]
V	Velocity [m/s]
W	Mass [kg]

Greek symbols

α	Void fraction
δ	Stefan-Boltzman constant ($5.67E10^{-8}$ [J/m^2-K^4-s])
ε	Gas holdup
ε	Emissivity
γ	Interfacial energy [N/m]
μ	Viscosity [kg/m-s]
ρ	Density [kg/m3]
Σ	Foaming index [s]
σ	Surface tension [N/m]
θ	Volume fraction
Π	Dimensionless number
τ	Foam lifetime [s]

Subcripts

c	Cross-section
c	Cylinder
eq	Equilibrium
r	Radius
s	Slag
s	Surface

1. Introduction

It has been suggested that the relative foam stability of metallurgical slags increases with decreasing temperature, decreasing basicity and increasing P_2O_5 content of the slag. Similar effects have observed in the additions of B_2O_3 and Cr_2O_3 to silicate melts. These changes in slag composition lower the surface energy (σ) and raise the viscosity (μ), when (σ/μ) ratio is lowered by changing the temperature and/or composition (Cooper and Kitchener 1959, Swisher and McCabe 1964).

The foams may have different morphologies and gas bubble cells with a large size range. Hence their stability degree can be very different. Foams can be divided into two categories; foam with spherical bubbles, kugelschaum (sphere foam) and polyhedron-shaped bubbles, called polyederschaum (polyhedron foam). The first ones consist of relatively small spherical bubbles. The second kind of foam is composed of large, polyhedron-shaped bubble cells with very thin liquid lamellae separating them. The stability of liquid foams depends not only on its intrinsic physical properties but also on the bubble size (Zhang and Fruehan 1995a).

Slag foams have very different structures. Foams with very fine bubbles have spherical bubble cells and they are stable. Foams, which contain larger bubbles have polyhedral bubble cells and are less stable (Zhang and Fruehan 1995a).

1.1 Benefits of slag foaming phenomena

Slag foaming phenomena are observed in many ferrous pyrometallurgical processes and are of interest in steelmaking, bath smelting and electric arc furnace processes (Pretorius and Nunnington 2002).

Slag foaming has become important for the modern electric arc furnace (EAF). The foaming practices are used to shield the refractory from the arc. The foamed slag stabilises the arc, shields the metal from the atmosphere and improves energy efficiency. The control of foaming height is required to maintain a steady operation (Pretorius and Nunnington 2002).

Foam acts as a thermal insulator between the hot bath and the surroundings, thus reducing the electrical power required to maintain the high operating temperature and limiting electrode consumption (Lotun and Pilon 2005).

Foaming slag stabilises the striking of the arc. This leads to a higher power input at a constant voltage. By applying the reproducible slag practice in stainless steel, the heat transfer increases between arcs and the metal, heat radiation is screened, chromium losses to slag decreases, electron consumption decrease due to longer arcs, and the need of injection material decreases. Foaming also promotes chromium recovery. This indicates the importance of a well-developed foam to achieve low chromium levels (Görnerup and Jacobsson 1998).

1.2 Complexity of slag foaming phenomena

However, there is a lack of knowledge concerning the foaming properties of slags used in stainless steel production. This prevents the effective development of slag foaming applications (Vidacak et al. 2002).

Slag foaming is a relatively complicated phenomenon in metallurgy, particularly in the manufacture of stainless steel, whereas the foaming phenomenon of low-alloyed carbon steelmaking is relatively well known. Maintaining sufficient foaming may be difficult in the manufacturing of stainless steels (Kerr and Fruehan 2000).

It can be complicated to control foaming properly, since the evolution of the chemical and physical conditions in the slag-steel system that affect foam height are generally unknown (Marique et al. 1999).

2. Gas generation

Gas generation is indispensable in order to succeed with a foaming slag practice. In stainless steelmaking, gas is mainly generated by the reduction of CrO and FeO with carbon forming CO-gas (Görnerup and Jacobsson 1998).

Gas causes foam bubbles to form on top of a dense layer of slag. The foam can be relatively small foam bubbles like foam on beer or larger bubbles like soap bubble foam on water. The small bubbles result from chemical reactions and the resulting foam is fairly stable. Gas injection, however, produces larger bubbles and less stable foam. True foaming should not be confused with simple gas holdup of bubbles in a liquid. In the case of gas holdup, the gas bubbles are distributed throughout the entire liquid and the expansion of the slag is due to the gas bubbles in the liquid. For gas holdup, expansion decays rapidly after the gas stops. True foam can be fairly stable and remain so for several minutes after gas generation stops (Matsuura et al. 2008).

The gas bubble generation reaction, the reduction of FeO_x in slag by added carbon and carbon dissolved in metal is shown in Eqs. (1) and (2).

$$FeO(s,l) + C(s) = Fe(l) + CO(g) \quad (1)$$

$$FeO(s,l) + [C] = Fe(l) + CO(g) \quad (2)$$

In carbon steelmaking, the FeO is generated in situ as the major oxidation product of the oxygen blow and is therefore the major component in the slag (> 20%). If the consistency of the slag is suitable for sustaining foam, the simple injection of carbon into slag causes the slag to foam (Pretorius and Nunnington 2002).

The relatively high reduction rate gives FeO the potential of generating a large amount of gas inside the foam, as in the case of low-alloyed steel melting. The reduction rate of iron oxide by carbon is considerably faster than the reduction rate of chrome oxide by carbon. The large FeO content in the slag during stainless steel melting causes an increase in gas generation. Additionally, the reduction reaction also consumes heat, which results in a local increase in the viscosity of the slag (Görnerup and Jacobsson 1998).

2.1 Gas generation in stainless steel slags

In the stainless steels, the main gas generation – the reduction of CrO_x to metallic chromium – is:

$$Cr_2O_3 + 3C(s) = 2Cr + 3CO(g) \quad (3)$$

This can be promoted by high Cr_2O_3 activity (high basicity slag), high carbon activity, low CO-gas partial pressure, high temperature and low chromium activity in the metal phase. The solubility of CrO is rather low in EAF slags, and carbon reduction should theoretically result in low chromium losses to the slag. Kinetics is a major limiting factor of the system. Many practical aspects related to the overall kinetics of the process are considered to promote gas generation (Görnerup and Jacobsson 1998).

In stainless steelmaking, the major oxidation products are SiO_2 and Cr_2O_3. SiO_2 fluxes and Cr_2O_3 is a very potent refractory component, which stiffens the slag. With stainless steel slags, the Cr-O buffer occurs at a much lower oxygen potential than FeO-buffer. Therefore, chromium is preferentially oxidised when compared with iron. Due to this, it is important that the Cr_2O_3 content of the slag has to be carefully controlled in order to make the slag consistency amenable for foaming conditions. The carbon dissolved in the steel may not play a vital role in the reduction of FeO_x in the slag (Pretorius and Nunnington 2002).

3. Slag requirements for optimal foaming

3.1 Early slag formation

The generation of the early liquid slag is a prerequisite for foaming in stainless steel slags. Reactions or processes that generate small bubbles and suitable slag properties as stable foam are common requirements for slag foaming with both carbon and stainless steel.

Oxygen injection into liquid steel during an early stage adds chemical heat to the slag soon after carbon injection into the slag. It increases mixing and evens out the temperature distribution in the furnace (Pretorius and Nunnington 2002).

The early slag formation is characterised by short arcs and poor melting efficiencies. Formation of early liquid slag is facilitated by the addition of wollastonite ($CaSiO_3$). It melts at steelmaking temperatures and provides a fluxing precursor. The silicon in the bath originates from the scrap and ferroalloys (Pretorius and Nunnington 2002).

The quicker the slag formation, the quicker the power levels can be increased. The early liquid slags can also be formed by the oxidation of silicon in the bath, or deliberate SiO_2 and lime additions. The addition of quartz requires energy to heat up and melt. However, the oxidation of silicon overall is exothermic and provides additional energy for melting the scrap – see Eqs. (4) and (5) (Pretorius and Nunnington 2002).

$$Si(s)_{25°C} + O_2(g) = SiO_2(l)_{1600°C} \tag{4}$$

For which $\Delta H° = -77.8 kWh/kg/Si$

$$SiO_2(s)_{25°C} + SiO_2(g) = SiO_2(l)_{1600°C} \tag{5}$$

For which $\Delta H° = 0.6 kWh/kg/Si$

Along with the SiO_2, the presence of FeO and CaO from lime additions causes the formation of liquid slag, which melts rapidly due to the fluxing effect of FeO (Pretorius and Nunnington 2002).

3.2 Stainless steel slags

Typical stainless steelmaking electric arc slag consists mostly of the components CaO, MgO, Al_2O_3 and SiO_2. Ideally, the Cr_2O_3 content of the slag should be less than 5% and can therefore often be ignored. The ideal final aim slag composition is at dual saturation with respect to both CaO and MgO. These dual saturated slags are basic enough to minimise Cr_2O_3-losses to liquid portion of the slag. They are also compatible with magnesia-chrome and magnesia-carbon refractory (Pretorius and Nunnington 2002) .

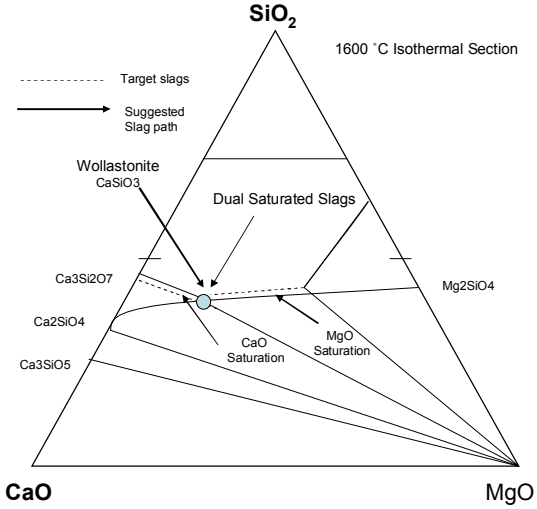

Figure 1. Isothermal section of CaO-MgO-SiO_2 system at 1600 ˚C (Pretorius and Nunnington 2002).

A critical requirement for these target phase slags to foam adequately is the control of Cr-Cr_2O_3 equilibrium in the bath. The solubility of CrO_x in the targeted slags is very low (< 5% Cr_2O_3). When the solubility of CrO_x is exceeded in the slag, the chromium containing phase precipitates. This has a negative impact on the ability of slag to foam. The purely isothermal CaO-MgO-SiO_2 system at 1600 ˚C can be shown as target slag for optimum foaming in Figure 1. Typical target compositions are in the area of saturation boundaries of CaO(Ca_2SiO_4) or MgO (Pretorius and Nunnington 2002).

The presence of suspended second-phase particles in the slag had a much greater impact on foaming than surface energy or viscosity. The optimum slags are not completely liquid, but are saturated with respect to CaO(Ca_2SiO_4). The second-phase particles serve as gas nucleation sites, which lead to a large number of small gas bubbles in the foaming slag (Pretorius and Nunnington 2002).

The slag composition is of great importance with an overall requirement of a limited amount of solid phase. This restricts the Cr_2O_3-and CaO content in the slag depending on temperature and basicity (Görnerup and Jacobsson 1998).

3.2.1 Effect of operation procedure

In the controlled melting (with respect to oxidation results) the initial Cr_2O_3 content is about 15%. The Cr_2O_3 content is more or less constant and the slag temperature increases at the start of injection. After the injection, the reduction of FeO proceeds and its content drops steeply. The number of available reaction surfaces is now at a high level and the reduction rate of Cr_2O_3 increases. The reduction of Cr_2O_3 is more pronounced when oxygen gas injection is stopped for a moment and the final carbon is injected. At the end of the reduction period, the Cr_2O_3 content in the slag is 7–9 wt%. The final reduction commences during the tapping. The Cr_2O_3 content can go down to 3 wt% if there is a sufficient amount of silicon dissolved in the steel along with the mixing of steel and slag. Figure 2 shows a schematic diagram of an ideal slag vs. time operation (Görnerup and Jacobsson 1998).

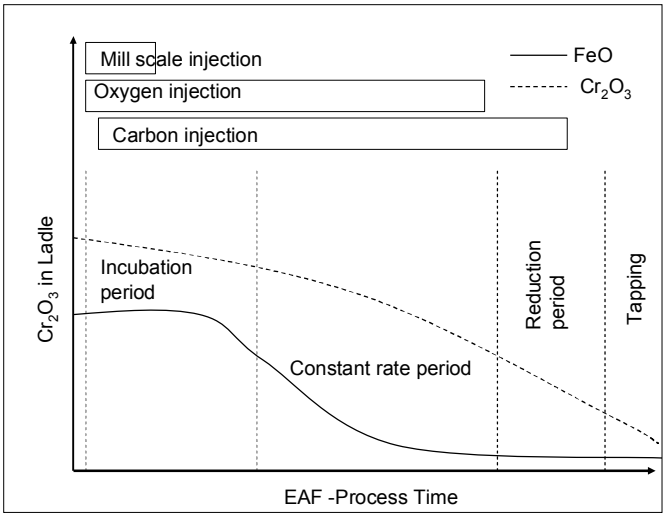

Figure 2. The principal slag foaming practice (Görnerup and Jacobsson 1998).

3.2.2 Effect of oxygen blowing

When oxygen is blown into a molten pool of steel, the metal species oxidise according to the affinity for oxygen and their activities in the bath. Aluminium and silicon have a greater affinity for oxygen and some of the chromium in the bath also oxidises. The CrO_x is absorbed into a liquid slag, then equilibrium conditions

can be approached after the oxygen blow and the chrome can revert back to the bath, providing the silicon content is high enough. The liquid slag enhances the mass transfer between slag and metal. If the oxidised chromium is present as solid phase ($MgCr_2O_4$, $CaCr_2O_4$) in a stiff slag, the recovery of chrome into the metal is poor, even if the silicon content of the steel is high (Pretorius and Nunnington 2002).

3.2.3 Effect of slag volume

A sufficient volume of slag is required to cover the arcs during foaming. This indicates the amounts of SiO_2, CaO, MgO and Al_2O_3 needed to achieve the desired volume in the furnace. The amount of slag needed to achieve the desired volume of slag in the furnace is defined by the silicon balance. It is important that the silicon level in the bath does not drop below a critical level (> 0.2 wt%), otherwise a significant amount of chromium can be lost to the slag. The amount of silicon remaining in the bath depends on the balance of chemical and electrical energy that is utilised to melt the scrap and heat the charge. If charge chrome with high silicon content is available, then enough silicon can be in the bath to match the oxygen input (Pretorius and Nunnington 2002).

3.2.4 Effect of timing of additions

The timing of additions is an important parameter of slag foaming in stainless steelmaking. The time slag composition takes to achieve its final target composition is crucial for controlling chromium losses and optimising the foamability of the slag. The generation of an early liquid slag during meltdown is an important requirement to enhance kinetics in the bath and control the amount of chromium lost to the slag (Pretorius and Nunnington 2002).

3.2.5 Effect of MgO (Doloma)

The initial MgO content in the slag is another important consideration. The MgO addition to wollastonite-type slag decreases the solubility of Cr_2O_3 due to the fact that the primary chromium saturation phase changes form eskolaite (Cr_2O_3) to spinel ($MgCr_2O_4$). However, the MgO-addition to CaO-SiO_2-slags lowers the melting point of slag and increases fluidity of the slag until MgO content becomes too high (15 wt%) (Pretorius and Nunnington 2002).

4. Foaming slags

The parameters of slag foaming are mainly foam height and foam life. The foam life cannot be measured in actual processes and its definition differs between authors (Hong et al. 1998).

After the creation of a slag that can sustain foam, the next step is the creation of the gas bubbles that make the slag foam. The injection of only argon or nitrogen gas into a slag with suitable viscosity can also create some foam (Pretorius and Nunnington 2002).

A cheaper and more effective option is to create CO-gas bubbles by the reduction of iron oxide by carbon according to Eqs. (1) and (2). This is achieved by the injection of carbon and iron oxide. Their particle sizes should be as fine as possible, as the reduction rate with finely divided particles is very fast at steelmaking temperatures. Maintaining an adequate silicon level in the steel together with continuous feeding of the mixture prevents the involvement of chromium in the steel bath as a reductant (Pretorius and Nunnington 2002).

4.1 Effect of carbonaceous particles

Free particles of coke or coal char act as foam destabilisers (Pretorius and Nunnington 2002). Thus, coke can be used to reduce the slag foaming in steelmaking. The top injection is reported to be effective in controlling excess foaming during the smelting reduction of chrome ore. The foam height is found to decrease significantly with the increase of the ratio of the weight of the carbonaceous particles to that of slag. The small gas bubbles have been known to rupture and spread over the surface of the coke particle present in the slag. Then bubbles coalesced and evolved from the top of the coke particle as a single large layer (Zhang and Fruehan 1995b).

4.2 Effect of FeO addition

In stainless steelmaking, the addition of iron oxide without the simultaneous addition of carbon leads to excessive chromium losses to the slag, which greatly diminishes the ability of the slag to sustain foam. The combined addition of iron

oxide with carbon into liquid slag ensures the availability of carbon to react with the iron oxide as it is dissolved into the slag. This decreases the possibility of FeO reacting with chromium in the bath according to Eq. (3). Foamy slag processes require carbon and mill scale additions or other foaming agents together with air or oxygen injection. The batch type additions will by default have cyclic periods of foam stability and instability (Pretorius and Nunnington 2002).

Since FeO is a requirement for slag foaming, the FeO addition method is critical for good foaming practice. The addition of FeO with scrap without carbon addition during melting causes a reduction of FeO by the silicon and chromium in the bath according to Eqs. (6) and (7) (Pretorius and Nunnington 2002):

$$2FeO(s,l)+[Si]=2[Fe]+SiO_2(l) \tag{6}$$

$$2FeO(s,l)+[Cr]=[Fe]+Cr_2O_3(s) \tag{7}$$

In the reactions FeO is removed from the slag. In Eq. (6) Cr_2O_3 is generated and this can lead to excessive solids and thus excessive slag viscosity values (Pretorius and Nunnington 2002).

4.3 Effect of mill scale injection

Mill scale (FeOx > 98.5%) injection is recommended to increase the reduction rate and foaming in the slag. Mill scale injection into the slag promotes foaming via increasing gas generations. The foaming thus increases chromium recovery.

Mill scale injection shows that the foaming slags have a higher initial FeO content and lower final FeO- and Cr_2O_3 contents. This suggests a strong effect of FeO on the rate of Cr_2O_3 reduction and gas generation. The mill scale is mainly injected during the initial period of carbon and oxygen injection to promote the start of slag reduction. The positive results can be confirmed by excellent gas generation. It is suggested that the reduction reaction of FeO produces liquid metal droplets that eliminate the difficulty of solid chromium nucleation (Eqs. (1) and (2)) (Görnerup and Jacobsson 1998).

Mill scale injection has been known to strongly promote gas production. This can be studied even by visual observations. Mill scale injection also is seen to be useful in starting the reduction and thereby, slag foaming (Görnerup and Jacobsson 1998).

5. Slag foams

The foaming of slag is well established in low-alloyed steel production. It consists of carbon and oxygen injection into the slag. The gaseous reaction is dominated by two routes. In the first route, oxygen injected into steel produces FeO, which is transferred to the slag phase. After this, it is reduced from the slag phase by injected carbon and forming CO-gas. The carbon dissolved in the steel also contributes to gas production. In the second route, injected or dissolved carbon reacts with injected oxygen gas, producing CO-gas (Görnerup and Jacobsson 1998).

The injection rate of oxygen and carbon is critical in achieving a stable foam in the slag. The range for optimum FeO_x content of the slag is rather large, 15–25 wt%. Both this and the quick reduction rate of FeO with carbon makes the foaming slag practice in low-alloyed steel production an easily controlled process (Görnerup and Jacobsson 1998).

5.1 Foaming of EAF slags in stainless steelmaking

The foaming slags have lower chromium content and a large initial reduction of FeO. Oxidative environment results in high initial levels of chromium in the slag. The foaming is found to promote chromium recovery (Görnerup and Jacobsson 1998).

In the production of high-alloyed steels, the high chromium contents have a large effect. The oxygen injected into steel produces CrO instead of FeO. The CrO presents different behaviour when dissolved in the slag. CrO has a low solubility in typical EAF slags depending on the (CaO/SiO_2)-ratio and temperature. The reduction rate of CrO by carbon is a slow reaction. The optimum range for the slag composition in the case of CrO content of slag is relatively narrow. There is a large possibility of uncontrolled oxidation with large chromium losses to slag and poor foaming (Görnerup and Jacobsson 1998).

Foaming of Cr_2O_3 in EAF slags in stainless steel melting is a difficult task. Both foaming and gas generation can be considered poor. The slag composition has minimal impact on the foaming of slag when it varies within the normal range of EAF slags. This is an indication of the importance of gas generation (Görnerup and Jacobsson 1998).

The slag which contains a larger amount chromium oxide (about 25 wt%), has a lower solubility limit and the emerging solid phase breaks the foam bubbles,

leading to precipitation of solid particles in the bulk and lower gas generation during foaming (Kerr and Fruehan 2004).

According to Kerr and Fruehan (2000), the poor foaming of stainless steel slag is due to a solubility limit of the slag which contains a greater amount of CrO, precipitation of solid particles in the bulk and lower gas generation during foaming. The slag foaming can be improved by controlling and manipulating its formation rate, composition and temperature.

5.2 The effect of slag composition

The slag composition has a small impact on the foaming in the range of typical EAF slags in stainless steel melting. This indicates that gas generation is critical (Table 1).

Table 1. Slag composition and temperature interval of typical EAF slag (Görnerup and Jacobsson 1998).

T, ˚C	(%CaO/%SiO_2)	%Al_2O_3	%FeO	%MgO	%Cr_2O_3	%MnO
1550-1650	1,0-1,8	0-7	0-10	0-15	2-20	0-4

The above considerations on slag foaming and gas generation can be summarised as a 'hypothetical phase diagram' in terms of the acid, basic and chrome oxide contents of the system (see Figure 3) (Görnerup and Jacobsson 1998).

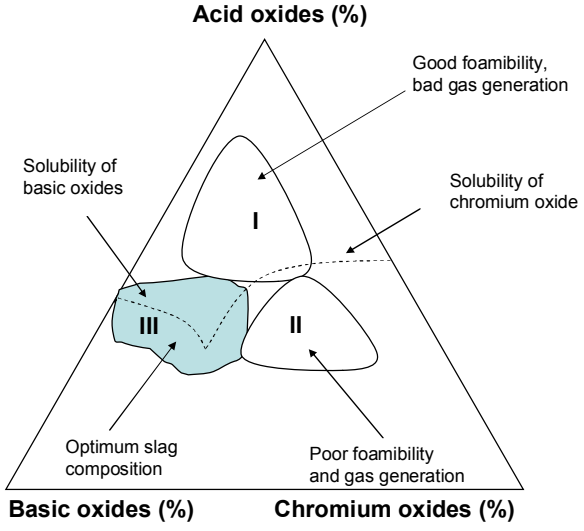

Figure 3. A hypothetical phase diagram shows the area of different foaming and reduction properties (Görnerup and Jacobsson 1998).

5.2.1 The effect of slag composition areas on foaming

Three important slag composition areas have been proposed and considered by Görnerup (Görnerup and Jacobsson 1998).

1) Low basicity slags with high viscosity favour good foaming. The gas generation is poor in this area, causing poor foaming due to low CrO activity. The overall result of this area is poor foaming with no industrial interest (Görnerup and Jacobsson 1998).
2) The area presents slag composition after uncontrolled oxidation during melting. The slag is partly solid with Cr_2O_3 complexes. The viscosity is far beyond the limits despite a large amount of Cr_2O_3 particles. The large proportion of solid particles is detrimental to the kinetics of gas generation (Görnerup and Jacobsson 1998).
3) This is the optimum area for foaming. The basicity is high, which promotes thermodynamic gas generation and low slag viscosity. However, by controlling the amount of undissolved (CaO/Cr_2O_3), the apparent viscosity increases and the foaming of the slag increases (Görnerup and Jacobsson 1998).

A foaming slag practice in stainless steel melting with controlled carbon and oxygen injection can be achieved with low Cr losses (< 3 wt% Cr_2O_3). This is possible with process control with respect to the total reductants/total oxygen ratio, chromium oxidation during melting should be minimised and injection mixture aimed at achieving reducing conditions. Silicon content should be high enough to protect chromium from oxidation and at the end to achieve a slag reduction at tapping (Görnerup and Jacobsson 1998).

The presence of surface-active species, such as V_2O_5, strongly promotes foaming. However, V_2O_5 is undesirable in stainless steels and thus does not offer a practical option. A higher content of FeO increases both the reduction rate of CrO and the foaming (Görnerup and Jacobsson 1998).

5.3 Chromium recovery

Increased foaming results in lower chromium losses and this emphasises the importance of slag foaming if low chromium losses are to be reached. Slag composition is of great importance in the overall requirement of a limited amount of solid phase. This restricts the Cr_2O_3 and CaO content in slag, depending on temperature and basicity (Görnerup and Jacobsson 1998).

Mill scale injection into the slag promotes foaming via increasing gas generation by adding FeO into slag. It is suggested that Eqs. (1) and (2) produce liquid metal droplets that eliminate the difficulty of solid chromium nucleation (Görnerup and Jacobsson 1998).

5.3.1 Controlling the chromium yield

According to Görnerup and Jacobsson (1998), the chromium yield in the EAF procedure is controlled by the following factors.

1) The degree of oxidation during melting. A high oxidation potential during melting results in high chromium levels in the slag. The local factors have a large effect on the reduction of Cr_2O_3. The achievement of low final chromium losses is impossible if the initial oxidation during melting is uncontrolled and Cr_2O_3 content is high (Görnerup and Jacobsson 1998).
2) The degree of reduction during injection period. During the refining period, reducing conditions have to be secured, which is a matter of controlling the (C/O_{tot}) injection ratio. In addition, the slag basicity has to be controlled for the whole of the injection period to limit the amount of undissolved materials in the slag (Görnerup and Jacobsson 1998).
3) The degree of reduction during tapping. The basicity and SiO_2 content decreases and a large amount of Cr_2O_3 is reduced during this period. It is possible that there is a certain minimum silicon content in the steel at tapping, which is an important parameter in achieving low final chromium losses. The mixing during tapping gives excellent conditions for dissolved silicon to reduce Cr_2O_3 in the slag (Görnerup and Jacobsson 1998).

6. Definition of the foaming index

According to Kerr and Fruehan (2004), the foam index is a parameter that quantifies the ability of slag to generate foam from either an injected gas or a gas that is generated within the slag of metal.

According to Ito and Fruehan (1989a), the foaming index (Σ) can be determined experimentally by modifying the foaming index used in aqueous foams. The superficial gas velocity is defined by Eq. (8), whereas the average gas travelling time or foaming index is defined in Eq. (9):

$$V_g^s = \frac{Q_g}{A} \tag{8}$$

$$\Sigma = \frac{\Delta h}{\Delta V_g^s} \tag{9}$$

Where (Q_g)[cm^3/s] is the gas flow rate, (A) is the cross-section area of the container and (Δh) is the change in slag height.

Superficial gas velocity $\left(V_g^s\right)$ is also correlated to the void fraction α, the volumetric fraction of gas and the actual gas velocity $\left(V_g\right)$[cm/s]:

$$V_g^s = \left(\alpha V_g\right) \tag{10}$$

The foam height (h) can be expressed as a function of void fraction (α) and the foam layer thickness (L), [cm]:

$$h = \left(\alpha L\right) \tag{11}$$

Finally, (Σ) can be expressed in terms of the foam layer thickness and the actual gas velocity $\left(V_g\right)$:

$$\Sigma = \left(\frac{\Delta L}{\Delta V_g}\right) \tag{12}$$

Eq. (12) is valid only when term (α) is independent of the foam height. The void fraction profile as measured has been discovered to be almost independent of position. Therefore, term (α) can be assumed to be constant (Ito and Fruehan 1989a).

According to Ozturk and Fruehan (1995), Eqs. (8) and (9) indicate that the foam height is independent of slag depth as long as there is a sufficient amount of slag to form foam. There is some controversy as to the effect of slag depth on foaming.

6.1 Foam life

The formation of foam is proportional to a gas flow rate and the rupture of foam is proportional to its height. The rate equation for the change in foam height can be presented in Eq. (13) (Ito and Fruehan 1989a):

$$\frac{dh}{dt} = \left(K_1 Q_g\right) - \left(K_2 h\right) \tag{13}$$

Where (K_1) and (K_2) are formation and rupture constants of foam. In the steady state conditions, the rate equation Eq. (14) for change in foam height can be presented:

$$\left(K_1 Q_g\right) = \left(K_2 h\right) \tag{14}$$

When the gas flow is ceased at the steady state ($Q_g = 0$):

$$\frac{dh}{dt} = -\left(K_2 h\right) \tag{15}$$

After integrating Eq. (15) from (t = 0) to (t = t) and from ($h = h^\circ$) to (h = h) the foam height can be presented as a function of time:

$$K_2 t = -\ln\left(\frac{h}{h^\circ}\right) \tag{16}$$

The rupture of foam can be expressed as the drainage of the liquid in the foam, by assuming that the drainage rate is of first order, the rate drainage rate given by Eq. (17) Ito and Fruehan (1989a):

$$\frac{dv}{dt} = k\left(V^0 - v\right) \tag{17}$$

Where (V^0) [cm^3] is the initial liquid volume in foam and (v) [cm^3] is the drained liquid volume. After the integration from (t = 0) it can be presented when the void fraction is almost constant:

$$kt = -\ln\left(\frac{h}{h^0}\right) \tag{18}$$

Finally, the average foam life (τ) can be obtained after modifications:

$$\tau = \frac{1}{V^0}\int_0^{v^0} t dv = k\int_0^{\infty} te^{-kt} dt = \frac{1}{k} \tag{19}$$

where (V^0) is the initial liquid volume in foam and (v) is the drained liquid volume, (k) is the drainage constant and (t) is the time.

6.2 The relation between foaming index and foam life

In an ideal system relation between foaming index (Σ) and foam life, for which (α) is constant, the foaming index can be related to average foam life (τ). The foam formation can be presented with constant (α) (Ito and Fruehan 1989a):

$$\frac{dh}{dt} = \alpha\frac{dL}{dt} = \frac{\alpha}{A}\frac{dV^{foam}}{dt} = \frac{Q_g}{A} \tag{20}$$

where (V^{foam}) is a volume of the foam, with constant (α), Eq. (21) can be presented from Eq. (16) with Eq. (13) (Ito and Fruehan 1989a):

$$K_1 = \frac{1}{A} \tag{21}$$

From the relationship of Eqs. (14), (19) and (21), the following relationship can be presented:

$$\frac{\tau}{A} = \frac{h}{Q_g} \tag{22}$$

Whereas the foam life in Eq. (23) can be presented using Eqs. (8), (9) and (22):

$$\tau = \frac{\Delta h}{\Delta\left(Q_s / A\right)} = \Sigma \tag{23}$$

In the ideal slag case, the foaming index (Σ) is equal to the average foam life (τ).

6.3 Foaming in the steelmaking process

The foaming for iron and steelmaking processes can be calculated by using the foaming index. The index for the particular slag can be estimated by evaluating the

liquidus composition from the phase diagrams and approximating the amount of suspended particles in the melt.

Using estimates of the foaming index, the foam height can be calculated via Eq. (24) (Ito and Fruehan 1989b):

$$h = \sum\left(V_g^s - V_g^*\right) + h^* \tag{24}$$

where $\left(V_g^*\right)$ is superficial gas velocity, and $\left(h^*\right)$ is the foam height when foaming begins.

The following assumptions have been made: $\left(V_g^*\right)$ and $\left(h^*\right)$ are expected to be small, the furnace is isothermal, flow regime is constant, the effect of the bubble diameter on the foaming index (Σ) is small, and the foamed slag is uniform. The absolute value of the calculated foam height may be different in actual operations in the EAF process, since there can be coal or coke in the slag, which can affect foaming (Ito and Fruehan 1989b).

6.4 Estimation of the slag physical properties

It is not possible to measure the physical properties of the slags in high temperature conditions. Therefore, simple models have been used to estimate the values of density, surface energy and viscosity. An additive method for the estimation of densities in the slag has been widely applied to complex systems. In this method, the molar volume (V) can be obtained as in Eq. (25) (Jiang and Fruehan 1991):

$$V = \sum_i x_i \overline{V}_i \tag{25}$$

where (x) and $\left(\overline{V}\right)$ are the mole fraction and the partial molar volume, respectively. The partial molar volume is usually assumed to be equal to the molar volume of the pure component, which is given in the literature (Mills and Keene 1987).

The estimations for surface energy of slag are based on the addition of the partial molar contributions of $\left(\overline{\sigma}\right)$ the individual constituent according to Eq. (26):

$$\sigma = \sum_i x_i \overline{\sigma_i} \tag{26}$$

The contribution of the surface-active component $\left(x_i \overline{\sigma_i}\right)$ is a function of the concentration itself and it is also given in the literature (Mills and Keene 1987).

6.4.1 The estimation of the viscosity of slags

The Urbain viscosity model (Urbain 1987) can be used in the estimation of the viscosity of slags according to Eq. (27) (Jiang and Fruehan 1991):

$$\mu = A \cdot T \cdot \exp\left(B / T\right) \tag{27}$$

where (A) and (B) are viscosity parameters, (T) is temperature [K], and (μ) is viscosity [Pas] or [Ns/m^2]. The results of this model agree within 15% of the measured values in systems for which reliable measurements are made (Jiang and Fruehan 1991).

6.4.2 The effect of second-phase particles

The stabilisation effect of particles on the slag foaming is believed to be caused by the increase in the viscosity of the slag. The diameter of the solid particles used in this is less than 100 μm, which is less than the bubble diameter. The effect of second-phase particles on slag foaming is described well by defining the viscosity of the mixture using the modified Einstein equations, Eqs. (28) and (29) (Ito and Fruehan 1989b):

$$\mu = \mu_f \left(1 + 5.5\varepsilon\right) \tag{28}$$

$$\mu = \mu_f \left(1 - \varepsilon\right)^{-2.5} \tag{29}$$

where (μ_f) is the viscosity of the liquid slag,

(Σ) is proportional to (μ). The (Σ/Σ_0) relation is equal to the (μ/μ_0) relation for the slag with particles, where superscript (0) is for slag without particles. The measured and calculated data is said to agree when the particle concentration is low (Ito and Fruehan 1989b).

According to Ito and Fruehan (1989b), if the slag contains second-phase particles CaO or Ca_2SiO_3, the viscosity is calculated using Eq. (28) and foaming index via Eq. (33). When the term (Σ) is proportional to (μ), the relation (Σ/Σ°) is equal to (μ/μ°) for slag with particles, where (Σ°) is for slag without particles (Ito and Fruehan 1989b).

The measured value of relation (Σ/Σ°) and the calculated lines for (μ/μ°) in Eqs. (28) and (29) are shown in Figure 4. The measured data and the calculated curve agree relatively well when the particle concentration is low. At higher particle concentrations the measured values are higher, since the interactions between the slag and particles are stronger (Ito and Fruehan 1989b).

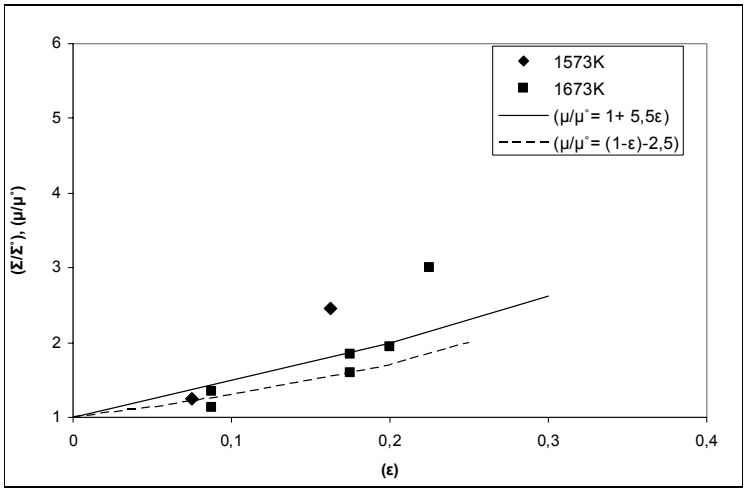

Figure 4. The effect of second-phase particle concentration on the foaming index ratio and viscosity ratio calculated from Eqs. (28) and (29) (Ito and Fruehan 1989b).

The effect of solid particles can also increase the bulk viscosity of the slag according to the Roscoe equation (Roscoe 1952):

$$\mu = \mu_0 \cdot \left(1 - n \cdot \Theta\right)^{-m} \tag{30}$$

where (μ) is the bulk effective slag viscosity, (μ_0) is viscosity of pure liquid slag, (Θ) is the volume fraction of the solid particles, and n and m are shape constants of the solid particles (Vidacak et al. 2002).

7. Experimental studies on the foaming index and dimensional analysis

7.1 Foaming of CaO-SiO_2-FeO slags

Ito and Fruehan (1989a) have experimentally studied the effect of CaO-SiO_2-FeO slag composition on foaming in iron and steelmaking processes. Argon was introduced into molten slag. The surface position was determined by electric probe. The foam height was defined as the increment of the slag surface level from the original slag surface $\left(V_g \approx 0\right)$ to the foaming slag surface. Mean bubble size is defined from the gas flow rate and the bubble formation frequency. The bubble formation frequency is determined by a pressure transducer.

Ito and Fruehan (1989b) then carried a dimensional analysis for the foaming index of CaO-SiO_2-FeO slag in order to study the effect of viscosity and surface energy on slag foaming. It was assumed that the effect of bubble diameter is negliable in the study of the foaming index. Taking foaming index (Σ [s]), density (ρ [kg/m^3], surface energy (σ [N/m]) viscosity (μ [Pas]) and gravitation (g [m/s^2]) into account, the following two dimensionless numbers can be obtained (Ito and Fruehan 1989b):

$$N_1 = \left(\frac{\gamma^{3/4} \cdot \rho^{1/4}}{\mu g^{1/4}} \right) \tag{31}$$

$$N_2 = \left(\frac{g^{3/4} \cdot \rho^{1/4}}{\sigma^{1/4}} \right) \tag{32}$$

A linear relationship was obtained between (N_1) and (N_2) for CaO-SiO_2-FeO-(Al_2O_3) slag. Due to this, the following experimental equation is derived for CaO-SiO_2-FeO-(Al_2O_3) slag (Ito and Fruehan 1989b):

$$\sum = 5.7 \times 10^2 \frac{\mu}{\sqrt{\sigma \rho}} \tag{33}$$

The foaming index for the slag with particles was calculated using Eq. (32) and Eq. (33) compared with the observed value in Figure 5. The values are in relatively good agreement with each other (Ito and Fruehan 1989b).

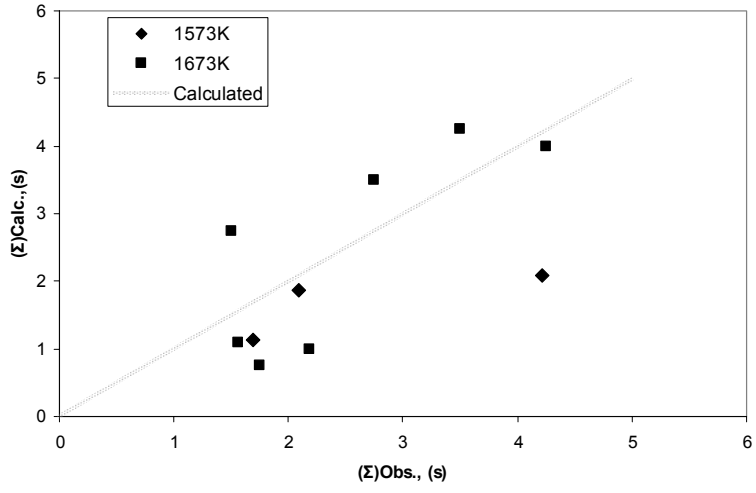

Figure 5. The comparison between foaming index for the slag containing second-phase particles with the observed (Ito and Fruehan 1989b).

According to Eq. (33), it seems that the viscosity is the most important parameter in determining foaming index (Σ). The validity of this equation for the slag containing surface-active species such as P_2O_5, C and CaF_2, was not studied due to the lack of experimental high temperature area surface energy or viscosity data. The effect of these components on the foaming index has to be approximated directly from the experimental data (Ito and Fruehan 1989b).

7.2 Slag foaming in bath smelting

Jiang and Fruehan (1991) experimentally studied slag foaming in terms of the foaming index for the bath smelting type of slags (CaO-SiO_2-FeO, CaO-SiO_2-MgO-Al_2O_3-FeO) at 1773 K in the argon gas injection. The foam was viewed by X-ray spectrometry. The foaming index (Σ) is determined by measuring the foam height for different gas flow rates under argon gas bubbling. The technique of dimensional analysis was applied in order to find the relationship describing the foaming index as a function of the slag properties.

7.3 Dimensional analysis technique

The technique of dimensional analysis was applied in order to find the relationship between the foaming index and slag properties. It can be assumed that the foaming index (Σ) is a function of all the variables and dimensional constants that can affect the value of foaming index (Σ) (Jiang and Fruehan 1991):

$$\Sigma = f\left(\rho, \mu, \sigma, g\right) \tag{34}$$

where (Σ) is foaming index[s], (ρ) is liquid slag density [kg/m^3], (μ) is slag viscosity [Pas], (σ) is slag surface energy, and [N/m] and (g) is gravity [m/s^2].

Two dimensionless groups can be obtained from the five variables and three fundamental dimensions of Eq. (34). It is useful to have a group that depends on viscosity and surface energy:

$$\Pi_1 = f\left(\rho, g, \Sigma, \underline{\mu}\right) \tag{35}$$

$$\Pi_2 = f\left(\rho, g, \Sigma, \underline{\sigma}\right) \tag{36}$$

Through dimensional analysis the final forms of Eqs. (35) and (36) are as follows:

$$\Pi_1 = \left(\frac{\Sigma g \mu}{\sigma}\right) \tag{37}$$

$$\Pi_2 = \left(\frac{\mu^4 g}{\sigma^3 \rho}\right) \tag{38}$$

The dimensionless number given in Eq. (38) is called the Morton number, which describes the balance between gravitational, viscous and surface energy forces. The Morton number is generally used to describe the velocity of bubbles in liquids. The dependence of the slag foaming index on the slag physical properties can be found by obtaining the relationship between these two dimensionless groups (Π_1, Π_2) (Jiang and Fruehan 1991).

7.3.1 Dimensional analysis results

From the measured foaming indexes and the defined slag physical properties, $\log(\Pi_1)$ vs. $\log(\Pi_2)$ was computed according to Eqs. (37) and (38). Using a least-square analysis, the slope of the straight line could be found. Taking into account the experimental error and accuracy of the slag property, the slope can be defined as (Jiang and Fruehan 1991):

$$\log\left(\prod_2\right) = -2\log\left(\prod_1\right) + 5.11 \tag{39}$$

The final equation can be shown:

$$\sum = 359\left(\frac{\mu}{\sqrt{\rho g \sigma}}\right) \tag{40}$$

or rewritten as Eq. (39):

$$\sum = 115\left(\frac{\mu}{\sqrt{\rho \sigma}}\right) \tag{41}$$

The analysis gave the same slag property dependence of the foaming index as that derived earlier in Eq. (33), except that there is difference in the value of the coefficient. The difference between the coefficients is believed to be due to the difference in the slag properties used for each analysis, since the previous values were extrapolated with respect to temperature and composition. According to Eq. (41), viscosity is more important than surface energy in determining the foaming index (Jiang and Fruehan 1991).

On the other hand, disregarding which dimensionless groups are used, the obtained results should be same. To verify this, the definition procedure was made for data to plot log(Π_1') vs. log(Π_2'), where (Π_1') vs. (Π_2') are dimensionless numbers from Ito and Fruehan (1989a). Then the following equation could be obtained using a least-square analysis (Jiang and Fruehan 1991):

$$\log\left(\prod\nolimits_2^{'}\right) = -1.05\log\left(\prod\nolimits_1^{'}\right) + 2.53 \tag{42}$$

From Eq. (42) it is possible to define the final equation describing the correlation:

$$\sum = 108\left(\frac{\mu}{\sqrt{\rho \sigma}}\right) \tag{43}$$

Within the accuracy of the determination, Eqs. (41) and (43) are identical. (Jiang and Fruehan 1991). According to Jouhari (2000), the discrepancies in the proportionality constant may be due to the accuracy in the estimate of the foaming index on the basis of slag properties as governed by the experimental conditions of composition and temperature.

7.4 The effect of the bubble size and chemical reactions on slag foaming

Zhang and Fruehan (1995a) have experimentally studied the effect of bubble size on slag foaming. The foam stability in terms of foam index for a bath smelting type of $CaO\text{-}SiO_2\text{-}Al_2O_3$ slag is determined for different bubbles. The average size of bubbles in the foam is measured by an X-ray video technique under argon gas bubbling.

The correlations used to predict the foam index for the liquid slag as a function of its physical properties and the size of the bubbles in the slag foam were obtained using dimensional analysis. The foam index is observed to increase with viscosity, whereas it decreases with density and bubble diameter. However, its value is relatively independent of surface energy (Zhang and Fruehan 1995a).

In the dimensional analysis based on the physical phenomena, the foam index (Σ) can be expressed as a function of all independent variables (Zhang and Fruehan 1995a):

$$C = f\left(\Sigma, \sigma, \mu, D_b, \rho, g\right) \tag{44}$$

where (C) is constant. The definitions and the dimensions of variables are: (Σ), foaming index [s], (ρ); liquid slag density [kg/m^3], (μ); slag viscosity [Pas], (σ); slag surface energy, [N/m], (g); gravity [m/s^2] and (D_b); average bubble diameter [m]. There are five variables and three fundamental dimensions in the equation; two dimensionless groups are to be obtained. It is useful to have a group, which depends on the viscosity and the surface energy. The average bubble diameter is as an independent variable. In reality, the bubble size is not a completely independent variable. It is easy to change the dimensions of the orifice and keep the physical properties constant (Zhang and Fruehan 1995a).

The following dimensionless groups can be obtained based on the principle of dimensional homogeneity (Zhang and Fruehan 1995a):

$$\Pi_1 = \left(\frac{\Sigma \mu g}{\sigma}\right) \tag{45}$$

$$\Pi_2 = \left(\frac{\mu^4 g}{\sigma^3 \rho}\right) \tag{46}$$

$$\Pi_3 = \left(\frac{\rho^2 D_b^3 g}{\mu^2}\right) \tag{47}$$

The dimensionless group $\left(\Pi_1\right)$ is denoted as (N_x). Furthermore, $\left(T_2\right)$ and $\left(\Pi_3\right)$ are defined as the Morton number (Mo) and Archimedes number (Ar) respectively. The Morton number signifies the ratio of the viscous force to the surface energy force and the Achimedes number describes the ratio of the buoyancy force to viscous force.

The dimensionless numbers (N_x), (Mo) and (Ar) were calculated from the measured foam index, the average bubble diameter and the physical properties. By taking logarithms on both sides and carrying multiple component linear regression analysis, coefficients α and β and the constant C were obtained.

$$N_\Sigma = \left(C \cdot Mo^\alpha Ar^\beta\right) \tag{48}$$

where (α) and (β) are exponential coefficients. The final result of the dimensional analysis is given by Eq. (49) (Zhang and Fruehan 1995a):

$$N_x = \left(900 Mo^{0.39} Ar^{-0.28}\right) \tag{49}$$

Taking account of the experimental error, the foam index is given by Eq. (50) (Zhang and Fruehan 1995a):

$$\sum = 115\left(\frac{\mu^{1.2}}{\sqrt{\rho D_b^{0.9}\sigma^{0.2}}}\right) \tag{50}$$

In addition, Ozturk and Fruehan (1995) have proposed a dimensional analysis relation deduced from Zhang and Fruehan (1995a) in order to predict the foaming index for a slag at a given bubble size:

$$\sum = 1.83\left(\frac{\mu^{1.2}}{\sigma^{0.2} d^{0.9}}\right) \tag{51}$$

where (σ) is the surface energy, (μ) is the viscosity and (d) is the bubble size.

7.5 The effect of carbonaceous particles on slag foaming

Zhang and Fruehan (1995b) have experimentally studied the effect of charcoal and coke particles on foams generated by argon gas injection at 1500 °C in the liquid CaO -60% -SiO_2-10%CaF_2 and 25.5CaO-51%SiO_2-8.5%CaF_2-15%Al_2O_3 slag systems. The liquid slag foam was examined by X-ray video photographic observation. In order to predict the initial foam indexes without the presence of carbonaceous particles, the correlation defined by dimension (Jiang and Fruehan 1991) was used due to the similarities between the injection nozzles.

7.6 Effect of temperature and slag volume on slag foaming

Ozturk and Fruehan (1995) have experimentally studied the temperature dependence of foaming index on 48% CaO-32%SiO_2-10% $Al2O_3$-10 %FeO slag at the temperature range 1773–1873 K. The argon gas injection is introduced and the foam-gas interface is detected by probes. The foaming height is measured as the difference between the top of the foam surface and the liquid slag surface at rest. A series of measurements were made at various argon gas flow rates in order to obtain an accurate value of the foaming index.

7.7 Effect of slag volume on slag foaming

In the experimental study carried out by Ozturk and Fruehan (1995) on the effect of slag volume on the foaming index, only the amount of slag used was changed, whereas all the variables were kept constant as in the previous temperature dependence study. A slag containing 40%SiO_2 -40%CaO-10%Al_2O_3-10%FeO is used. The maximum amount of slag in the experiments is limited to about 200 g in the experimental equipment.

7.8 Effect of gas type and pressure on slag foaming

Zhang and Fruehan (1995c) have experimentally studied the effect of gas type and pressure on slag foaming. They injected gas to bubble liquid slag at 1400 and 1500 ˚C temperatures. The foam height and bubble sizes were studied using X-ray equipment and the electric probe technique.

The helium and hydrogen gases were used to bubble liquid 20%CaO-60%SiO_2-10%CaF_2 slag at 1500 ˚C. The slag was without FeO in order to eliminate the gas phase reaction. The foam heights at the different gas flow rates were compared with those obtained with argon gas injection.

The effect of gas phase pressure on foam index of 34%CaO-37.5%SiO_2-5%FeO-14%Al_2O_3-9.5%BaO slag was studied by argon gas injection at nearly (2 atm) pressure and 1450 ˚C temperature. The results were compared with the measured values at the normal atmospheric pressure (1 atm) with the same slag at the same conditions (Zhang and Fruehan 1995c).

7.9 Surface energy and foaming behaviour of melts in CaO-FeO-SiO_2 system

Skupien and Gaskell (2000) have studied slag foaming along with surface energy and viscosity. The surface energies values of CaO- (30%)FeO -SiO_2 slags with varying basicities were defined experimentally using the hollow cylinder technique at the temperature range 1573 to 1708 K. The extrapolated viscosity and density values measured by Lee (1974), dimensional groups derived by Jiang and Fruehan (1991) and measured surface energy values were used in the definition of the foaming index values.

$$\log \prod_1 = \left(\frac{\sum g\mu}{\gamma} \right) \tag{52}$$

$$\log \prod_2 = \left(\frac{\rho \gamma^3}{\mu^4 g} \right) \tag{53}$$

The variation of ($\log\Pi_1$) with ($\log\Pi_2$) is a straight line given by Eq. (53) in Skupien and Gaskell (2000):

$$\log\prod_2 = \left(-2.6\cdot\log\prod_1 + 6.79\right) \tag{54}$$

This yields the correlation:

$$\sum = 100\left(\frac{\mu^{0.54}}{\sqrt{\rho^{0.39}\sigma^{0.15}}}\right) \tag{55}$$

7.10 Steady state thickness of foams

According to Pilon et al. (2001), the steady state foam height can be presented by Bikerman's theorem (Bikerman 2001) as a function of the superficial gas velocity (j). The theorem suggests that below a critical superficial gas velocity (j_{cr}), the steady state foam thickness $\left(H_\infty\right)$ increases linearly with the gas flux:

$$H_\infty = \left(\Omega j\right), if\left(j \le j_{cr}\right) \tag{56}$$

where the constant $\left(\Omega\right)$ is called the "unit of foaminess" or "foaming index". It is considered to be a physical characteristic of the liquid corresponding to the residence time of a bubble in the foam. Beyond the critical mass flux (j_{cr}), the entrainment of the liquid into the foam by rising bubbles cannot be balanced by drainage and the foam thickness increases without limit (Pilon et al. 2001).

Hrma (1990) has developed a model for a steady state foam blanket. The foam behaviour is described in terms of two limiting gas fluxes. The threshold flux (j_m) corresponding to the minimum gas flux required to generate foam and the critical flux (j_{cr}) corresponding to the breakdown of steady state conditions is given as:

$$H_\infty = \left(2r_0 + 2r_0 b_h\right)\left(\frac{\left(1/j_m - 1/j_{cr}\right)}{\left(1/j - 1/j_{cr}\right)}\right) \tag{57}$$

where (r_0) is the average radius of bubbles in the foam, (b_h) is a constant depending on the gravitational drainage, and on the survival time of a critically thin film separating the foam from atmosphere. Furthermore:

1. If ($j < J_m$), the gas flux j reaching the liquid surface is not sufficient to create a foam layer. If ($j = J_m$), the foam layer consists of a monolayer of bubbles whose thickness is $2r_0$, where r_0 is the average radius of bubbles.

2. If ($J_m < J < J_{cr}$), the foam is steady and its thickness increases as the gas flux increases according to the expression.
3. If ($j > J_{cr}$), the excess of mass flux over (j_{cr}) cannot be released at the top of the foam and has to be stored within foam. Therefore, the foam volume grows continuously and a steady state is never reached until all available liquid is dispersed in the foam. Beyond a certain mass flux, vent holes start developing within the foam and the foam thickness stops growing and even starts decreasing.

7.10.1 Procedure of dimensional analysis technique

The isothermal conditions were assumed to prevail and thermophysical properties were constant across the foam layer. The following independent dimensionless variables were used (Pilon et al. 2001):

$$z^* = \frac{z}{H\infty},\ r^* = \frac{r}{r_0},\ j^* = \frac{j}{(j - j_m)},\ t^* = \frac{t}{\tau} \tag{58}$$

where (H_∞) is the steady state foam thickness, (r_0) is the average bubble radius, (j_m) is the superficial gas velocity of the onset of foaming, and (τ) is the characteristic time for the foam formation. The dimensional analysis was performed based on the governing equation for the transient foam thickness. In the dimensional analysis, two dimensionless parameters can be shown after modifications (Pilon et al. 2001):

$$\prod_1 = \left(\frac{\rho g r_0^2}{\mu(j - j_m)} \right) \tag{59}$$

$$\prod_2 = \left(\frac{\mu H\infty (j - j_m)}{\sigma r_0} \right) \tag{60}$$

Term (Π_1) can be defined as the ratio of the gravitational force to the viscous force on an average bubble radius (r_0) having velocity (j-j_m). Term (Π_2) corresponds to the ratio of the viscous force to the surface energy force times the ratio of the steady state foam characteristic height to the bubble characteristic dimension. The term (j_m) is the superficial gas velocity of onset of foaming, (μ) is viscosity, (σ) is surface energy, (r) is the radius of the bubble and (g) is gravity (Pilon et al. 2001):

$$\prod_1 = \left(\frac{\rho g r_0^3}{\mu(j - j_m) r_0} \right) = \frac{Gravitational\ Force}{Viscous\ Force} = \left(\frac{\mathrm{Re}}{Fr} \right) \tag{61}$$

$$\prod_2 = \left(\frac{\mu(j - j_m) r_0}{\sigma r_0} \right) \times \left(\frac{H\infty}{r_0} \right) = Ca \left(\frac{H\infty}{r_0} \right) \tag{62}$$

where (Re), (Fr) and (Ca) are Reynolds, Froude and Capillary numbers respectively, defined as:

$$\mathrm{Re} = \left(\frac{\rho(j - j_m) r}{\mu} \right) \tag{63}$$

$$Fr = \left(\frac{(j - j_m)^2}{gr} \right) \tag{64}$$

$$Ca = \left(\frac{\mu(j - j_m)}{\sigma} \right) \tag{65}$$

where (ρ) is the density of the liquid, (j) is the superficial gas velocity, (j_m) is the minimum superficial gas velocity required for foaming, (μ) is the viscosity, (σ) is the surface energy, (r) is the average bubble radius at the bottom of the foam layer, and (g) is specific gravity. The Reynolds number represents the ratio of the inertial and viscous forces; the Capillary number is the ratio of the inertial and the gravitational forces acting on the bubbles (Pilon et al. 2001).

The superficial gas velocity for the onset of foaming (j_m) is determined by assuming a linear relationship between the steady state foam thickness (H_∞) and the gas flux (j). Then it can be written $H_\infty = a(j - j_m)$ as shown in Figure 6 (Pilon et al. 2001).

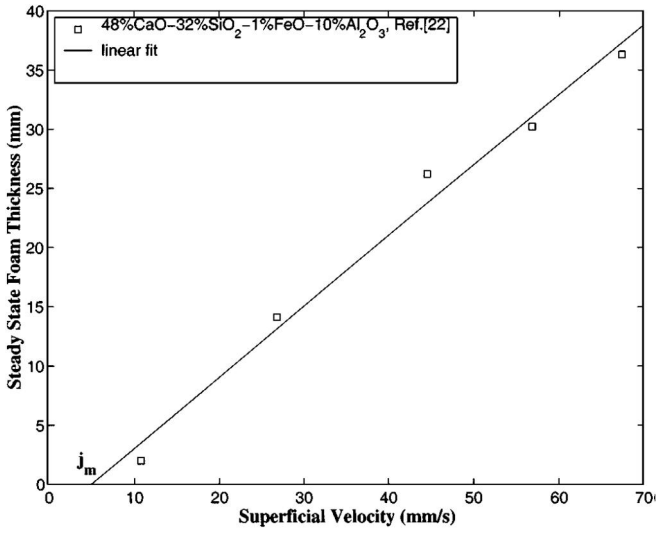

Figure 6. Steady state foam thickness vs. superficial argon velocity (Pilon et al. 2001).

The relationship between (Π_1) and (Π_2) is assumed to follow a power law (Pilon 2001):

$$Ca\left(\frac{H\infty}{r_0}\right) = K\left(\frac{\mathrm{Re}}{Fr}\right)^n \tag{66}$$

where (K) and (n) are constant parameters from experimental data. Then, an expression for the steady state foam thickness $\left(H_\infty\right)$ can be defined. The choice of power law to relate the dimensionless numbers is arbitrary. It presents the advantages of capturing a wide variety of possible functional relationships between $\prod_1 = \left[\mathrm{Re}/\,Fr\right]$ and $\prod_2 \left[= Ca\left(H_\infty / r_0\right)\right]$. Figure 7 shows the relationship between the dimensionless parameters (Π_1) and (Π_2) (Pilon et al. 2001).

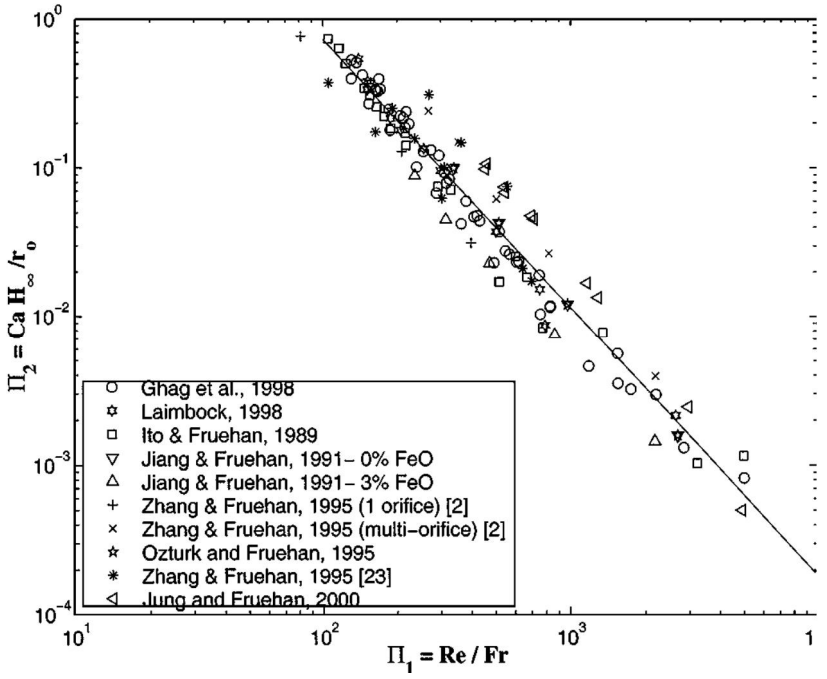

Figure 7. Correlation of dimensionless numbers (Π_1) vs. (Π_2) (Pilon et al. 2001).

As per the experimental data on steady state foam thickness for low-viscosity fluids, Eq. (67) can be presented between two dimensionless numbers (Pilon et al. 2001):

$$\left(\frac{H\infty}{r_0}\right) = \frac{2905}{Ca}\left(\frac{\mathrm{Re}}{Fr}\right)^{1.8} \tag{67}$$

The final correlation is obtained by assuming a power law relationship, whose empirical constants were found from a wide variety of experimental data for high viscosity fluids:

$$H_\infty = 2905\left(\frac{\sigma\left[\mu\left(j - j_m\right)\right]^{0.8}}{\left(\rho\sigma\right)^{1.8} r^{2.6}}\right) \tag{68}$$

From Eqs. (67) and (68) it is possible to conclude that the steady state foam thickness $\left(H_\infty\right)$ appears to be proportional to $\left(j - j_m\right)^{0.80}$, confirming the assumption made in determining the minimum superficial gas velocity for foaming (j_m), i.e. $H_\infty \alpha \left(j - j_m\right)$.

The velocity (j_m) should be determined iteratively in general, but this is not judged necessary due to the proximity of the exponent 0.8 to unity due to the

experimental uncertainty on both thermophysical properties and the experimental conditions. Then (j_m) in Eq. (68) is obtained by assuming a linear relationship between $\left(H_\infty\right)$ and $\left(j - j_m\right)$.

In addition, the steady state foam thickness increases with an increase in the superficial gas velocity (j). As the viscosity of the liquid phase increases, the drainage rate is reduced, the lamellae become thicker and more stable along with the foam thickness increase. In contrast, the gravity and an increase in the liquid density (ρ) cause the foam to drain faster and to reduce its steady state thickness (Pilon et al. 2001).

Eq. (68) is valid for foams formed from high viscosity liquid bubbles with nitrogen, air or argon gas injected though single-orifice or multi-orifice nozzles or a porous medium. The accuracy of this semi-empirical correlation and experimental data yields a 35% error margin. In addition, predictions are very sensitive to the average bubble radius (Pilon et al. 2001).

7.10.2 Role of surface energy

The effect of surface energy seems to be in contradiction with intuitive consideration since it has been discovered that an increase in the surface energy tends to reduce the steady state foam thickness. This can be interpreted based on the fact that a decrease in the surface energy reduces the interfacial energy. Similarly, this increases foam stability and the steady state foam thickness. The contradiction is evident if we assumed that the surface energy and the average bubble radius are independent. However, in reality they are not. When considering the effect of the surface energy on the foam thickness as presented in Eq. (68), the effect of the bubble radius has to be accounted for as well. Then the ratio $\sigma / r_0^{2.6}$ represents the effect of surface energy. According to the Young-Laplace equation, the bubble radius is proportional to the surface energy, when the pressure in the bubble is assumed to be constant and equal to the pressure of injection. Due to this, Eq. (68) suggests that if the surface energy decreases, the bubble radius decreases by the same order and the ratio $\sigma / r_0^{2.6}$ increases. Thus, according to Eq. (67), the foam index increases as the surface energy decreases in agreement with experimental observations (Pilon et al. 2001).

7.11 Physical modelling of slag foaming for various operating conditions

Lotun and Pilon (2005) have developed a correlation to slag foaming by using the Buckingham Pi theorem with variables commonly used in previous studies on slag foaming.

The Buckingham pi theory is a widely applied dimensional analysis tool to obtain correlations between foaminess and liquid properties. However, there is no systematic rule to which variables should be chosen as repeating variables. Dimensional analysis may not always lead to a physically sound set of dimensionless numbers so that field equations and boundary condition can be provided (Lotun and Pilon 2005).

The two dimensionless numbers from Pilon's et al. (2001) study on foam thickness can be expressed as a function of the four dimensionless numbers derived from the Buckingham pi theorem. The empirical coefficients were obtained from experimental data for foams made of various fluids with different chemico-physical properties. The predictions of the correlations compares well with the experimental data for high viscosity liquids (Lotun and Pilon 2005).

The concept of foaminess is disregarded as an idealisation since it is not supported by experimental evidence. However, the Buckingham Pi theorem is applied to basic variables describing the foam and its constituents. It also addresses the apparent contradiction due to the presence of the surface energy in the numerator (Lotun and Pilon 2005).

The steady state foam thickness (H), depends on six variables: the liquid viscosity (μ), surface energy (σ) , the average bubble radius (r), the liquid density(ρ), specific gravity (g) and reduced superficial gas velocity($j_r = j-j_m$). The Buckingham Pi theory is applied to those variables by disregarding foaminess. The seven variables consist of a combination of three basic physical dimensions for length [L], mass [M] and time [T]. According to the theorem, a function relating to these seven variables can be expressed in terms of four dimensionless parameters (Lotun and Pilon 2005):

$$\prod_1 = \frac{H}{r} \tag{69}$$

$$\prod_2 = \frac{\sigma}{j_r \mu} = \frac{1}{Ca} \tag{70}$$

$$\prod_3 = \frac{gr}{j_r^2} = \frac{1}{Fr} \tag{71}$$

$$\prod_4 = \frac{\sigma r j_r}{\mu} = \mathrm{Re} \tag{72}$$

where (Π_2) and (Π_3) are the reciprocals of the Capillary and Froude numbers, while (Π_4) is the Reynolds numbers defined in Eq. (63). The solutions for the set of dimensionless numbers has the form (H/r) = g(Ca,Re,Fr), respectively. Assuming the power law relationship it can be assumed that (Lotun and Pilon 2005):

$$\left(\frac{H}{r}\right) = kCa^{\alpha}\,\mathrm{Re}^{\beta}\,Fr^{\gamma} \tag{73}$$

The constant (k) and the exponents (α) and (β) were obtained from the experimental data. The final expression can therefore be expressed in terms of the dimensionless numbers as in Eq. (74), or the chemico-physical properties as in Eq. (75) (Lotun and Pilon 2005):

$$\left(\frac{H}{r}\right) = 2617\,Ca^{-1.01}\,\mathrm{Re}^{-1.74}\,Fr^{1.77} \tag{74}$$

$$\left(\frac{H}{r}\right) = 2617\,\frac{\mu^{0.79}\,j_r^{0.79}\,\sigma^{1.01}}{\rho^{1.74}\,g^{1.77}\,r^{3.51}} \tag{75}$$

The foam thickness equation and experimental results have a good agreement, but the presence of surface energy in the numerator instead of the denominator seems to contradict intuition based on the thermodynamic principle. To address this, the dependence of the bubble radius on the chemico-physical properties of the system and particularly the surface energy should be discussed along with the physical mechanism responsible for bubble formation. The bubble radius forming the foam depends on numerous factors such as the method by which the bubbles are formed and the chemico-physical properties of the foaming liquid (Lotun and Pilon 2005).

The dependence of the bubble radius on the ratio of density and surface energy can be described by the average bubble size equation $\left(\sigma / \rho\right)^{0.5}$. In the variation of the average bubble radius with surface energy, if the surface energy is in the denominator, it can be seen that an increase in surface energy decreases foam thickness. Therefore, the predictions from the correlations do not contradict the fact that foam stability increases with decreasing surface energy. However, the bubble radius cannot be written solely in terms of the liquid properties since it is also dictated by the formation mechanism (Lotun and Pilon 2005).

8. Experimental foaming studies in the industry

8.1 Foaming slag practice in electric stainless steelmaking

Görnerup and Jacobsson (1998) have studied the potential of slag foaming practice on an industrial scale during full-scale experiments in the Avesta Sheffield UHP-AC-Electric Arc Furnace. The effect of FeO addition on slag was particularly studied in the experiments. The experiments were divided to two groups according to the Cr_2O_3 content in the slag.

The experimental work consisted of raw material charging with balanced input, slag formers, oxygen injection, and coal injection in conjunction with oxygen injection. Mill scale (FeO > 98.5%) injection is performed initially; nitrogen injection is used for stirring. Sampling is made as a function of process time.

The foaming level of the slag is graded according to a foaming scale. The reported value is estimated after visual inspection. The sound of the furnace is a good indicator of the slag foaming. The noise level is observed to be reduced strongly by foamy slag covering the arcs. The foaming of slag is graded from 1 to 5 according to Table 2. If the foaming changed during the experiment, the heat is given two grades (Görnerup and Jacobsson 1998).

Table 2. Foaming grades in the experimental trials (Görnerup and Jacobsson 1998).

Grade	Visual impression
1	No foam, arcs fully visible
3	Foam, arcs partially covered with slag; electrode tips partially visible
5	Severe foam; lower parts of the electrodes fully covered by foam
Grade	**Audial impression**
1	Loud noise with clear sound of the striking arcs
3	Reduced noise level; noise peaks of striking arcs partly damped
5	Very low noise level: noise peaks of striking arcs fully damped

8.2 Observation of foaming EAF slags in the production of stainless steel

Vidacak et al. (2002) have studied the foaming of EAF slags with high and low Cr_2O_3 content in the production of stainless steel. The experiments were carried out using the EAF process at AB Sandvik Steel's plant. In the definition of foaming characteristics, a mathematical KTH model was used to define the viscosities of multi-component slags in the temperature range 1773–1923 K. The predicted foaming behaviour is then compared to estimations of foaming determined visually and acoustically by operators.

The foaming degree can be estimated visually by the operators or sound measurements. Fast Fourier Transform (FFT) analysis of the generated sound is conducted in order to find the frequencies that were sensitive to the foam amount. The sound intensity is attenuated by the foam and by using a microphone, amplifier and digital signal-processing hardware, and the foam height can be determined from just the sound signals. MatLab software is used to read and analyse data files. During the sound sampling, the operators also estimated the foam level based on what they can hear from the process during arching. The time and foam level were noted and later compared with sound analysis. Slag and steel samples were taken manually from the vessel after tapping the EAF. The slag samples were analysed by X-ray spectrometer (Vidacak et al. 2002).

The foaming index was predicted by using Eq. (76):

$$\sum = K_{Slag}\left(\frac{\mu}{\sqrt{\rho\sigma}}\right) \tag{76}$$

where (K_{Slag}) is empirical constant, (μ) is viscosity, (ρ) is density and (σ) is surface energy.

The density and surface energy of slags were defined as the average values on the molar composition of the oxide components according to the literature data (Vidacak et al. 2002).

8.3 Online control of the foamy slag in EAF process

Marique et al. (1999) have developed a control method of the slag foaming operation based on noise emitted by EAF vessel. The method was first implemented at the Hoogovens-UGB steelshop (DC single vessel furnace).

In the EAF plant procedure, the material is charged in two buckets along with carbon and oxygen injection and argon gas bubbling. The foaming starts soon after the charging of the second bucket.

In the first stage with oxygen injection, the FeO level in the slag increases and renders it more fluid. The foam can already appear during the first stage when the injected oxygen reacts with carbon present in metal.

In the second-phase, the carbon and oxygen are injected simultaneously into the furnace in order to achieve a high foamy slag level. The gains in the electric energy consumption and on the steel nitrogen content can be achieved by the optimisation of the foaming formation.

Nowadays, according to Marique et al. (1999) the slag height and the foam formation is estimated in most installations by subjective acoustic and visual means of the surface operator, the operating practices being either rigidly pre-established or left to the free interpretation of the furnace operators.

8.3.1 Experimental procedure

In the characterisation of the theoretical foaminess of slags a use has been made of the foaming model proposed by Ito and Fruehan (1987):

$$\sum = 1.15 \times 10^2 \frac{\mu}{\sqrt{g\sigma\rho}} \tag{77}$$

where (μ) is slag viscosity [Pas], (ρ) is slag density [kg/m^3], (σ) is surface energy [N/m] and (g) is the gravity [m/s^2].

8.3.2 Sonicmeter equipment

According to Marique et al. (1999), the sonicmeter also provides a means for better positioning of the consumable lances and for a reduction of the splashing and skull problems.

The correlation between sonicmetric signals and the volume and quality of the foaming slag present in the vessel makes online guidance of the carbon and oxygen injection possible.

The analysis of the signals has been performed with the FFT method. The foaming slag signal is possible to maintain at predefined optimum levels during the refining period by correctly modulating the carbon injection.

The sound information on slag foaming has been complemented by a further treatment of the signal in the frequency range 1000–10000 Hz in order to derive an indication on the position of the oxygen lance and its immersion in the slag.

8.4 The additions to generate foam in stainless steelmaking

Kerr and Fruehan (2004), using the constant volume pressure increasing (CVPI) technique, have experimentally studied the capability of slag additives to generate gas at sufficient rates. The master slag composition is 12wt%MgO-42.4wt%CaO-42.5wt%SiO_2-3wt%Al_2O_3. The study focused on the ability of WOB material (oxide briquettes), limestone, hydrated calcium nitrate, NiO or carbon additions to provide significant foaming.

The foam index for stainless steelmaking slag is found to be similar to foaming carbon steelmaking slag, which foam adequately. The most likely cause for poor foaming is assumed to be low gas generation during the injection of carbon into EAF. Due to this, the slag additives capable of generating gas at sufficient rates induce foaming (Kerr and Fruehan 2004).

The CVPI technique measures the rate at which gas is generated as a result of the additives. The basic principle of CVPI is to measure the pressure increase due to the generation of gas in a closed system and relate it to the moles of gas generated.

The subsequent pressure increase in the furnace tube is measured with a pressure transducer. The data collected by the pressure transducer generated a calibration curve that converted the change in pressure to the moles of gas. Finally, argon gas injected during calibration is vented and the experiment commences when a graphite disc is lowered and submerged completely into the slag. This phase of experiment is completed when the measured pressure approaches the maximum calibration pressure by raising the graphite disc from the slag. The mass spectrometer is used to provide insight into identifying the product gases resulting from additions (Kerr and Fruehan 2004).

9. Modelling studies

9.1 Behaviour of slag foaming with reduction of iron oxide in molten slags by graphite

Hong et al. (1998) have experimentally studied at 1573 K the conditions of iron oxide reduction by graphite in CaO-Li_2O-SiO_2-Al_2O_3-slag systems under argon or CO-gas atmosphere with a flow rate 1000 Ncm^3/min. The main focus of the study is a slag foaming phenomena originating from the gas forming chemical reaction between FeO in molten slag and graphite. The immersed graphite rod is used to study the slag foaming behaviour caused by chemical reaction.

The experiments were carried out in a curved alumina tube, with the initial FeO content in the slag at 3–15%. The sulphur is added as CaS to the slag system. The sulphur content is maximum 0.68%.

The slag foaming is affected by the CO-gas evolution rate. When the CO-gas evolution rate is less than a critical value the slag is not foamed. An increase in the CO-gas evolution rate leads the slag foaming to become rigorous. The addition of sulphur suppresses the slag foaming and SiO_2 addition favours slag foaming to a lesser extent.

The FeO content of the slag sample is determined by the EDTA-titration method and slag height is defined by measuring the slag length attached to the rod. A simple fluid mechanics model, drift-flux analysis, is used to fit the experimental results.

9.1.1 Determination of gas evolution rate

In the experimental work, CO-gas is generated by a reduction of iron oxide in molten slag with solid carbon, according to Eq. (78) (Hong et al. 1998):

$$FeO(slag) + C(s) = Fe(l) + CO(g) \tag{78}$$

The reaction between iron oxide in molten slag and graphite follows the first-order rate equation:

$$d(\%FeO)/dt = -r_A \times (\%FeO) \tag{79}$$

where the term (r_A) is apparent reaction rate [1/s] and t is time [s].

The gas evolution rate is determined from the change in iron oxide content of molten slag over time. The rate of CO-gas follows the first-order rate equation (Hong et al. 1998):

$$Q_{CO} = (RT/P)(\%FeO)_0 W_S k_A \exp(-k_A t)/(100 M_{FeO}) \tag{80}$$

Then the average gas evolution rate can be expressed:

$$\overline{Q}_{CO} = (RT/P)(\%FeO)_0 W_S \{1-\exp(-k_A t)\}/(100 M_{FeO}) \tag{81}$$

where (Q_{CO}) is the CO-gas evolution rate at time t [cm^3/s], $(\overline{Q}_{CO})$ is the average CO-gas evolution rate from time 0 to t [cm^3/s], (%FeO) is the initial iron oxide content in slag [mass%], (W_S) is the mass of molten iron oxide [g/mol], (T) is temperature [K], (P) is pressure [MPa] and (R) is gas constant [J/molK].

9.1.2 Evaluation of the slag foaming

Instead of slag foaming parameters, foam height and foam life, the slag foaming is evaluated by gas holdup, (ε), namely volume fraction of gas in the foaming slag (Hong et al.1998):

$$\varepsilon = V_g / V_s = 1 - V_0 / V_S = 1 - h_0 / h \tag{82}$$

where (V_g) is the volume of gas [cm^3], (V_S) is the apparent volume of foaming slag [cm^3], (V_0) is the volume of dense slag before foaming [cm^3], (h_0) is the height of dense slag before foaming [cm], and (h) is the height of foaming slag [cm].

The average value of form time 0 to (t) is given as:

$$\overline{\varepsilon} = (1 - h_0 / \overline{h}) \tag{83}$$

where $(\overline{h})$ [cm] is the average foaming slag height for time 0 to (t). The average values of gas forming rate and gas holdup from 60 to 300 s are used to evaluate the slag foaming behaviour.

9.1.3 Drift-flux analysis

A two-phase flow model, the drift-flux analysis, is used in the analysis of gas-liquid flow systems, where a considerable relative velocity exists between the two phases. The analysis can be used to correlate the experimental results (Hong et al. 1998).

In the gas-slag system, (υ) represents the phase velocity, the symbol (j) [flux, cm/s] is used to represent the volumetric flux of the volumetric flow rate per unit area, and flux is related to the local gas holdup (ε), and the velocity (Hong et al. 1998):

$$j_g = \varepsilon \upsilon_g \tag{84}$$

$$j_s = (1-\varepsilon)\upsilon_g \tag{85}$$

$$j \equiv \left(j_g + j_s\right) \tag{86}$$

where the subscripts (g) and (s) represent the gas and the slag phase, respectively. The drift flux represents the volumetric flux of phase relative to the average mixture velocity (j):

$$j_{gs} = \varepsilon\left(\upsilon_g - j\right) \tag{87}$$

$$j_{sg} = (1-\varepsilon)\left(\upsilon_s - j\right) \tag{88}$$

A distribution parameter (α) can be defined:

$$\alpha = \langle \varepsilon j \rangle / \left(\langle \varepsilon \rangle \langle j \rangle\right) \tag{89}$$

where $\langle\ \rangle$ marks the average over the cross-section. The parameter represents the effect of radially non-uniform flow varying from 1 to 1.5 depending on the profile of the system.

Averaging term by term, the above equations (84) and (89) can be presented:

$$\left\langle j_g \right\rangle = \left\langle \varepsilon \upsilon_g \right\rangle \tag{90}$$

$$\left\langle j_{gs} \right\rangle = \left\langle \varepsilon\left(\upsilon_g - j\right) \right\rangle \tag{91}$$

Combining the equation with (α), it can be presented:

$$\left\langle j_g \right\rangle / \langle \varepsilon \rangle = \alpha \langle j \rangle + \left(\left\langle j_{gs} \right\rangle / \langle \varepsilon \rangle\right) \tag{92}$$

In terms of the volumetric flow rates the following Eqs. (86–88) are valid:

$$\langle j \rangle = \left(Q_g + Q_s\right)/\left(A_c\right) \tag{93}$$

$$\left\langle j_g \right\rangle = \left(Q_g\right)/\left(A_c\right) \tag{94}$$

$$\left\langle j_s \right\rangle = \left(Q_s\right)/\left(A_c\right) \tag{95}$$

where (A_c) is the cross-sectional area of crucible.

9.1.4 Steady state foaming

In a steady foaming state, the net slag flow in the system is zero (Q_S = 0), and then the foaming can be shown (Hong et al. 1998):

$$Q_g / \langle \varepsilon \rangle = \alpha Q_g + \langle j_{gs} \rangle A_c / \langle \varepsilon \rangle \tag{96}$$

The drift flux, $Q_d \left(= \langle j_{gs} \rangle A_c / \langle \varepsilon \rangle \right)$ is correlated to the physical properties of the slag. On the basis of simple analytical consideration, (Q_d) for the particular steam-water flow system can be expressed (Hong et al. 1998):

$$Q_d = A_p \left(\frac{\sigma \rho \Delta \rho}{\rho_L^2} \right)^{1/4} \tag{97}$$

where (A_p) is the system parameter, (σ) is the surface energy of slag, (g) is the acceleration of gravity, (Δρ) is the density difference between slag and gas, and (ρ_l) is the density of slag.

Drift-flux analysis is applied to the average gas holdup obtained in the experimental study. When the CO-gas evolution rate is smaller than the critical value (ε = 0), ($Q_{CO,c}$), which is characteristic of the slag system. This is due to the coalescence of small bubbles at the surface of the graphite rod and bubbles can escape along the graphite rod surface to the atmosphere directly without dispersing into the slag phase. In this case, no slag foaming can be observed. The effective gas flow rate for slag foaming can be expressed (Hong et al. 1998):

$$\overline{Q}_{CO,e} = \overline{Q}_{CO} - Q_{CO,c} \tag{98}$$

($Q_{CO,c}$) has specific values for every slag composition [cm^3/s]. The linear drift correlation in Eq. (99) provides a good correlation for the experimental data at the steady foaming state. (Q_s) is not zero for the unsteady slag foaming and it is possible to evaluate a value for it:

$$\left(Q_{S,t_n} \right) = \left(1 - \varepsilon_{t_n} \right) \frac{\left(V_{s,t_n+1} - V_{s,t_n-1} \right)}{t_{n+1} - t_{n-1}} \tag{99}$$

where the subscript (t_i) refers to a value at a given time.

The drift analysis can be applied to the average gas holdup data obtained experimentally in earlier studies. When (ε) is zero, the evolution rate of CO-gas has a smaller value than a critical value, ($Q_{CO,\,cr}$), which is characteristic of the slag system. This is due to the coalescence of small bubbles at the surface (Hong et al. 1998).

9.2 Thermodynamic model of the EAF process for stainless steel

Arnout et al. (2006) have developed a time-dependent thermochemical model for the EAF process for stainless steel production. Time dependency is implemented by a stepwise input of energy and matter into the equilibrium reactor. The equilibrium calculations were performed using data from the Fact database and implemented using the ChemApp programming library. The input data for material and energy was taken from industrial data. The data is reconciliated and scaled though an efficiency factor. Data reconcialition is used to close mass balance in order not to disturb model results with mass balance errors. The model is applied to industrial data of the furnaces of Ugine & ALZ and simulation results were compared with typical heating practice.

9.2.1 Modelling

The model is implemented in Fortran and equilibrium calculations are performed with the commercially available ChemApp routine library. Databases for FactSage are used to generate free energy files for the used set of elements and phases. Tables 3-6 show the elements, formalism, input and output streams of the model, respectively.

Table 3. Elements of the calculation (Arnout et al. 2006).

Fe, C, Mn,Si, Al,Cr, Mo, Ni, Ca, Mg, O, F

Table 4. FactSage – Input model formalism (Arnout et al. 2006).

Solid Solution	Model	Gas	Model
Monoxide	QKTO	IDEAL	FACT
$(Ca,Mg)_2SiO_2$	QKTO		
Pure phase	MODEL		
All	FACT		

Table 5. FactSage – Input stream formalism (Arnout et al. 2006).

Steel	Solid	Alloying	Solid	Other	Solid	Other	Solid
Stainless	fcc	FeSi	fcc	Coke	Graphite	Dolomite	Pure oxide
Carbon	bcc	FeCr	fcc	Fluorspar	CaF_2	Calcia	Pure oxide
		FeNi	fcc	Oxygen	(O_2)-gas	Stone	Pure oxide

Table 6. FactSage – Output streams formalism (Arnout et al. 2006).

Steel	Slag	Gas
Liquid	Liquid	(CO)

9.2.2 Data reconcialition

Data reconciliation is used in correction of total masses of all streams by minimising the weighted sum of squares of the corrections. Then the optimisation problem can be formulated (Arnout et al. 2006):

$$\min_m \left(\sum_s \frac{\left(m_{tot,s} - \bar{m}_{tot,s}\right)^2}{\sigma_{tot,s}^2} + \sum_s \sum_{el} \frac{\left(c_{el,s} - \bar{c}_{el,s}\right)^2}{\sigma_{el,s}^2} \right) \tag{100}$$

$$s.t. \forall : \sum_{s(in)} m_{el,s} = \sum_{s(out)} m_{el,s} \tag{101}$$

$$\forall s : \sum_{el} m_{el,s} = m_{tot,s} \tag{102}$$

$$\sum_{el} \frac{\left(m_{el,s} \cdot n_{el}\right)}{M_{el}} = \frac{m_{O,s}}{M_O} \tag{103}$$

The objective function (100) weights the corrections of concentrations ($c_{el,s}$) of the elements (el) in the streams (s), and of total weights of streams ($m_{tot,s} \cdot c_{el,s}$), and ($m_{tot,s}$) are the corresponding measured values. The terms ($\sigma_{,tots}$) and ($\sigma_{el,s}$) are the weighting factors. The constraints (101) are mass balances. The total weight of a stream is equal to the sum of the elements (102), and the oxide streams are subject to stoichiometry constrains (103). Unknowns are the total masses ($m_{tot,s}$) of the streams (s) and the masses ($m_{el,s}$) of the elements (el) in the streams. With this approach, the constraints are linear (Arnout et al. 2006).

When the concentrations and total masses are unknown it can yield a least-square problem with non-linear constraints. In this approach the objective function is complicated, since the corrected concentrations in the objective function also have to be expressed as a function of the masses. A small number of terms have to add in the denominator to prevent division by zero. The reconciliation calculations were performed in Fortran using the DLCONF numerical optimisation routine from the IMSL library (Arnout et al. 2006).

9.2.3 Model

The electric arc furnace is modelled as a homogenous equilibrium reactor. Thus the temperature is the same throughout the entire content at every time step, and

the output of the previous step is the input. Most of the energy and mass addition, which are made in this step according to industrial data, are also added in the model. After every equilibrium calculation, the results are stored. Energy input is approximated as constant during every arc period. Energy loss approximations and efficiency factors are fitted to industrial data. The enthalpy difference is defined as remaining added energy. The output temperature is a result of every time step and the resulting phases are entered into the next step at this calculated temperature. The mass additions in the model were made at the measured time step at room temperature. The measured weights were reconciled before using them. The measured amount of oxygen is added in the model at the time of injection. The mass needed to close the oxygen balance is added as a constant flux during the heat. The equilibrium model energetically forms the most favourable phases. However, it is not possible to predict the behaviour of dust, since this is mechanically formed. The dust is not allowed in the reconciled output. With this approach, the mass is then distributed over steel and slag. The concentration of these phases cannot be affected since this can strongly raise the objective function and because the dust has a concentration similar to the average of steel and slag (Arnout et al. 2006).

9.3 Decarburisation and slag formation model for the electric arc furnace

Matsuura et al. (2008) have developed a decarburisation and slag formation model based on a mass balance and the kinetic equations for decarburisation and the reduction reaction between carbonaceous materials and iron oxide in slag. The model is applied to two-bucket charge operations in the EAF process. The dynamic metal and slag compositions were calculated as a function of time. The model calculates various melting patterns for scrap and pig iron. The variations of carbon content in the metal and iron oxide content in slag were also calculated. The model can be used to optimise oxygen injection, flux additions, carbon injection and yield as well as slag foaming.

9.3.1 Modelling

The model is applied to a two-bucket charge operation furnace and the charge of melt and slag compositions were defined based on the operational results. The model can predict iron yield and carbon loss with the discharged slag. The pig iron melting behaviour has a large role in determining the carbon content in the model. The decarburisation and slag formation model is based on a mass balance for each component in metal and slag phases. The rate equations are based on the decarburisation and the reduction of iron oxide in slag by injected carbonaceous materials. The complete optimisation of parameters needs many sources of heat, together with the proper optimisation tool such as a sequential quadratic programming SQP algorithm (Matsuura et al. 2008).

9.3.2 Oxidation of carbon and other elements by oxygen

The calculation algorithm consists mainly of melting of scrap and pig iron, along with the dissolution of impurities, oxidation of carbon, iron and other elements by injected oxygen, reduction of iron oxide by injected carbon materials, slag discharge or flushing and finally mass balance calculations. Melting and mass balance calculations have to be repeated until the end of the refining by the time step. In the model the injected oxygen oxidises the first elements (silicon, aluminium, manganese), which oxidise more easily than carbon and iron (Matsuura et al. 2008).

The decarburisation reaction proceeds as in oxygen steelmaking practice. The injected oxygen first reacts with iron to form FeO in slag. Then the carbon diffuses in the metal, reducing the FeO to metallic iron and producing CO-gas. With higher carbon contents, the driving force for mass transfer is sufficient to reduce all of the formed FeO. The rate of decarburisation is limited by the oxygen mass flow rate, whereas at lower carbon contents, the mass transfer rate decreases and not all of the FeO is reduced. Thus, the FeO content of the slag increases. Then the decarburisation is controlled by liquid phase mass transfer of carbon at lower carbon content (97) or by (98) oxygen gas flow rate at higher carbon content (Matsuura et al. 2008).

$$\frac{d[\%C]_t}{dt} = -\frac{kA\rho}{W_t^{Melt}}\left([\%C]_t - [\%C]_r^e\right) \tag{104}$$

$$\frac{d[\%C]_t}{dt} = -\frac{V_t^{Oxy} \times (1000/22.4) \times (2 - R_{PC}) \times 0.012}{W_t^{Melt}} \tag{105}$$

where k is the liquid phase mass transfer coefficient of carbon, A is the interfacial area where decarburisation occurs, ρ is the density of melt, W_t^{Melt} is the weight of metal phase at time t, $V_t^{Oxy}$is the oxygen gas injection rate at time t and R_{Pc} is the post-combustion ratio. The equilibrium carbon content is negligibly small compared to carbon content in melt – it is assumed to be zero. The changing point of rate mechanism is called the critical carbon content. The value of term kA is extrapolated from oxygen steelmaking operations by assuming the parameter is proportional to the oxygen flow rate. In the model, the CO-gas can be further oxidised to CO_2-gas by post-combustion. Due to the heterogeneous distribution of solid and liquid in an EAF process during melting, it is difficult to get a representative liquid metal sample during the first half of the oxygen injection period. When the carbon content decreases below the critical value, the oxidation reaction of iron becomes dominant and iron oxide is produced. It is absorbed by the slag phase. The reactions between decarburisation and iron oxide are completive and the proportion between those two reactions is determined by carbon content (Matsuura et al. 2008).

9.3.3 Reduction of FeO by injected carbonaceous material

During EAF steelmaking, coke and coal are injected into the slag to reduce iron oxide in slag phase to make the slag foam. The reduction rate of FeO is assumed to be controlled by mass transfer of FeO in the slag or chemical kinetics and the surface area of carbon is proportional to its weight in slag (Matsuura et al. 2008):

$$r_t^{red} = k_{red} W_t^{CM} \left(\frac{(\%FeO)_t}{100} \right) \tag{106}$$

where (k_{red}) is the reaction rate constant between carbon and iron oxide in the slag, (W) is the mass of carbon existing in slag at time (t). In the model, reduced iron return to metal phase and (k_{red}) is considered as a constant value throughout the refining time. The reaction rate constant (k_{red}) does not affect carbon content in metal considerably though FeO content changes. Decreasing the rate constant increases FeO content in slag, and FeO and carbon also increase at the same time (Matsuura et al. 2008).

9.3.4 Definition of FeO amount in the slag

The FeO amount in the slag is determined from oxygen injected minus any oxygen used in carbon burning, post-combustion and the oxidation of alloying elements. In the EAF, part of the oxygen reacts directly with the solid scrap, producing FeO. When the scrap melts, FeO on the scrap is transported to the slag phase. The calculated FeO content formed in the model is based on a mass balance in which the oxygen not used for carbon, CO-gas or elements in the metal oxidises iron. Therefore, the formation of FeO by the reaction of oxygen gas with scrap is accounted for. The formation of FeO by the reaction of oxygen with scrap is accounted for, though not explicitly calculated. In the model, the iron dust is neglected. This can result in a slightly lower actual yield (Matsuura et al. 2008).

9.3.5 Definition of mass balance

The mass balance definitions in metal and slag phases in the refractory dissolution is not taken into account. The dust losses are not considered in the calculation. In addition, the mass balance definitions are performed for each component of metal and slag phase. Post-combustion depends on the actual operations (Matsuura et al. 2008):

For the metal phase:

$$\left(W_t^{Melt}\right) = \left(W_t^{Fe} + W_t^{C} + W_t^{Mn} + W_t^{Si} + W_t^{Al}\right) \tag{107}$$

$$\left(W_{t+\Delta t}^{Melt}\right) = \left(W_t^{Fe} + \left(r_{1t}^{Pig} \cdot C_{Pig}^{Fe} + r_{1t}^{Scrap} \cdot C_{Scrap}^{Fe}\right) \cdot \Delta t - W_t^{Fe-Oxi} + W_t^{Fe-\mathrm{Re}\,d}\right) \tag{108}$$

For the slag phase:

$$\left(W_t^{Slag}\right) = \left(\Sigma W_t^{MeO_n}\right) \tag{109}$$

$$\left(C_{t+\Delta t}^{MeO_n}\right) = \left(\frac{W_{t'}^{MeO_n}}{W_{t'}^{Slag}}\right) \tag{110}$$

$$\left(W_{t+\Delta t}^{MeO_n}\right) = \left(W_{t'}^{slag} - r_{2t}^{Dis} \cdot \Delta t\right) \cdot \left(C_{t+\Delta t}^{MeO_n}\right) \tag{111}$$

where (W) refers to mass and (C) to mass fraction of a component, (t) to the current time and (Δt) to time increment. Reaction rates (r_1) and (r_2) are given in Eq. (112) and (113), respectively.

9.4 Slag foaming in an electric arc furnace

Matsuura and Fruehan (2009) have studied slag foaming in the high productivity North American electric arc furnace by using a mathematical model to compute the CO-gas generation rate and slag chemistry along with laboratory measurements of the foam index. Their aim is to understand and predict foaming in EAF steelmaking. In order to achieve this, the foaming characteristics of the slag must be known.

In the study, the rate of reaction was determined by measuring the volume of CO-gas generated as a function of time after adding the carbonaceous material. The resulting foam height is measured with an electrical probe. The foam index decreased from about 6–8 s at 15% FeO content to 2–4 s at 45% FeO content at 1773 K. The foam height appeared to be at a maximum at about 25% FeO content, despite the gas generation continuing to increase at higher contents. The foam height is limited by foam stability or from the amount of slag present (Matsuura and Fruehan 2009).

In EAF steelmaking, it has been found that at the end of the process, the foam becomes unstable and its height decreases. It is hypothesised that FeO content increases initially as CO-gas generation goes up, causing an increase in foaming. However as the FeO content increases the slag viscosity decreases and density increases causing the bubbles to drain more rapidly, to decrease and foam to decay. There is observed to be a critical FeO content below which foaming increases with FeO content and above which the foam is unstable. This is about 20–40% FeO, depending on other conditions. The foaming characteristics of the slag and the CO-gas generation rate have to be known. EAF steelmaking is complex when compared with oxygen steelmaking. Lime (CaO) and carbon are continuously injected and slag is flushed out of the furnace continuously and periodically (Matsuura and Fruehan 2009).

9.4.1 Methodology of model

The slag viscosities, densities and surface energies were computed using simple models in which the property is related to its molar composition. The foam index is used in the definition of potential foam height according to the correlation of Zhang and Fruehan (1995a). The extrapolation of the measured foam indexes to the EAF case is small and the estimated uncertainty is about 20%. The key factor – furnace temperature – varies between 1823–1953 K during the operation. The temperature is not calculated by the present EAF model. If the temperature is lower than 1823 K, the foam index and the computed foam height are higher. For example, at 1823 K they are about 25% higher. Otherwise, if the temperature is higher, the foam height is lower. Again, for example at 1923 K they are about 25% lower (Matsuura and Fruehan 2009).

The reaction rate r_1 in Eq. (108), which is the formation rate of CO-gas, is assumed to be proportional to the amount of carbon in slag (Matsuura and Fruehan 2009):

$$r_1 = \frac{k_1 W_C (\%FeO)}{100} \tag{112}$$

where (k_1) is the rate constant, term (W_C) is the mass of carbon in the slag defined from the EAF model.

The reaction rate r_2 in Eq. (109) is controlled by mass transfer of carbon in the metal:

$$r_2 = \frac{kA\rho}{100}\left[\%C - \%C^e\right] \tag{113}$$

Where (k), (A) and (ρ) are the mass transfer coefficient of carbon in the metal, the area of metal drops and the density of iron, respectively. (%C) and ($\%C^e$) are the carbon content and the carbon content in equilibrium with the slag. The CO-gas generation rate and the slag composition depend on the assumed melting rates of scrap and pig iron (Matsuura and Fruehan 2009).

10. Results of experimental foaming studies

10.1 Foaming of $CaO-SiO_2-FeO$ slags

Ito and Fruehan (1989a) have experimentally studied the effect of $CaO-SiO_2-FeO$ slag composition on foaming in iron and steelmaking processes. As described above in Section 7.1, argon gas was introduced into the molten slag to initiate the foaming process. Surface positioning was determined using an electric probe. The foam height was defined as the increment of the slag surface to the foaming surface. Mean bubble size was defined from the gas flow rate and the bubble formation frequency. The bubble formation frequency was determined by pressure transducer.

The foaming index was correlated to the retention or travelling time of the gas in the slag and the average foam life. Slag foaming increased with viscosity and decreased with surface energy. Suspended second-phase solid particles stabilised the foam and had a larger effect on foaming than changes in viscosity and surface energy for the slag studied (Ito and Fruehan 1989a).

10.1.1 Foaming index and foam life

The relation between foam height (h) and gas flow rate (Q_g) is shown in Figure 8 for different sizes of crucibles. The height foam increases with increasing gas flow rate. In the case of the same flow rate, the foam height is larger with smaller crucibles (Ito and Fruehan 1989a).

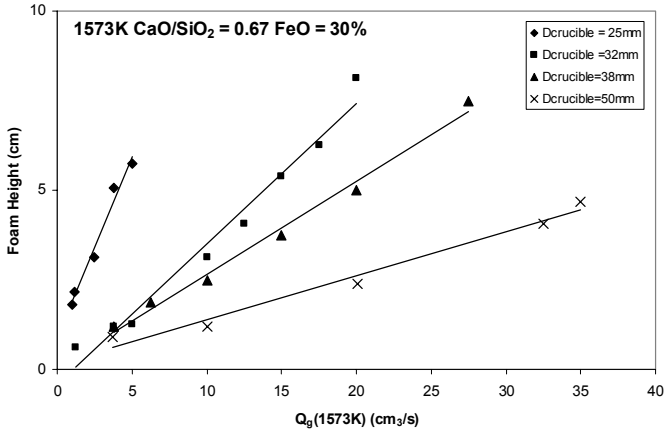

Figure 8. The relation between foam height and superficial gas flow rate for various crucible sizes (Ito and Fruehan 1989a).

Figure 9 shows the dependency of foam height (h) and the average gas travelling time in the foaming slag (Σ) on the superficial gas velocity. The foam height increases linearly with increasing $\left(V_g^s\right)$, and (Σ) becomes constant after a certain flow rate is reached. With larger crucible sizes, the results seem to be independent of the crucible diameter, since they increase at the rate that is a function of the superficial gas velocity. On the other hand, Figure 10 shows the relationship between time and $\left(-\ln\left(h/h^0\right)\right)$ in the results of foam life measurements.

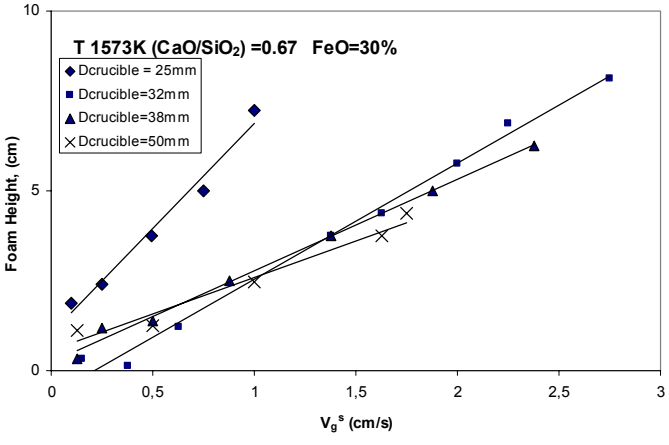

Figure 9. The relation between foam height and superficial gas velocity for various crucible sizes (Ito and Fruehan 1989a).

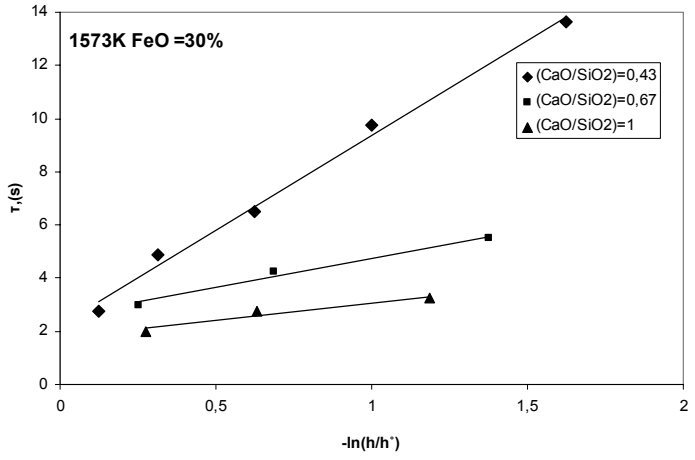

Figure 10. The relation between time and $\left(-\ln\left(h/h^0\right)\right)$ (Ito and Fruehan 1989a).

10.1.2 Effect of basicity

The foaming index and foam life for CaO-SiO_2-FeO slag as a function of basicity index in wt% CaO/(SiO_2 + Al_2O_3) at 1573 K is shown in Figure 11. Both (Σ) and (τ) decrease with increasing basicity. The high basicity slags have a higher surface energy (σ) and lower viscosity (μ), which destabilises the foam. In addition, Figure 11 shows that (Σ) and (τ) have approximately the same value in the case of ideal slag.

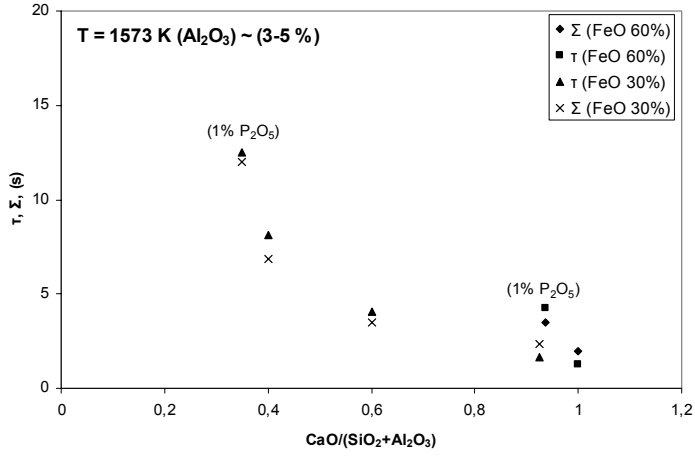

Figure 11. The change of foaming index (Σ) and foam life (τ) with basicity index (CaO/SiO_2) of the CaO-SiO_2-FeO slag (Ito and Fruehan 1989a).

According to the results of Skupien and Gaskell (2000), the foaming index decreased with increased basicity and temperature. The surface energy values were observed to increase and viscosity values decrease with the increase of basicity of SiO_2-FeO-CaO-slag. Figure 12 shows the variations of composition of the foaming index measured by (Ito and Fruehan 1989b) in Eq. (33).

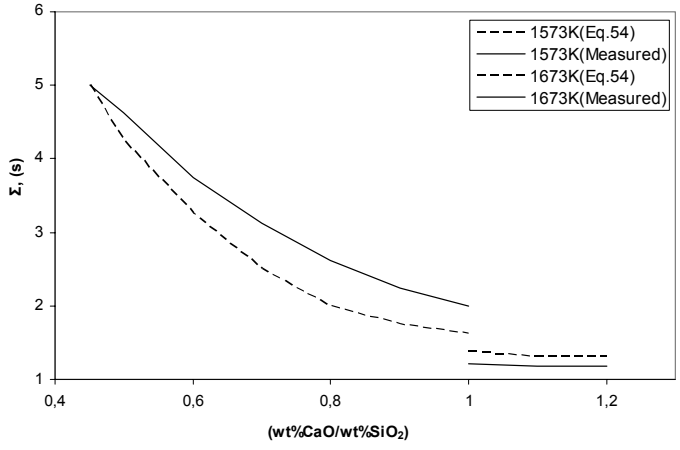

Figure 12. The variations with composition of the measured foaming indexes and the values defined from Eq. (55) (Skupien and Gaskell 2000).

10.1.3 Effect of second-phase particles

According to experimental observations, slag foaminess can be characterised by the average gas travelling time and average foam time. They are equal for an ideal gas (Ito and Fruehan 1989a).

Figure 13 shows the relationship between volumetric particle concentration and foaming. The term (Σ°) is the foaming index without second-phase particles. The value of term (Σ) increases with increasing particle concentration (Ito and Fruehan 1989a).

The foaming index as a function of slag basicity (wt%CaO/wt%SiO_2) is shown in Figure 14. The foaming index is observed to decrease with the basicity up to (1.20) at 1573 K and (1.22) (liquidus composition) at 1673 K. The surface energy increases and viscosity decreases with increasing CaO content. Therefore, low surface energy and high viscosity stabilises the slag foaming. The term (Σ) increases with the increasing basicity, when basicity is in excess of the liquidus composition. The solid particles, (SiO_2.CaO), precipitate at higher CaO contents and thus increase the foam stability. However, with greater basicity values it increases due to the presence of second-phase particles (CaO or $2SiO_2$.CaO), which have a large effect on foam stability (Ito and Fruehan 1989a).

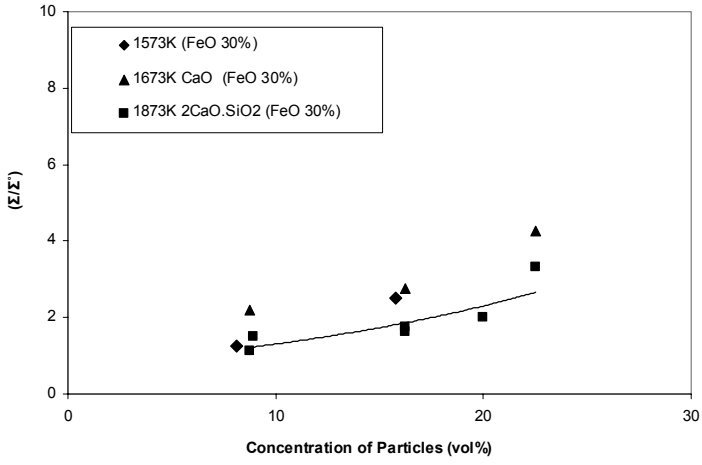

Figure 13. The relation between foaming index (Σ) and the basicity index for CaO-SiO_2-FeO slag (Ito and Fruehan 1989a).

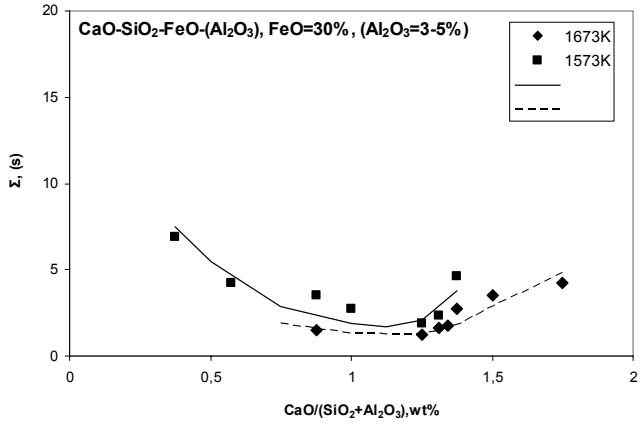

Figure 14. The effect of the second-phase particles such as CaO and 2CaO.SiO_2 on the foaming index (Ito and Fruehan 1989a).

10.1.4 Effect of surface-active components

Figure 15 shows the effect of the surface-active components, sulphur, P_2O_5, CaS and MgO on the foaming index. The term (Σ°) is the foam index for slag without the additives. The P_2O_5 addition slightly increases, whereas sulphur marginally decreases foaming index. CaF_2 decreases foam index (Σ) by lowering the viscosity

of the slag and increasing CaO solubility, whereas the MgO addition increases (Σ) by increasing the amount of solid particles in the slag (Ito and Fruehan 1989a).

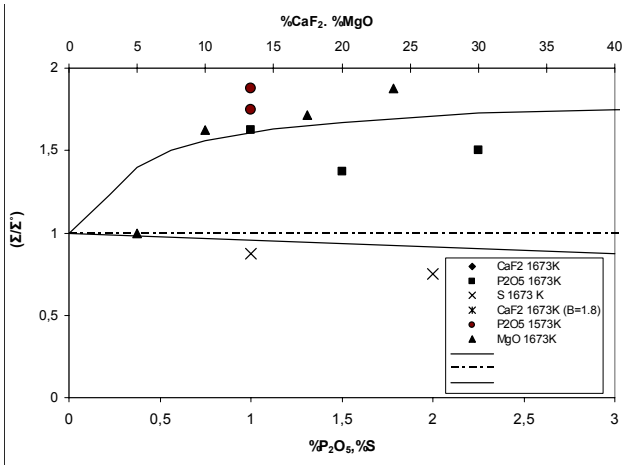

Figure 15. The effects of CaF, P_2O_5, S and MgO on the foaming index (Ito and Fruehan 1989a).

10.2 Effect of viscosity and surface energy on CaO-SiO_2-FeO and SiO_2-PbO slag foaming

The relation between the foaming index and the surface energy of the slag for the CaO-SiO_2 – FeO system is shown in Figure 16. The surface energy data is taken from Gunji and Dan (1974) and Kawai et al. (1976). The value of the logarithm of (Σ) varies approximately linearly and decreases with an increase in the logarithm of surface energy. When SiO_2 decreases surface energy and increases viscosity, the effect of the viscosity on the foaming index can be expected (Ito and Fruehan 1989b).

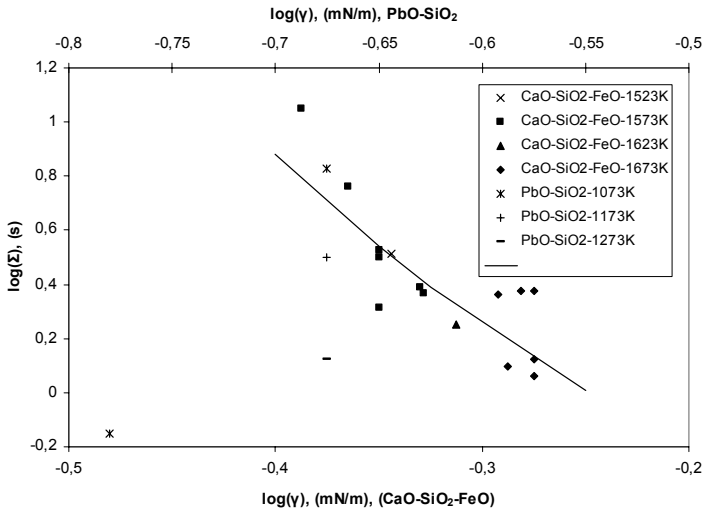

Figure 16. The relation between the foaming index and surface energy for CaO-SiO_2-FeO and PbO-SiO_2-slags (Ito and Fruehan 1989b).

It can be complicated to determine whether the increase in the foaming index with SiO_2 content is primarily due to the increase in viscosity or the increase in surface energy. Therefore, the measurements for slag foaming were made experimentally for the PbO-SiO_2 system at 1073 to 1273 K, since SiO_2 increases both surface energy and viscosity in this system. In this system, the foaming index does not depend on the surface energy, suggesting that in the CaO-SiO_2-FeO system, the change in the foaming index is due to the change in viscosity. Thus, the role of surface energy is smaller (Ito and Fruehan 1989b).

The relation between foaming index and slag viscosity in the CaO-SiO_2-FeO and PbO-SiO_2 system is shown in Figure 17. The foaming index increases with increasing viscosity in both systems. However, in the CaO-SiO_2-FeO system there is a lot of scatter in the relationship (Ito and Fruehan 1989b).

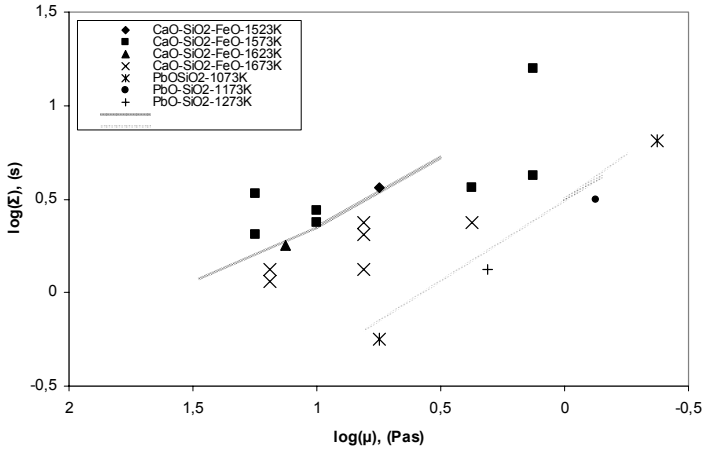

Figure 17. The relation between the foaming index and viscosity for CaO-SiO_2-FeO and PbO-SiO_2-slags (Ito and Fruehan 1989b).

However, the foaming index decreased with increased slag viscosity in both systems. It seems that the low surface energy enhances and stabilises the foaming, whereas the high viscosity prevents the drainage of liquid slag from the film between the bubbles (Ito and Fruehan 1989b).

Figure 18 shows the relation between two dimensionless numbers, (log N_1) and (log N_2) obtained by dimensional analysis for CaO-SiO_2-FeO-Al_2O_3 slags without solid particles. According to the dimensional analysis data, viscosity is the most important parameter in determining (Σ), compared with surface energy and density. The PbO-SiO_2 system has a similar linear relationship with the CaO-SiO_2-FeO system according to Figure 3. Due to the similarity of the measurement points and the difference between the constants, it can be expected that another dimensionless number – such as the Marangoni number – is needed for the complete dimensional analysis. It characterises the surface flow and may strongly depend on the slag system (Ito and Fruehan 1989b).

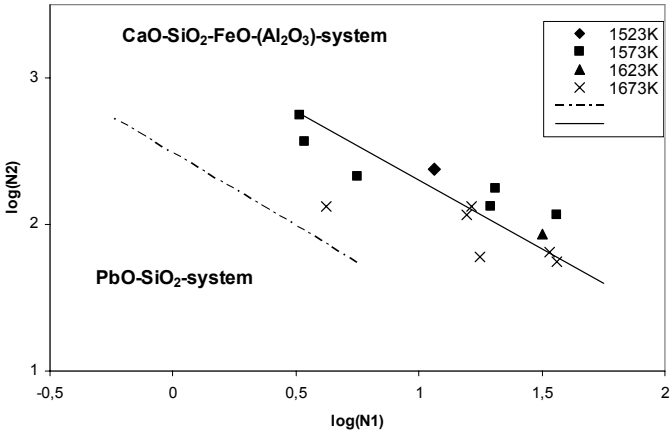

Figure 18. The results of the dimensional analysis (Ito and Fruehan 1989b).

10.2.1 Results of the foaming behaviour of melts in the system CaO-FeO-SiO_2

According to Skupien and Gaskell (2000), the foaming behaviour of silicate slags is defined by both surface energy and viscosity, and it seems that the viscosity has a greater role than surface energy. The isothermal addition of a small amount of surface-active solute has little influence on viscosity but causes a decrease in surface energy. The increased temperature of a melt of fixed composition is observed to decrease both viscosity and surface energy. This indicates that the influence of foam life on decreasing viscosity is greater than that of foam life increasing surface energy (Skupien and Gaskell 2000).

10.2.2 Results of steady state thickness of liquid–gas foams

Pilon et al. (2001) have developed a correlation to predict the thickness of isothermal foams produced by blowing gas in liquid solution under steady state conditions. The experimental data such as viscosity density, surface energy, gas superficial velocity and average bubble radius is derived from literature values. Their correlation is valid for foams formed from high viscosity liquids bubbled with nitrogen, air, helium, hydrogen and argon gas injected though single multi-orifice nozzles of porous medium. The correlation is sensitive to the average bubble radius. In the comparison with experimental data, the results of correlation showed relatively good agreement, about 35%. Figure 19 shows a comparison between steady state foam thicknesses obtained experimentally.

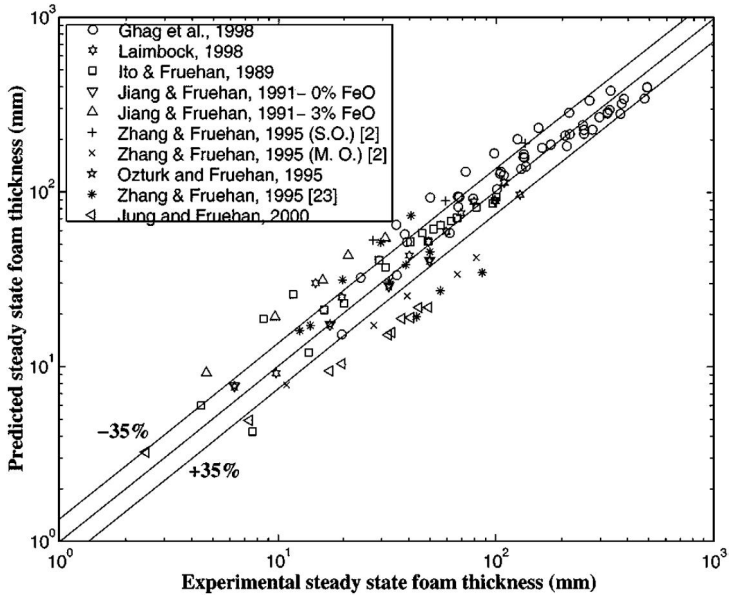

Figure 19. Comparison between experimental data and predictions of the steady state foam thickness. S.O. stands for single-orifice and M.O. for multiple orifice nozzle (Pilon et al. 2001).

10.3 Effect of FeO or NiO on slag foaming phenomena

10.3.1 Foaming height in the electric arc furnace

Ito and Fruehan (1989b) have defined the foaming height of an EAF slag with ($CaO/SiO_2 \approx 3$) at 1873 K as a function of FeO content using actual operating conditions as shown in Figure 20. The foam height increases linearly with increasing oxygen blowing rate. The foaming significantly increases with decreasing FeO content due to the lower viscosity and the greater amount of second-phase particles. The gas flow rate in EAF process is assumed to be controlled by the oxygen gas injection rate in Figure 20. In some foaming slag practices, coke is injected into the slag, which reacts with FeO to generate the foaming gas. Then the gas velocity is given by Eq. (115) (Ito and Fruehan 1989b).

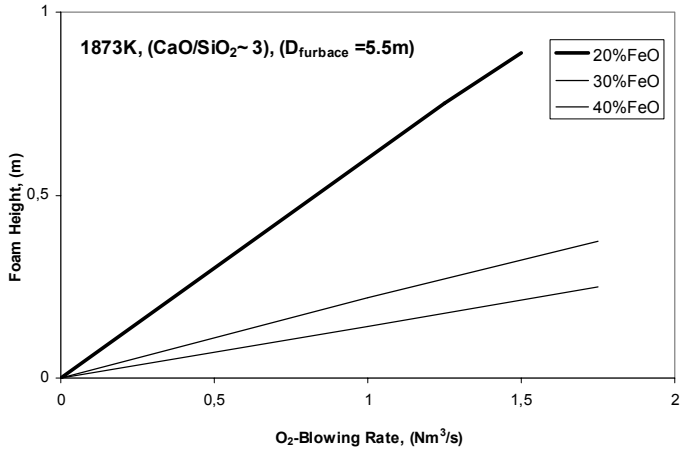

Figure 20. The foaming height of the slag for an EAF operation as a function of the oxygen injection rate (Ito and Fruehan 1989b).

Figure 21 shows the calculated foaming height in EAF for slag with (CaO/SiO_2 ~3) at 1873 K as a function of FeO content. The superficial gas velocity is obtained from Eq. (115) by using a reaction rate defined for graphite in Eq. (116) (Ito and Fruehan 1989b).

The reaction between FeO content in slag and solid coke (carbon) suspended in controls the gas velocity (Ito and Fruehan 1989b):

$$(FeO)_{slag} + C_{solid} = Fe(l) + CO(g) \tag{114}$$

$$V_g^s = \frac{TK_r A_s}{273 A_c} \tag{115}$$

$$K_r = 2.88 \exp\left(-\frac{39700}{RT}\right) a_{FeO} (mol - FeO/cm^2 s \tag{116}$$

where (T) is temperature, [K], (A_s) in the interfacial area between slag and solid carbon, (A_c) is the cross-sectional area of the vessel and (R) is the gas constant.

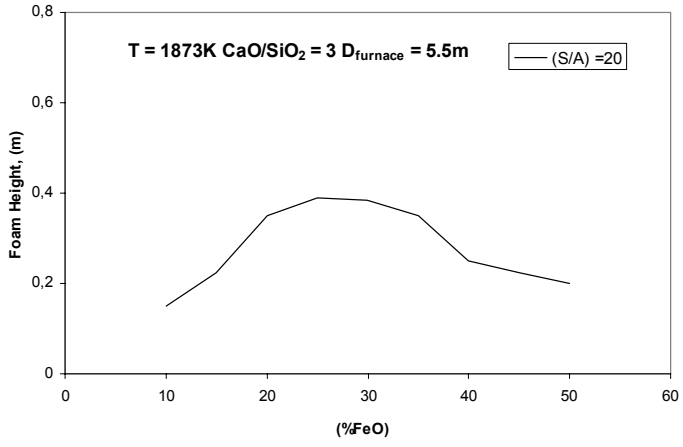

Figure 21. The foaming height of the slag during EAF -operation as a function of FeO content. The reduction of FeO is assumed to determine the gas velocity in the furnace (Ito and Fruehan 1989b).

The ratio of areas (S/A) is assumed to be 20. This corresponds the slag that contained 1 wt% of coke particles. The maximum foaming height is found when FeO content is 25 to 30%. The maximum foaming height is found to be with 25–30% FeO content in the slag. Then the higher FeO contents decrease the foaming by decreasing viscosity, but the higher FeO contents also increase the rate of gas generation. This has a larger effect on foam height (Ito and Fruehan 1989b).

10.3.2 Foaming index of bath smelting slag

Jiang and Fruehan (1991) have experimentally studied the foaming index on the bath smelting type of slags by measuring the foam height with different gas flow rates. It is expected that slag foaming in terms of the foaming index can be related to the slag's physical properties. Figure 22 shows the typical results.

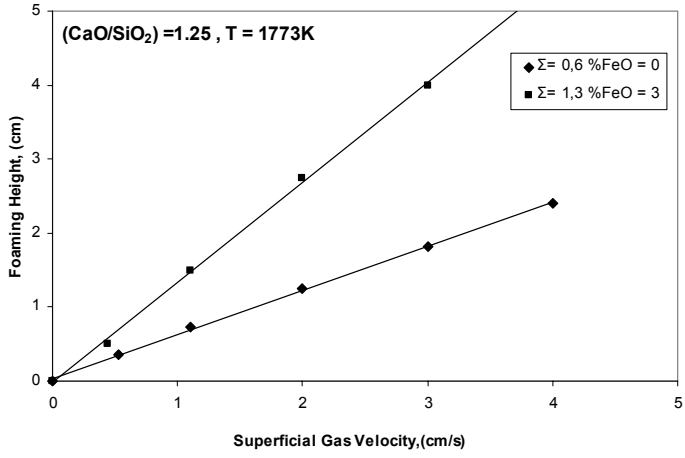

Figure 22. Foam height of $CaO\text{-}SiO_2$-FeO slag as a function of superficial gas velocity at 1773 K (Jiang and Fruehan 1991).

The foam stability decreases with increasing FeO content and basicity as shown in Figure 23. No stable foaming is observed with very low FeO contents. The maximum foam index occurred at 2 wt% FeO content. The higher foaming index observed for lower basicity slags (B~1) is due to their higher viscosities. The slag foaming is observed to increase with FeO content going to maximum and then it decreases (Jiang and Fruehan 1991).

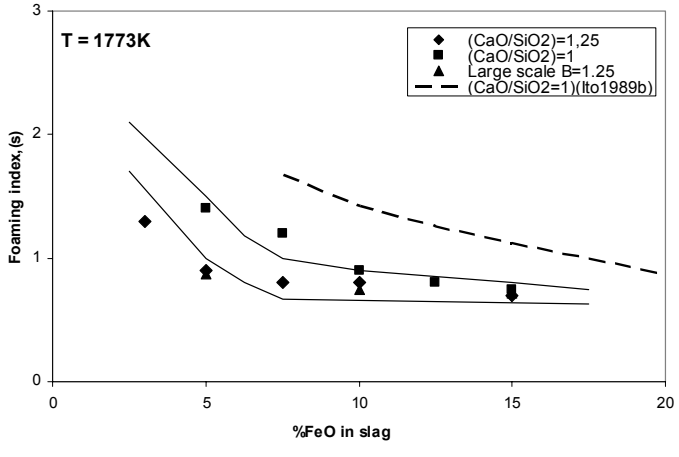

Figure 23. The foaming index for $CaO\text{-}SiO_2$-FeO slags at 1773 K (Jiang and Fruehan 1991).

A similar phenomenon is observed with $CaO\text{-}SiO_2$-NiO slags in respect of NiO. The foaming index reached a maximum value for this slag system at around 4% NiO as shown in Figure 24. From the experimental observations it is assumed that the $CaO\text{-}SiO_2$ slag do not foam without FeO or NiO in the slag. The slag is then too viscous to foam significantly. The slags with low FeO or NiO contents have a high melting point and viscosity and the bubbling gas channels through the slag. The maximum foaming index corresponds to the slag composition at which the slag has a critical viscosity, which allows foaming (Jiang and Fruehan 1991).

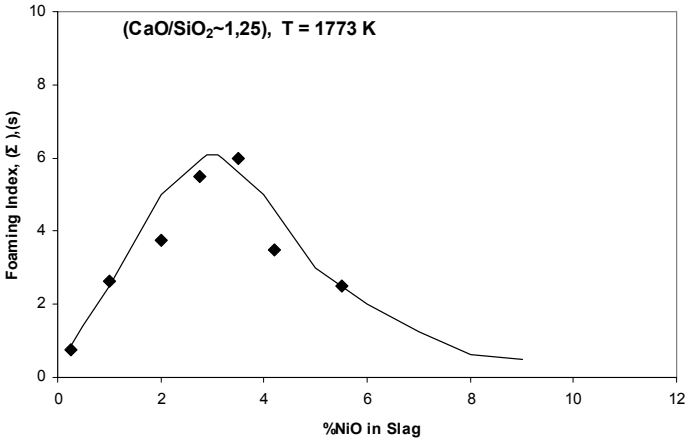

Figure 24. The foaming index of $CaO\text{-}SiO_2$-NiO slag as a function of %NiO at 1773 K (Jiang and Fruehan 1991).

10.4 Effect of the bubble size and chemical reactions on slag foaming

10.4.1 Foaming generated argon gas bubbling

Ito and Fruehan (1989a) measured bubble diameter as a function of argon gas flow rate at 1573 K as shown in Figure 25. The results are in good agreement with the line proposed by Sano and Mori (1977). The P_2O_5 addition decreases the bubble diameter since it decreases the surface energy of the slag. The line developed by Sano and Mori (1977) is used to determine the bubble diameter with high gas velocities (Ito and Fruehan 1989a).

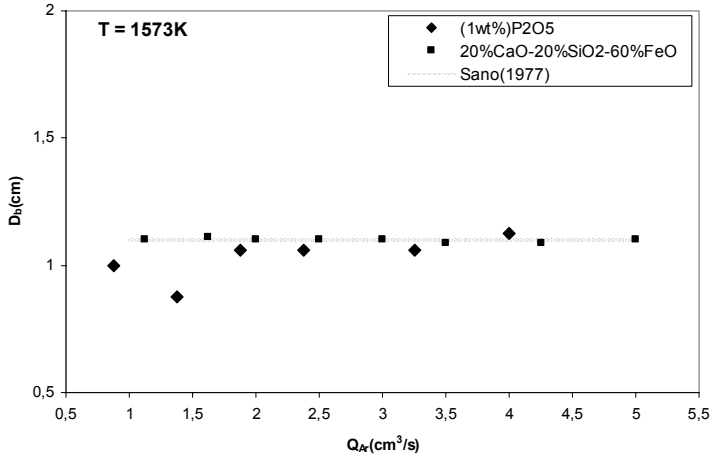

Figure 25. The relation between mean bubble diameter and gas flow rate at 1573 K (Ito and Fruehan 1989a).

Figure 26 shows the measured foam heights by Zhang and Fruehan (1995a) at different superficial gas velocities using a single-orifice and a multi-orifice nozzle, when slag contains 5% FeO. The foam height with multi-orifice nozzle increased by 70% with respect to the foam height measured using the single-orifice nozzle. These results agree with the results of Jiang and Fruehan (1991) and Zhang and Fruehan (1995a).

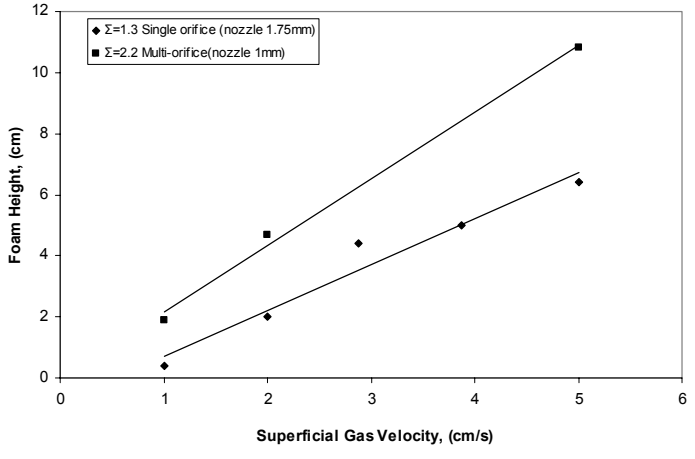

Figure 26. Measured foam height as a function of the superficial gas velocity for the single-orifice and multi-orifice nozzles (Zhang and Fruehan 1995a).

The distribution of the bubble sizes in the foams generated by both kinds of nozzles under the same conditions is shown in Figure 27. The average bubble diameter for a single-orifice nozzle is about 13.5 mm, whereas the foam generated by a multi-orifice nozzle is about 7.5 mm (Zhang and Fruehan 1995a).

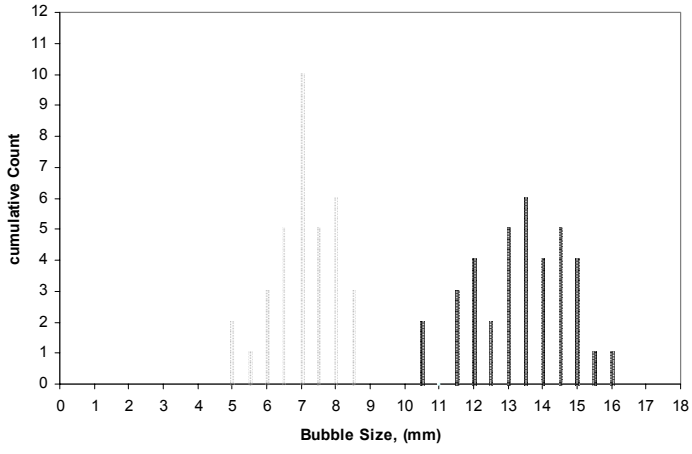

Figure 27. Measured bubble size in the slag foams generated by gas injection (Zhang and Fruehan 1995a).

10.4.2 Foaming generated by the slag/metal interfacial reaction

According to the experimental results of Zhang and Fruehan (1995a) the foam index is observed to decrease as the bubble size increases for a slag containing 45%CaO-45%SiO_2-5%FeO-5%Al_2O_3. The physical properties of this slag at 1400 ˚C were relatively similar to those of 34%CaO-37.5%SiO_2-5%FeO-14%Al_2O_3-9.5%BaO. Therefore, the foam indexes measured for the single-orifice and the multi-orifice nozzles at 1500 ˚C were extrapolated to 1400 ˚C by using correlation developed by Jiang and Fruehan (1991). The ratio of foam indexes at the temperatures is assumed to be equal to the ratio of property terms of Eq. (34).

In the experiments, the foaming of slag generated by the slag/metal interfacial reaction the reaction rate was measured in terms of CO-gas flow as a function of time. By measuring the foam height corresponding to the constant gas flow rate at the maximum reaction rate, the foaming index was determined. This type of foam is composed of very fine spherical gas bubbles and it is very stable (Zhang and Fruehan 1995a).

The increase of sulphur content in liquid metal decreases the foam index. This is due to the increase of the size of CO-gas bubbles formed at the metal/slag interface by the sulphur in the metal phase as a result of chemical reaction (Zhang and Fruehan 1995a).

The bubble size generated by nucleation at the slag/metal interface is expected to be a strong function of the interfacial energy and the contact angle between the liquid slag and metal. The average bubble size is observed to increase markedly as the sulphur content of the metal increases. Due to the large size of the bubble cells, the foam became polyhedron type (Zhang and Fruehan 1995a).

Therefore, it is possible to plot the foam index against the reciprocal of the average bubble diameter as shown in Figure 28, for which foams were generated either by argon gas injection or the slag metal interfacial reaction. The foam is inversely proportional to the bubble size for slags having the same physical properties (Zhang and Fruehan 1995a).

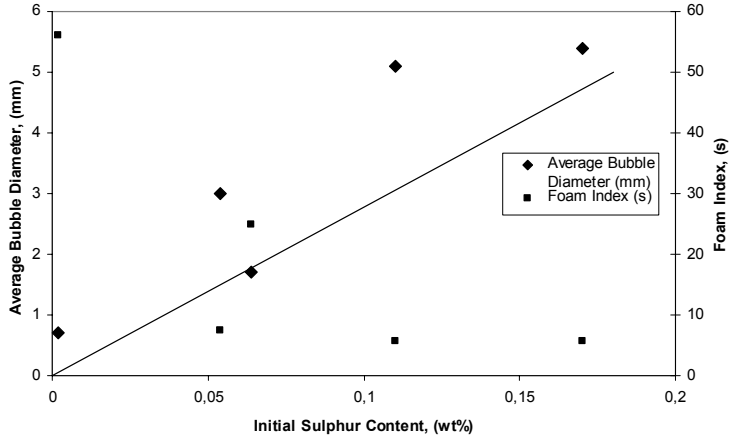

Figure 28. The foam index as a reciprocal of the average foam index (Zhang and Fruehan 1995a).

The size of bubbles in foams generated by the slag/metal interface reaction depends on the sulphur activity in liquid metal. The maximum bubble size detaching from the interface is determined by a balance between buoyancy and interfacial energy. Therefore, its value depends on the contact angle. Sulphur as a surface-active element in liquid iron increases the contact angle, resulting in larger bubbles and less stable foams (Zhang and Fruehan 1995a).

10.4.3 Effect of sulphur in liquid metal on the bubble size

When the sulphur content was relatively high, the highest foam level corresponded to the maximum gas flow rate. As the reaction rate decreased, the foam height decreased accordingly. However, with high sulphur content the initial foam level that corresponds to the maximum gas flow rate is not the highest, due to the large bubble size. As a portion of sulphur transferred from metal to the slag phase, the

bubble size decreased. Consequently, the foam height increased as a function of time, even with lower reaction rates. The foam index is observed to be approximately inversely proportional to the average bubble diameter. The sulphur has a large role in the determinations of the sizes of bubbles. As a surface active element in iron, it increases the contact angle, resulting in larger bubbles and less stable foams (Zhang and Fruehan 1995a).

Figure 29 shows the average bubble diameter in the slag foam as a function of sulphur content in the liquid metal. Figure 30 shows that the average bubble diameter in the slag is plotted against the activity of sulphur relative to 1 wt% in the liquid iron (Zhang and Fruehan 1995a).

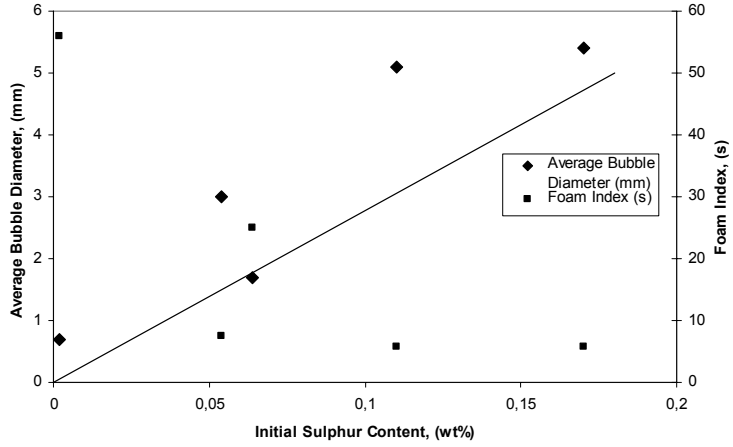

Figure 29. Average bubble diameter in the foam and foam index generated by the slag/metal reactions as a function of the sulphur content in the liquid metal (Zhang and Fruehan 1995a).

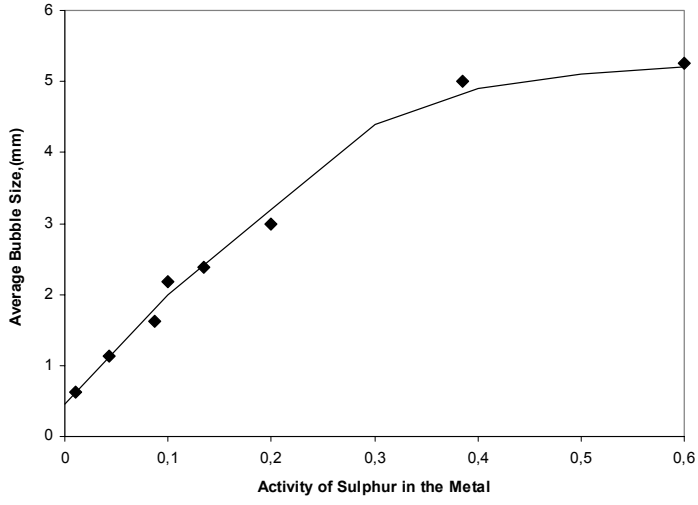

Figure 30. Average bubble diameter as a function of sulphur activity in 1 wt% standard state in the metal phase (Zhang and Fruehan 1995a).

Various sized crates were observed in the photographic study on the surfaces of Fe-C-S-metal samples. This phenomenon can indicate CO-bubble formation at the slag/metal interface. The bubbles sizes were larger with higher sulphur content samples. These observations reflected the bubble formation and growth at the slag/metal interface at the temperature where the reaction commenced. It also indicated that the bubble size is determined by the interfacial phenomena (Zhang and Fruehan 1995a).

The size of CO-gas bubble detaching from the slag/metal interface after growth may be considered to be governed by the balance between buoyancy force the balance between the buoyancy force and surface energy forces. In addition, the size of bubbles detaching from the interface may be affected by the turbulent flow induced the local surface energy gradient due to the temperature difference as well as chemical reactions (Zhang and Fruehan 1995a).

10.5 Effect of carbonaceous particles on slag foaming

The experimentally measured foam heights by Zhang and Fruehan (1995b) are shown in Figure 31 at the presence of coke spheres as a function of superficial velocity of gas at 1500 °C. The measured foam index reduced strongly along with added coke particles. The same phenomenon is observed with 10-mm and 3-mm diameter coke spheres. In addition, the coal particles have a similar antifoam effect, as indicated by the results shown in Figure 32 (Zhang and Fruehan 1995b).

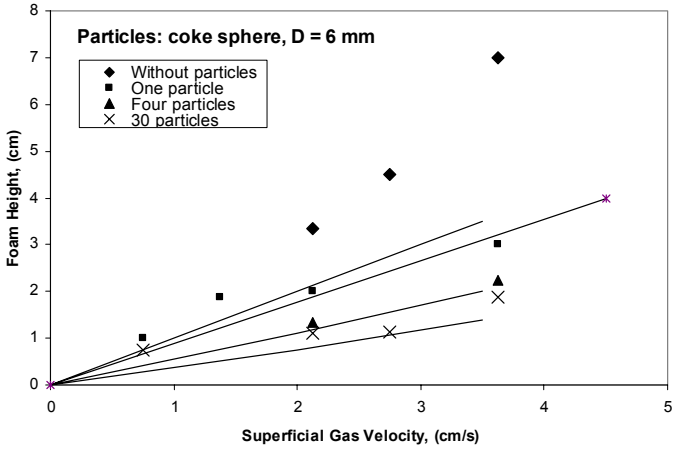

Figure 31. Effect of coke spheres (6 mm) on the foam height (Zhang and Fruehan 1995b).

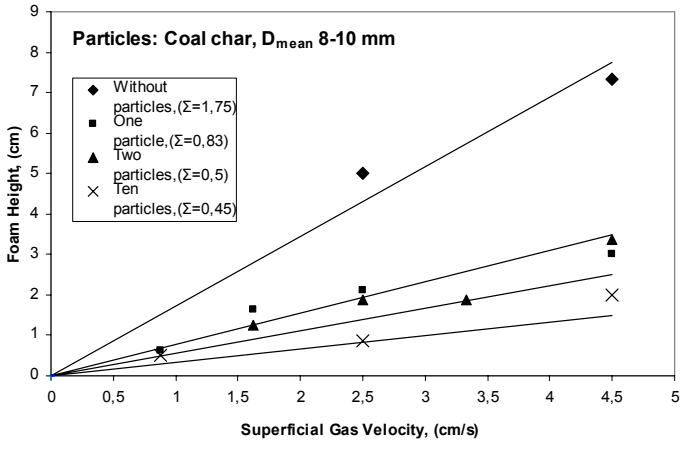

Figure 32. Effect of coal char particles in slag on the foam height (Zhang and Fruehan 1995b).

The predicted initial foam index of 25.5%CaO-51%SiO_2-8.5%CaF_2-15%Al_2O_3 slag is 4 s at 1500 ˚C without the presence of carbonaceous particles. Figure 33 shows the experimentally measured foam index of this slag with coke discs (8 mm). The foam index is observed to reduce with increasing carbonaceous particles. The similar phenomenon is also observed with larger particles (10 mm) (Zhang and Fruehan 1995b).

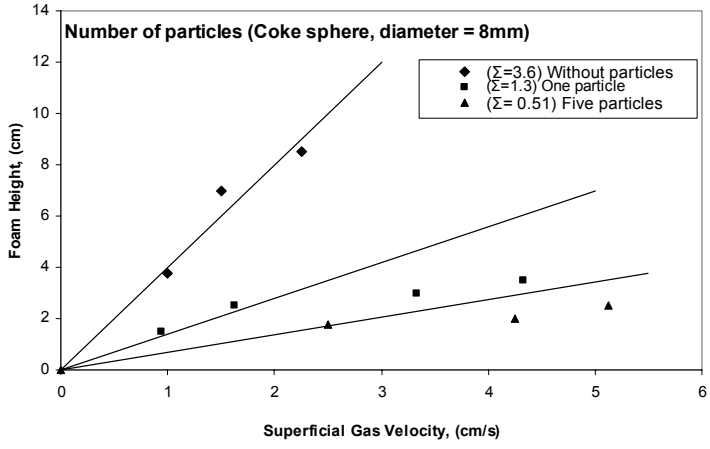

Figure 33. The effect of coke spheres (8mm) in slag on the foam height, with the initial foam index of 4 s (Zhang and Fruehan 1995b).

The effect of carbonaceous particles in suppressing slag foams is most likely due to its interfacial behaviour with liquid slag film of the foam. Both coke and coal char have contact angles greater than 90˚ with liquid slag, which make these particles non-wetting to the slag. When the particle contacts a liquid slag film, it aligns itself in such a way that its largest cross-section becomes parallel to the gas/liquid interface. Thus, the reduction of foam index of the slag depends on the coverage of its surface by the carbonaceous particles.

The non-wetting particles, coke and char coal, have a tendency to rupture foam when they come into contact with the liquid slag bubble. The wetting particles, such as alumina and iron oxide pellet, cannot break the foam. It can be concluded that two possible mechanisms of a carbonaceous particle rupturing a slag film are either the rapid thinning of the film driven by difference between the instantaneous contact angle and the equilibrium contact angle or the de-wetting of the liquid slag from the interface.

10.6 Effect of temperature on slag foaming

Ozturk and Fruehan (1995) have carried out experimential studies on the temperature dependence of foaming at temperature range 1773 and 1873 K. The foam height for 48% CaO-32%SiO_2 -10%Al_2O_3-10%FeO slag at 1773 K is shown as a function of superficial gas velocity in Figure 34.

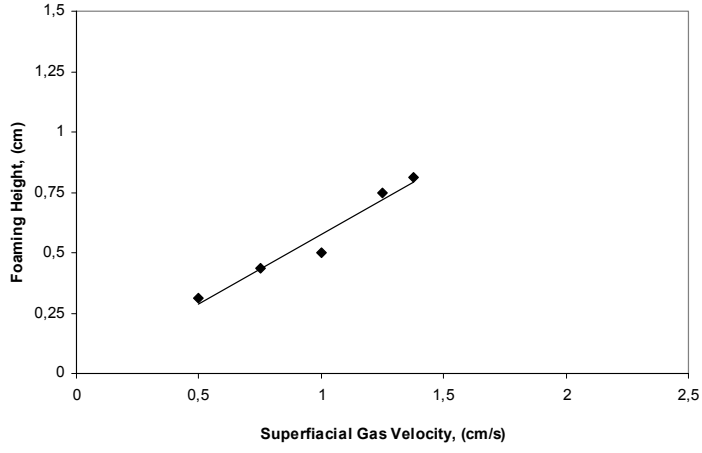

Figure 34. The relation between foam height and gas flow rate for a 48% CaO-32%SiO_2-10%Al_2O_3-10%FeO at 1873 K (Ozturk and Fruehan 1995).

Foam height increased linearly with increasing superficial gas velocity. The foaming index is obtained from the slope of the line in Figure 34. Similar experiments were also carried out at different temperatures. The foaming index decreased with temperature according to the results shown in Figure 35 (Ozturk and Fruehan 1995).

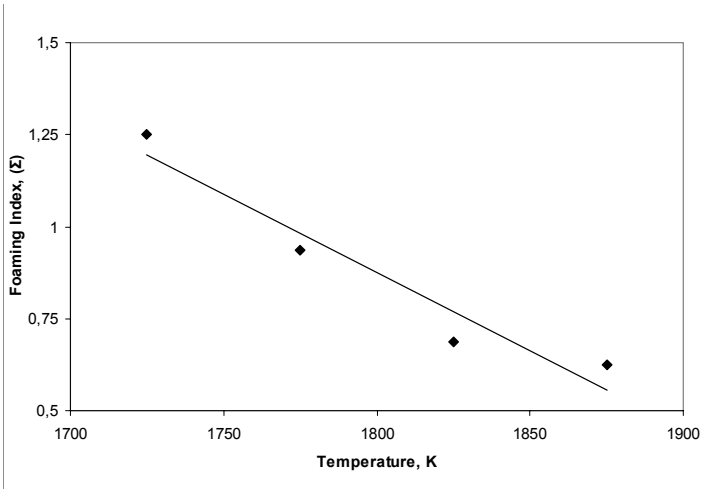

Figure 35. The effect of temperature on foaming index for a slag containing 48%CaO-32%SiO_2-10%Al_2O_3-10%FeO (Ozturk and Fruehan 1995).

The temperature dependence of the foaming index and viscosity for a slag containing 48% CaO-32%SiO_2-10%Al_2O_3-10%FeO is shown Figure 36.

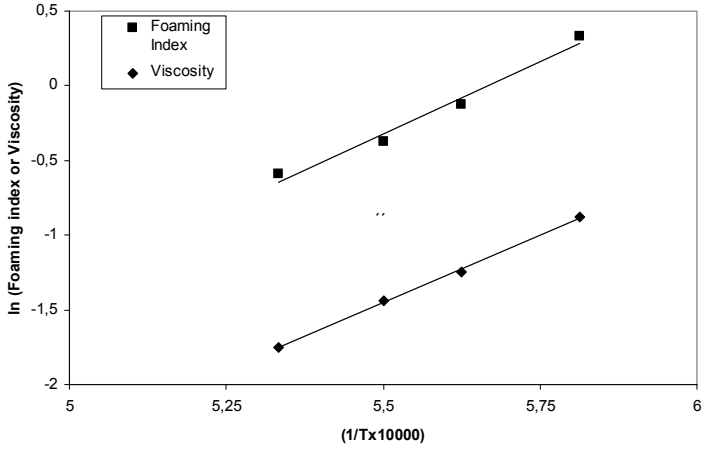

Figure 36. The temperature dependency of foaming index (s) and viscosity (Pas) for a 48% CaO-32%SiO_2-10%Al_2O_3-10%FeO (Ozturk and Fruehan 1995).

From the data given in Figure 36, the temperature dependence of the foaming index can be obtained (Ozturk and Fruehan 1995):

$$\Sigma = 1.78 \cdot 10^{-5} \exp\left[\frac{16.97}{T}\right] \tag{117}$$

However, Eq. (117) is valid only for the slag and the experimental conditions used in this investigation (Ozturk and Fruehan 1995).

Ito and Fruehan (1989a) have experimentally studied the temperature dependency of the foaming index at the temperature range of 1250–1400 ˚C. Figure 37 shows that the log (Σ) is inversely proportional to temperature. When the temperature drops from 1350 to 1250 ˚C, (Σ) increases by a factor of two. Since the temperature coefficient for surface energy is considered positive and that for viscosity negative, decreasing temperature can be expected to stabilise the foams.

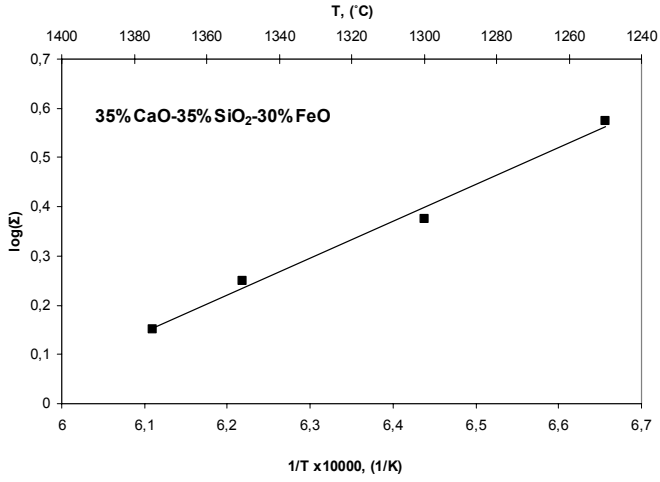

Figure 37. The temperature dependency of the foaming index for a 35%CaO-35%SiO_2-30%FeO slag (Ito and Fruehan 1989a).

10.7 Effect of slag volume on slag foaming

According to Ozturk and Fruehan (1995), the experiment results of the foaming index is nearly independent of the 40%SiO_2-40%CaO-10Al_2O_3-10%FeO slag volume. The small change in the foaming index may be due to the gas holdup in the slag. The results represented in Figure 38 are in the agreement with the foaming index value 2.07 s at 1723 K defined in Eq. (51) developed by Zhang and Fruehan (1992).

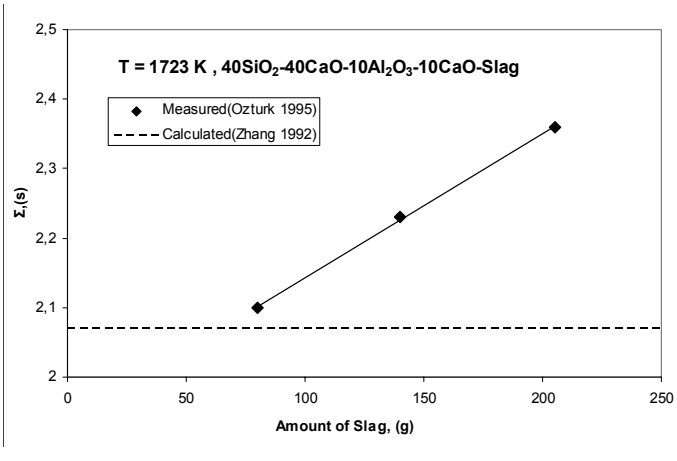

Figure 38. The effect of slag amount of foaming index for a slag containing 40%SiO_2-40%CaO-10Al_2O_3-10%FeO slag (Ozturk and Fruehan 1995).

10.8 Effect of gas type and pressure on slag foaming

The experimental results obtained by Zhang and Fruehan (1995c) showed that when using different gases other than argon, less foam is generated in 25.5%CaO-51%SiO_2-8.5%CaF_2-15%Al_2O_3 slag as shown in Figure 39. The defined foam index of slag at 1500 ˚C dropped from 1.8 s in argon gas injection to 0.8 s with helium and 0.5 s with hydrogen under the same experimental conditions.

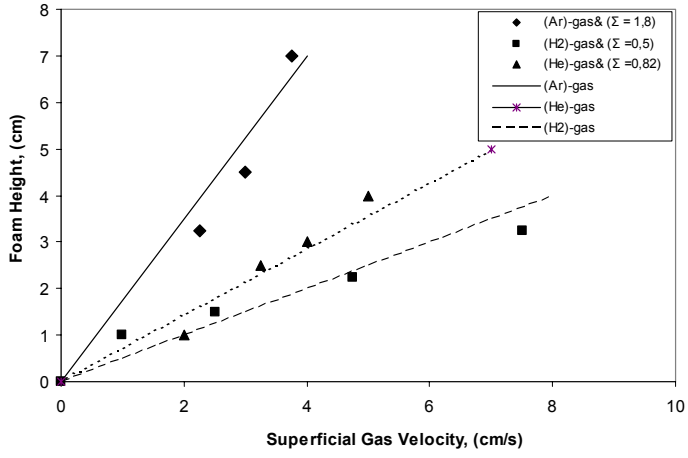

Figure 39. Foam index measured with hydrogen and helium bubbling at 1500 ˚C with 30%CaO-60%SiO_2-10%CaF_2-slag (Zhang and Fruehan 1995c).

In the experiments at 1400 ˚C the used slag contained 25.5%CaO-51%SiO_2-8.5%CaF_2- 15% Al_2O_3. As shown in Figure 40 the foam index for helium instead of argon is reduced from 12.4 to 9.8 s (Zhang and Fruehan 1995c).

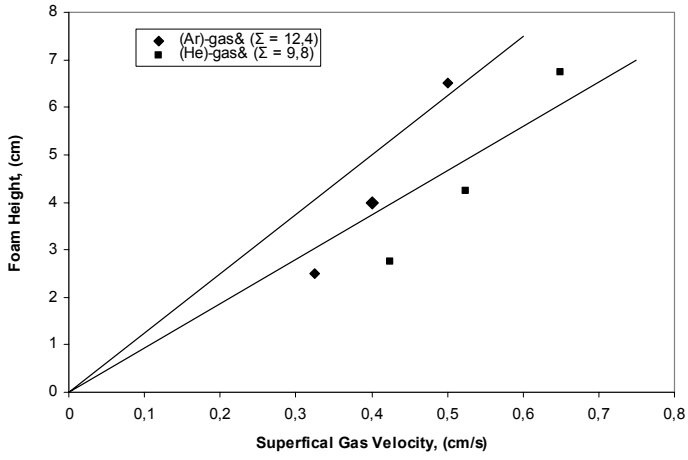

Figure 40. Foam index measured with helium gas bubbling at 1400 ˚C by electric probe technique with 25.5%CaO-51%SiO_2-8.5%CaF_2 and 15%Al_2O_3 slag (Zhang and Fruehan 1995c).

Figure 41 shows that the foaming index of the same slag with hydrogen gas injection is only 3.1 s compared with 10 s with argon gas injection. In addition, the X-ray observations indicated that there is no change in appearance or the size of the bubble cells in the foam, no matter what type of gas is used (Zhang and Fruehan 1995c).

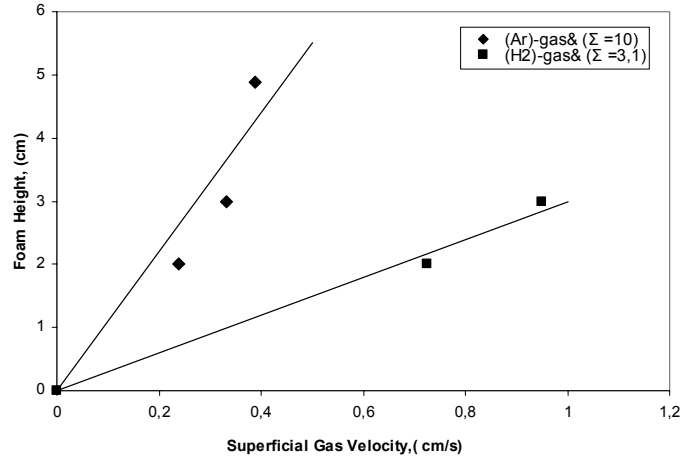

Figure 41. Foam index measured with hydrogen gas bubbling at 1400 ˚C by X-ray video technique with 25.5%CaO-51%SiO_2-8.5%CaF_2 and 15%Al_2O_3-slag (Zhang and Fruehan 1995c).

As shown in Figure 42, the measured foam height at the same volumetric gas flow rate of the same gas superficial velocity but different pressures are equal. If the mass flow rate is kept constant, an increase in the system pressure causes a decrease in the superficial gas velocity. In addition, the results in Figure 42 show that gas pressure did not affect the foam index under the present conditions. The X-ray observations showed that the size and appearance of bubbles were constant. As the gas phase pressure increased from 1 to 1.9 atm, its density nearly doubled. It seems that the gas density does not have much effect on the slag foam index. The increased gas pressure reduces the volume of the gas phase at a fixed mass flow rate and therefore decreases the foam volume (Zhang and Fruehan 1995c).

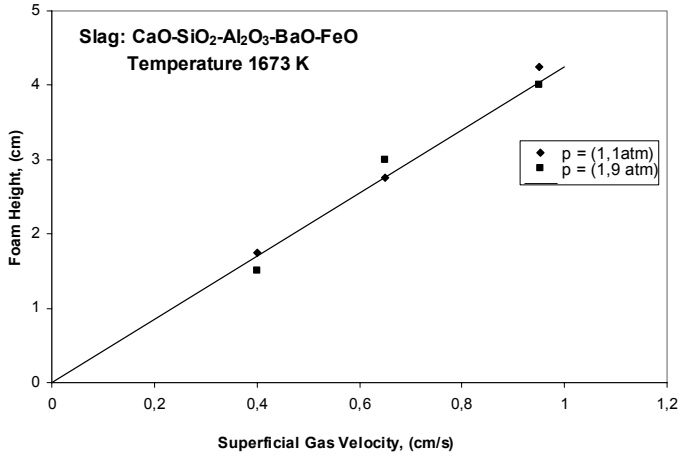

Figure 42. The effect of gas phase pressure on slag foaming at 1450 ˚C with 34%CaO-37.5%SiO_2-5%FeO-14%Al_2O_3-9.5%BaO slag (Zhang and Fruehan 1995c).

11. Results of experimental foaming studies in industrial scale

11.1 Results of foaming slag practice in electric stainless steelmaking with full-scale industrial experiments

Görnerup and Jacobsson (1998) have studied the potential of slag foaming practice in the industrial scale during full-scale experiments. The effect of FeO addition on slag is studied in particular in the experiments. The experiments were divided into two groups according to the Cr_2O_3 content in the slag.

11.2 Experimental results

The Cr_2O_3 content in the slag was high in the first group, indicating that the oxidation conditions were high. As shown in Figure 43, the foaming was also observed to promote chromium recovery. The well-developed foam is important for achieving lower Cr_2O_3 contents in the slags (Görnerup and Jacobsson 1998).

In the first group of experiments, the results showed that the oxidation level during the melting period is important. The chromium losses are caused by oxidising conditions resulting in high initial levels of chromium in the slag. No significant reduction of Cr_2O_3 content is observed during tapping due to a lack of reductants. The foaming heats were observed to have lower chromium content in the slag and a large initial reduction of FeO content. The foaming is also observed to promote chromium recovery (see Figure 43) (Görnerup and Jacobsson 1998).

The results can be divided according to their foaming characteristics, as shown in Table 7; the lower Cr_2O_3 content heats were more foaming. The foaming group had also a higher initial FeO content and finally a lower content (Görnerup and Jacobsson 1998).

Table 7. Sample analysis of foaming and non-foaming heats of the first group of experiments (Görnerup and Jacobsson 1998).

	Content(%)	1:Meltdown	2: O2-Injection Stop	3:Before Tapping	4:Transfer Ladle
Foaming	Cr_2O_3	24,8	23,8	20,3	16,3
7(Heats)	FeO	7,9	5,4	2,9	2,2
Nonfoaming	Cr_2O_3	25,7	25,9	21,4	18,7
6(Heats)	FeO	6	5	3,4	2,4

In the second group, the final Cr_2O_3 content in the slag is low and foam covered the electric arcs. The relation of foaming to Cr_2O_3 content looks similar to first group. The oxidation during melting is restricted and the curve is shifted to lower Cr_2O_3 contents as shown in Figure 44. Nevertheless, the slag foaming indicates the promotion of chromium recovery (Görnerup and Jacobsson 1998).

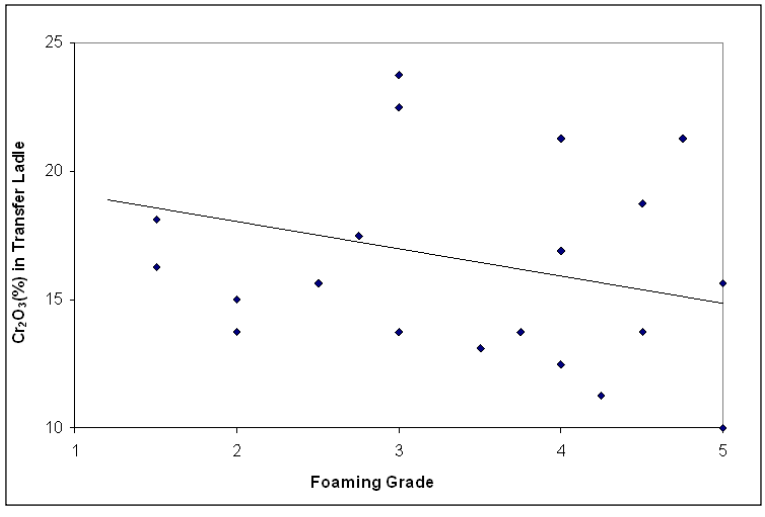

Figure 43. The first group of experiments shows that foaming promotes Cr-recovery (Görnerup and Jacobsson 1998).

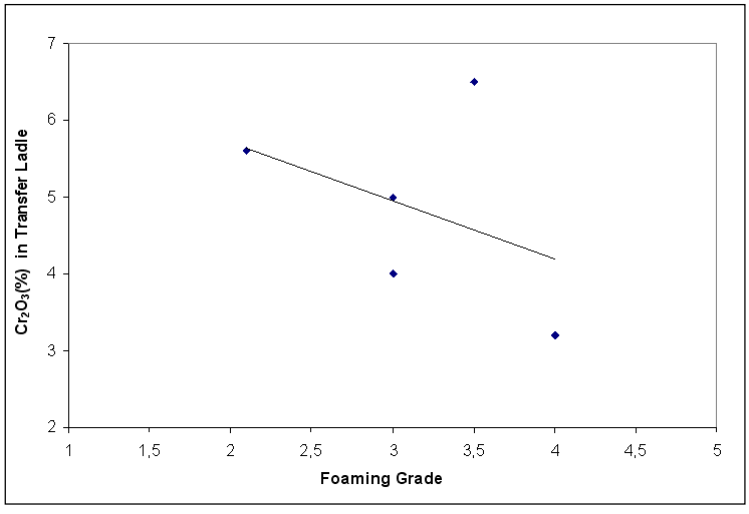

Figure 44. Cr-recovery was also observed in the second group of experiments (Görnerup and Jacobsson 1998).

The results of the second group are presented in Table 8. These results have a low final chromium content in the slag and foam covering the electric arcs (Görnerup and Jacobsson 1998).

Table 8. Operational results from the second group of experiments (Görnerup and Jacobsson 1998).

Number of experimental heat					
Content(%)	1	2	3	4	5
Cr_2O_3 Meltdown	14				15,1
Cr_2O_3 Before Tapping	7,6	7,4	6,9	7,2	12,6
Cr_2O_3 Transfer Ladle	4,1	5	3,1	5,6	6,7
CaO/SiO_2 Meltdown	1,3				1,6
CaO/SiO_2 Before Tapping	1	1,4	1,6	1,6	1,5
CaO/SiO_2 Transfer Ladle	1,1	1,3	1,5	1,5	1,3
Si Meltdown	0,57				0,49
Si Before Tapping	0,37	0,13	0,3		0,62
Si Transfer Ladle	0,25	0,06	0,09	0,04	0,19
Number of experimental heat					
Foaming grade	3,5	3,5	4	3	4
FeO-injection(kg)	320	400	520	160	360
O_2-injection(Nm^3)	346	709	531	857	472
C-injection(kg)	902	902	1103	587	800

Finally, the mill scale injection is observed to promote gas production. At least the visual observations during mill scale injection showed a dramatic increase in gas production soon after the start of injection (Görnerup and Jacobsson 1998).

11.2.1 Recommendations based on experimental results

Material charge balance in the reducing conditions is useful to limit Cr_2O_3 content in the slag below 15 wt%, the total oxygen input during meltdown has to be counterbalanced by ferrosilicon and raw material charging should aim for high silicon content 0.1wt% during tapping. The slag former addition should be carried out continuously to avoid a large amount of undissolved material in the slag. Minor MgO additions decrease refractory wear. Oxygen injection into liquid steel should begin at an early stage in order to add chemical heat to the slag soon after carbon injection into slag. Sufficient time has to be allowed before tapping for the slag reduction to reach reasonable Cr_2O_3 contents. The remaining Cr_2O_3 content reduces due to slag/metal mixing. Mill scale injection has been seen to strongly promote gas production. At least visual inspections during mill scale injection tend to show an increase in gas production soon after the start of injection. The injection can be seen to be useful in starting the reduction and thus slag foaming (Görnerup and Jacobsson 1998).

11.3 Results of observation of foaming of EAF slags in the production of stainless steel

Vidacak et al. (2002) have studied the foaming of EAF slags with high and low Cr_2O_3 content in the production of stainless steel. According to the experimental results, the foaming index is similar for the used slags, although their compositions were quite different. This is due to the similarities between viscosity, density and surface energy data for these slag compositions as shown in Table 9 and Table 10, respectively.

Table 9. Slag viscosities calculated using the KTH model and other physical properties at 1873 K (Vidacak et al. 2002).

Heat	μ(Pas)1773K	μ(Pas)1823K	μ(Pas)1923K	μ(Pas)1873K	ρ(g/cm^3)1873K	σ(mN/m)1873K	Σ1873K
CH-1	0,23	0,17	0,1	0,13	3,25	316	0,004
CH-2	0,21	0,16	0,11	0,12	3,26	319	0,006
CH-3	0,24	0,18	0,1	0,13	3,4	347	0,004
CH-4	0,21	0,15	0,1	0,11	3,49	361	0,003

Table 10. Composition of slags after tapping in the ladle (Vidacak et al. 2002).

Heat	$\%Al_2O_3$	%CaO	$\%Cr_2O_3$	%FeO	%MgO	%MnO	$\%SiO_2$	B = $(\%Al_2O_3/\%SiO_2)$
CH-1	5,4	44	1,1	0,7	10	0,6	26	1,68
CH-2	5,7	42	2,1	1	12	1	25	1,68
CH-3	3,5	41	10	4,3	6,1	2,4	27	1,66
CH-4	3,4	40	16	5,2	7,6	1,7	24	1,52

In the SEM microscopy analysis of slag samples, it is observed that the slag with high Cr_2O_3 content has solid precipitations. This confirmed the findings from the phase diagram that the slag is in the two-phase region and the solid particles can be expected (Vidacak et al. 2002).

The foaming degree determinations by operators showed that the slags with lower Cr_2O_3 content had higher foaming levels than the higher Cr_2O_3 content ones. This is unexpected since the higher Cr_2O_3 content slags with solid particles enhance the viscosity and foaming (Vidacak et al. 2002).

The estimated slag foaming is observed to be higher with increased Cr_2O_3 content. The foaming increases since solid particles are present in the slag due to their slag viscosity increasing effect. If the amount of secondary particles in the slag is moderate, the viscosity and foaming index are higher. However, at higher Cr_2O_3 contents in the slag, the large solid particles destroy the bubble network and become detrimental to the foaming of the slag (Figure 45).

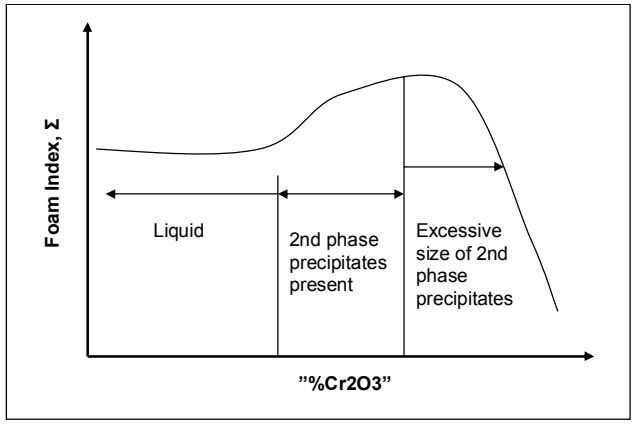

Figure 45. Relationship between foaming index and second-phase particles (Vidacak et al. 2002).

11.3.1 Results of sound measurement experiments

The sound measurements were also used to determine slag foaming during experiments. A tendency for increasing foaming with a decrease of sound intensity was observed. The foam was judged on a 5-point scale, where 1 corresponded to

no foaming and 5 to maximum foaming. Table 11 shows the average estimated foam level and Cr_2O_3 content for each plant trial (Vidacak et al. 2002).

T**able 11**. Foaming degree and chromium content (Vidacak et al. 2002).

Heat	MW/Active effect	Cr_2O_3(wt%)	Average foam (0-5)
CH-1	27	1,1	4
CH-2	26	2,1	3
CH-3	28	10	2
CH-4	36	16	1

The degree of foaming is determined using both sound measurement and manual observation by experienced operators for each of the trials. Figure 46 shows an example of the average sound intensity plotting versus the estimated foam level for heat CH-3.

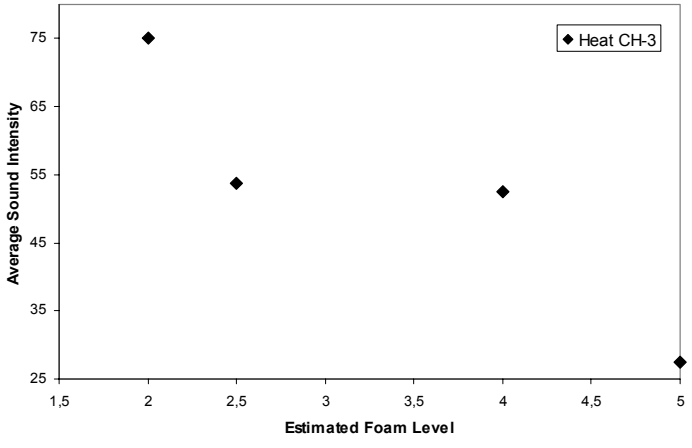

Figure 46. Variation in magnitude with frequency, heat CH-3 (Vidacak et al. 2002).

The highest average sound intensity corresponds to the lowest foam level (2) and the lowest sound intensity to the highest foam level (5). However, for the sound intensity of 50 both foaming levels (2.5) and (4) was estimated. It was considered probable that the human ear is not able to distinguish between such small changes in sound intensity. Thus, the foaming observations based on sound measurements have to be compared with more reliable data (Vidacak et al. 2002).

11.4 The results of the online control of the foamy slag in electric arc furnace

Marique et al. have developed and recently published (1999) a control method of the slag foaming operation based on noise emitted by the EAF. The established correlations between the sonicmeter signals and the volume and quality of the foaming slag present in the vessel allow for online guidance of the carbon and oxygen injection.

11.4.1 Detection and characterisation of the slag foaming

For characterising the heats, the average level of the signal during the refining period was calculated. The relationship between the average noise level and the foamy slag quality appraised is defined (Marique et al. 1999.

The heats were classified into four different categories according to noise levels; no slag (noise level > 4), thin slag layer (noise level 2–3), emulsified slag volume (Arc nearly submerged), (noise level 2) and formation of high foam slag volume with slopping (noise level < 2) (see Figure 47).

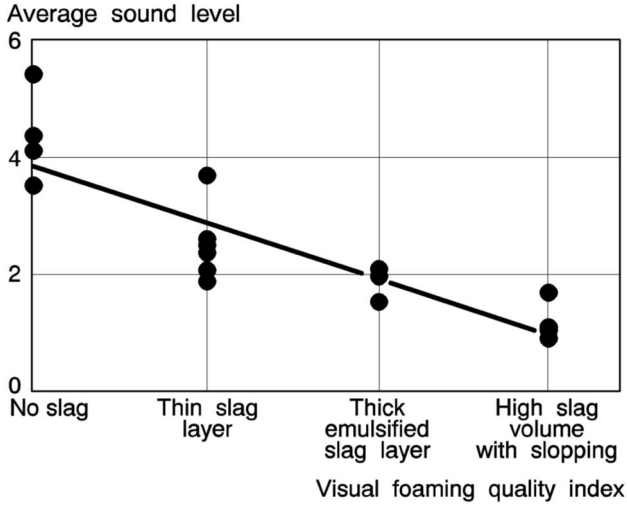

Figure 47. Appraisal of the slag foaming quality in the EAF with sonicmeter (Marique et al. 1999).

Correlations have been established between the sound signal and the volume and quality of the foamy slag present in the vessel during refining, allowing an in-line guidance of the carbon and oxygen injections. A more regular and reliable control of the foamy practice allow gains on the electric energy consumption and on the steel nitrogen content. Another way to express the foaming slag quality is to define

the ratio between the duration when the arc is covered by the foamy slag (noise level < 2) and the power on time. The high ratio indicates that a good foamy slag had rapidly been formed and controlled during almost the entire refining step (Marique et al. 1999).

11.4.2 Foamy slag quality

According to Marique et al. (1999), from a metallurgical viewpoint the steel nitrogen content is the only parameter that has been highlighted as being directly influenced by the foaming slag practice. It is a difficult element to remove and control on a regular basis in the EAF process. The achieved nitrogen level in the liquid steel at tapping depends particularly on the metallic input. The significant reduction of the average nitrogen content can be obtained mainly due to an effective desorption induced by a more intense melt decarburisation (see Figure 48).

A decrease in the nitrogen level from 70 to 20 ppm can be obtained when the working practice leads to a very low foam signal during most of the refining period. The foamy slag plays an important role for a more efficient protection of the melt against the nitrogen pick-up coming from the atmosphere (see Figure 49).

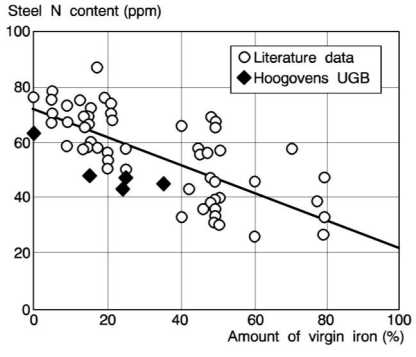

Figure 48. Limitation of the nitrogen content by the addition of virgin iron in the EAF (Marique et al. 1999).

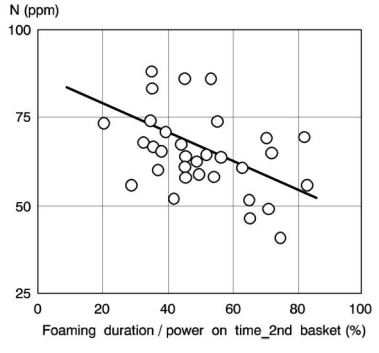

Figure 49. Relation between the steel nitrogen content and the percentage of the time when the arc is covered by a good foaming slag (Marique et al. 1999).

The influence of the foamy slag quality is considered separately for heats with the same scrap mix and virgin iron input. The presence of a good foamy slag during the longest part of the refining period (noise level < 2) allows for a reduction in electric consumption (Marique et al. 1999).

11.4.3 Influence of the slag composition

According to Marique et al. (1999), the slags used in the experiments are characterised by a relatively low theoretical foaming index with high basicity ($CaO/SiO_2 \approx 4$). It is far from the optimal zone with basicity of 1.5–2.0 and FeO content in the slag 15–25% (see Figure 50). The practice is driven by the need to maximise the desulphurisation reaction in the furnace to comply more easily with the end specifications on the products.

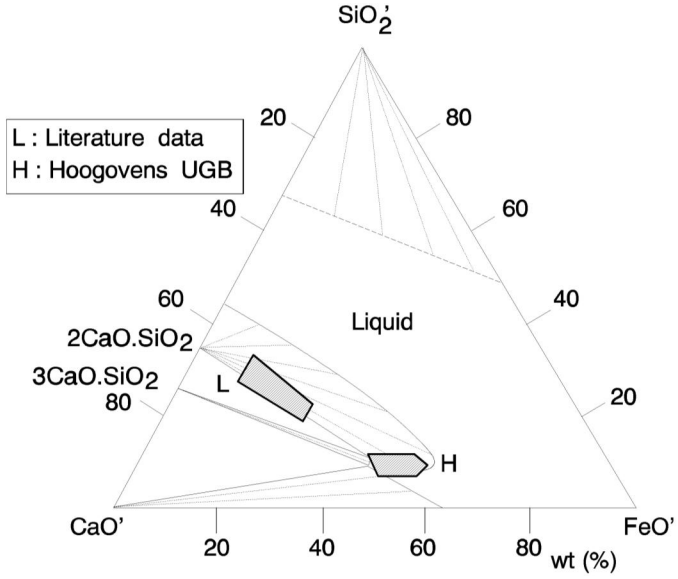

Figure 50. Composition of EAF slag (Marique et al.1999).

A high value of the theoretical foaming index corresponds to a better foaming proneness. The slags with high basicity and high iron content are characterised by a relatively low theoretical foaming index (see Figure 51). According to this, the theoretical foaming index is a function of measured noise level (see Figure 52), and no relationship has been highlighted. However, the suitable slag foaming can be achieved with the appropriate working practice with a good combination of carbon and oxygen gas injections (Marique et al. 1999).

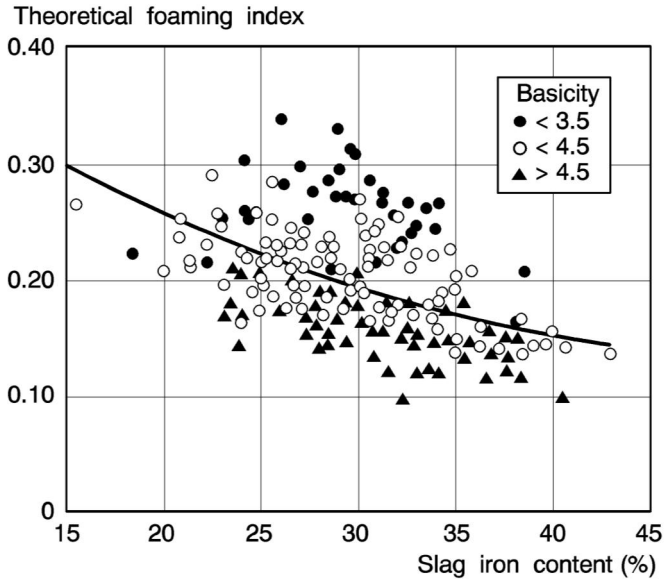

Figure 51. The effect of the slag composition to foaming index (Marique et al. 1999).

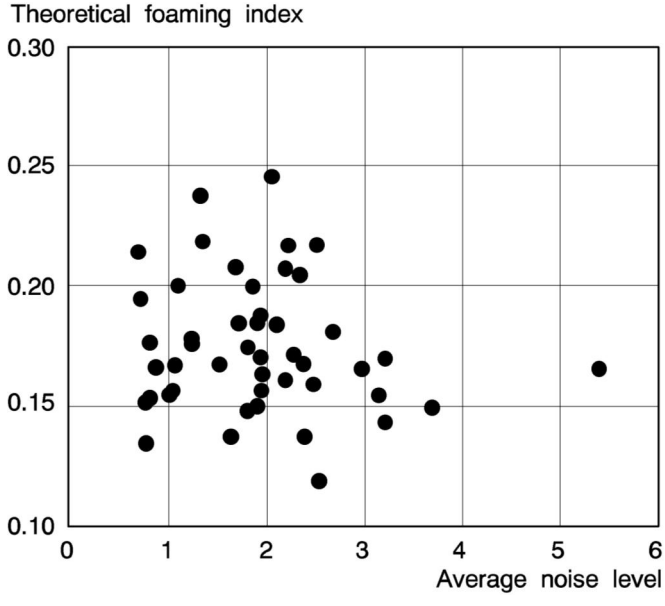

Figure 52. The relation between the foaming index and the average noise level (Marique et al. 1999).

11.5 The results of additions to generate foam in stainless steelmaking

Kerr and Fruehan (2004) have experimentally studied the capability of slag additives to generate gas at sufficient rates using the CVPI technique. They determined the gas generation rates and rate-controlling mechanisms for each additive. From these results, the expected foaming in actual steelmaking operations can be predicted. The NiO and carbon additions do not appear practical for generating foam, whereas limestone and calcium nitrate briquettes provide foaming.

11.5.1 Gas generation rates from hydrated calcium nitrate additions

Calcium nitrate has been suggested for use in foaming. Calcium nitrate dissociates according to Eq. (118) and calcium nitrate containing carbon reacts at 1550 ˚C as shown in Eq. (119). It can be assumed that calcium nitrate and a calcium nitrate/carbon mixture dissociates as heating and the reaction in Eq. (119) is only hypothetical (Kerr and Fruehan 2004):

$$Ca(NO_3)_2(H_2O)_2 = CaO + N_2 + 2H_2 + 2.5O_2 \quad (118)$$

$$Ca(NO_3)_2(H_2O)_2 + 5C = CaO + N_2 + 2H_2 + 5CO \quad (119)$$

Table 12 shows the quantity of gases produced as a function off temperature, when one mole of pure calcium nitrate heats up, whereas Table 13 shows the quantity of gases generated as a function of temperature when one mole of calcium nitrate and five moles of carbon heats up. Both of the results were obtained at atmospheric pressure from FactSage software. An excellent agreement between the total quantity of gas predicted by the FactSage software and the quantity of gas measured during the CVPI technique (Constant Volume Pressure Increase) is observed. The basic principle of the CVPI technique is to measure the pressure increase due to the generation of gas in a closed system and relate it to the moles of gas generated (Kerr and Fruehan 2004).

Table 12. Dissociation of one mole of calcium nitrate (Kerr and Fruehan 2004).

T/K	H_2O/mol	O_2/mol	N_2/mol	Gas total/mol
300	0	0	0	0
400	1,9	0,2	0,1	0,2
500	2,5	1	1	4,5
600	2,5	1	1	4,5
700	2,5	1	1	4,5
800	2,5	2	1	5,5

Table 13. Dissociation of calcium nitrate and carbon mixture (Kerr and Fruehan 2004).

T/K	CO_2/mol	H_2O/mol	N_2/mol	H_2/mol	CH_4/mol	CO/mol	Gas/Mol
300	1,5	9,1	1	0	0	0	2,6
400	1,6	1,8	1	0	0,1	0	4,5
600	1,7	1,5	1	0,1	0,2	0	4,5
700	1,8	1,4	1	0,3	0,2	0	4,7
800	1,8	1	1	0,7	0,2	0,3	5

The mass spectrometer results for pure calcium nitrate dissociation are shown in Figure 53 and Figure 54 for nitrate and carbon reaction. The results were in agreement with the FactSage software. The mass spectrometer identified oxygen, water and nitrogen as the product gases, in agreement with the products predicted by the FactSage software.

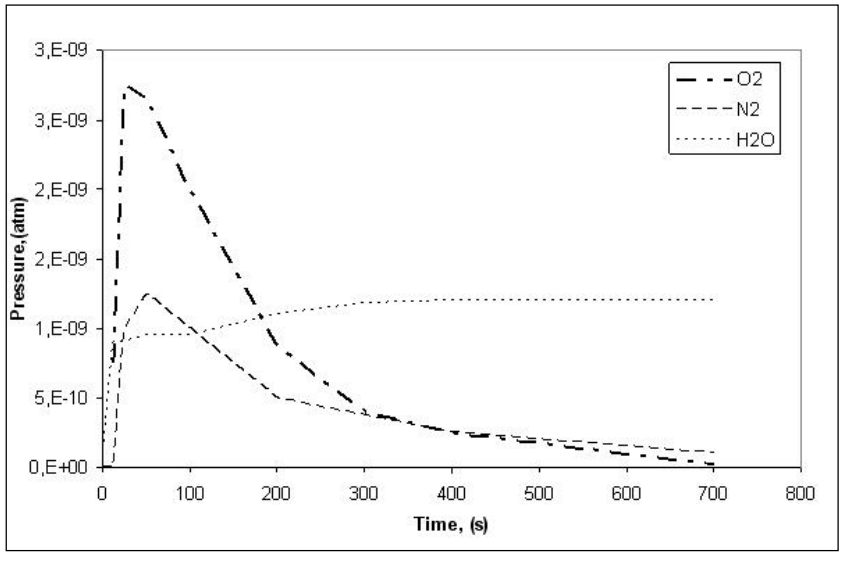

Figure 53. Mass spectometer results from the dissociation of calcium nitrate (Kerr and Fruehan 2004).

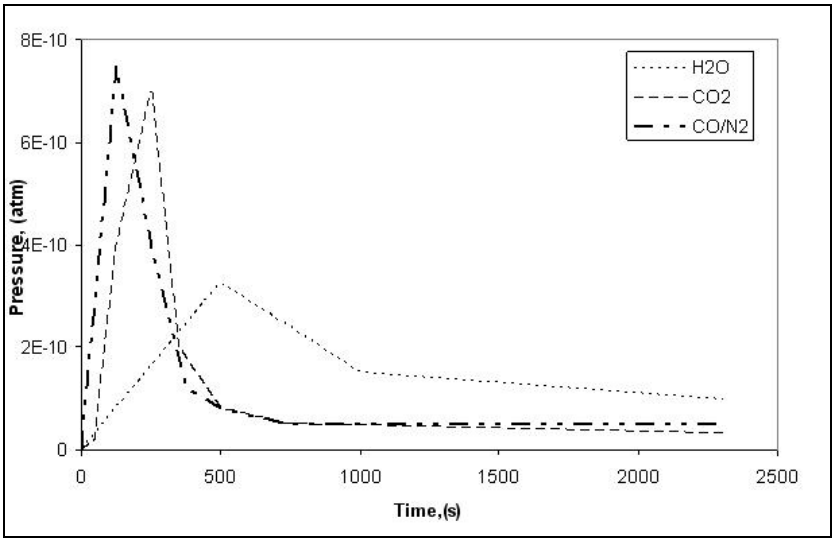

Figure 54. Mass spectrometer results of the calcium nitrate and carbon reaction (Kerr and Fruehan 2004).

11.5.2 Gas generation in the WOB additions

The WOB additions are assumed to proceed at 1550 ˚C in the CVPI technique. The reasons for the superior gas generation rate of the WOB addition were; WOB additions contained Fe_2O_3, which have a faster reduction rate than FeO has to metallic iron; diffusion did not limit the reduction rate, since the iron oxides and carbon were in direct contact throughout the experiment; and a larger surface area is available for reactions to commence due to the small constituent particles. The FeO occurred as a separate phase and consequently its activity is unity. This increases the rate of CO_2-gas. The equilibrium CO_2-gas pressure reaction is shown in Eq. (120), the reduction of Fe_2O_3 to FeO is high, thus emphasising the importance of the CO_2-gas equilibrium pressure in the reduction processes (Kerr and Fruehan 2004):

$$Fe_2O_3 + CO = CO_2 + 2FeO \tag{120}$$

Figure 55 shows the amount of gases measured by the mass spectrometer during a WOB reduction.

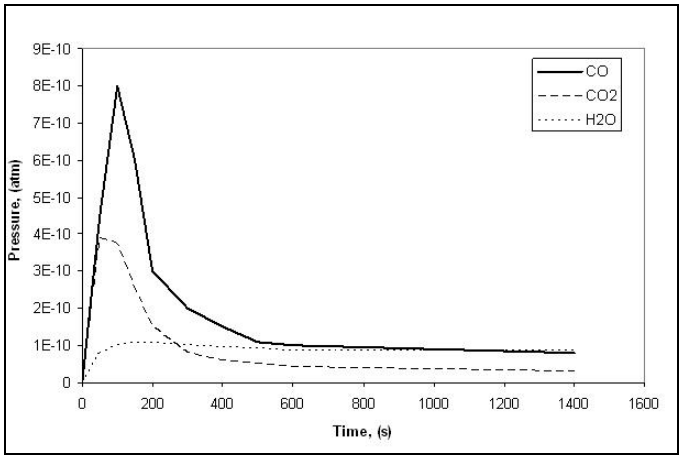

Figure 55. Gases measured by the mass spectrometer during a WOB reduction (Kerr and Fruehan 2004).

11.5.3 Gas generation from NiO and CoO additions

Iron oxide reduction proceeds though the following process: diffusion of the oxide from the bulk of the slag to the slag-gas interface, reduction of oxide at the slag-gas interface, diffusion of CO_2-gas from the slag-gas interface to the gas-carbon interface and oxidation of graphite.

The oxidation is shown in Eq. (121) and the corresponding reaction rate is given by Eq. (122) (Kerr and Fruehan 2004):

$$CO_2(g) + C = 2CO(g) \tag{121}$$

$$Rate = k_{GC}\left(p^{FeO}_{CO_2,eq} - p^{GC}_{CO_2,eq}\right) \tag{122}$$

where $\left(k_{GC}\right)$ is the rate for reaction in Eq. (121) and $\left(p^{GC}_{CO_2,eq}\right)$ is the CO_2–gas Eq. pressure at the carbon-gas interface. In addition, Eq. (123) simulates the iron oxide reduction process when the FeO diffusion though the slag controls the overall reduction rate:

$$Rate = \left(\frac{1}{\left(\frac{100MW_{FeO}}{m\rho}\right) + \left(\frac{1}{K_{GC}K^{'}Cp_{CO}}\right)}\right)\left(FeO\%\right) \tag{123}$$

where m is the mass transfer coefficient of FeO thought the slag, ρ is the slag density (kg/m^3), K_{eq} is the equilibrium constant at the slag-gas interface, C is the

constant relating FeO activity to FeO wt%, k_{GC} is the rate constant for the reaction, and p_{CO} is the equilibrium CO-gas pressure at the slag-gas interface (1 atm). The measured and the calculated FeO and CrO reduction rates are in good agreement (Kerr and Fruehan 2004).

The FeO and CrO experimental results indicate that the oxidation rate of carbon partially controls the reduction rates. Any oxides that are selected for analysis of their capability to induce foaming should create a relatively large CO_2-gas pressure at the slag-gas interface. The NiO has a large equilibrium CO_2-gas pressure and thus its gas-generating capability was examined. Figure 56 shows the results from NiO CVPI experiments and Eq. (124) describes the NiO reduction rates (Kerr and Fruehan 2004):

$$Rate = \left(\frac{1}{\left(\frac{100 MW_{NiO}}{m\rho} \right) + \left(\frac{1}{K_{GC} K_{eq}^{'} Cp_{CO}} \right)} \right) (NiO\%) \tag{124}$$

where $\left(K_{eq}^{'}\right)$ is the equilibrium constant for CO + NiO = CO_2 + Ni.

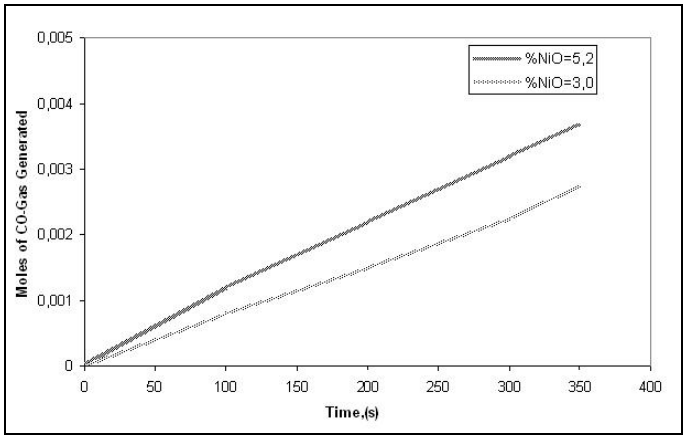

Figure 56. Quantity of CO-gas generated with time during a NiO CVPI experiment. The lines describe the approximated mean value of CO-gas generation as a function of time (Kerr and Fruehan 2004).

The gas-carbon rate constant can be determined according to Eq. (125) (Kerr and Fruehan 2004):

$$k_{GC} = \frac{k_{lm}}{RT} \tag{125}$$

where (k_{lm}) is the rate constant for limited mixed control.

The mass transfer coefficient can be presented (Kerr and Fruehan 2004):

$$m = \left(\frac{12Dv(1-B)}{\pi d_b} \right) \tag{126}$$

where (D) is the diffusivity, (d_b) is the average bubble diameter, (v) is the rate of evolution of gas per unit area, and (B) is the degree of surface coverage.

The diffusivity of NiO can be approximated with Eq. (127), which defines the self-diffusion of iron in CaO-FeO-SiO_2 melts between 1250 and 1540 ˚C (Kerr and Fruehan 2004):

$$\log D_{Fe} = \left(-\frac{5450}{T} - 1.93 \right) \tag{127}$$

However, it seems probable that a significant source of error in the calculated NiO reduction rate is estimating the D_{NiO} with the D_{Fe}. Regardless, it seems that the calculated NiO rates are still in modest agreement with the measured data (Kerr and Fruehan 2004).

11.5.4 Gas generation rates from limestone additions

Limestone calcination evolves CO_2-gas during reduction. Limestone calcination is endothermic and the calcination is controlled by heat transfer rate to the limestone.

The calculation of Biot number supports the hypothesis that limestone temperature during calcinations remained constant at 897 ˚C and resulted in the constant gas generation pattern. After the heat up, the mode on heat transfer to the limestone cylinder changed from convection to radiation according to Eq. (128) (Kerr and Fruehan 2004):

$$Biot - Number = \left(\frac{hV}{KA} \right) \tag{128}$$

where (h) is the average convection heat transfer coefficient, (V) is the volume of the solid, (A) is the surface area of the solid and (K) is the thermal conductivity of the solid.

The Biot number is a dimensionless number and it represents the ratio between convection heat transfer resistance and the conduction-heat-transfer resistance. If the value of the Biot number is small, the conduction resistance to heat transfer within a solid is significantly less than the convection resistance through a boundary layer to the solid. It is reasonable to assume a uniform temperature distribution

across the solid at any time during process. If the convection-heat-transfer coefficient can be replaced with the radiation heat-transfer coefficient, then the Biot number represents the ratio of the radiation heat-transfer resistance to the conduction heat-transfer resistance. Low surface temperatures decrease the rate at which heat is transferred by radiation between surfaces and result in lower temperature gradients in the colder body – the limestone cylinder according to Eq. (129) (Kerr and Fruehan 2004):

$$h_r = \varepsilon\delta\left(T_c + T_s\right)\left(T_r^2 + T_s^2\right) \tag{129}$$

where (h_r) is the average radiation heat-transfer coefficient, ε is the emissivity of limestone, (δ) is the Stefan-Boltzman constant (5.67E10^{-8} W/m^{2}K^4), T_c is the cylinder temperature (897 ˚C) and T_s is the slag temperature (1550 ˚C). At the smaller Biot-number the temperature gradient in the limestone cylinder is negligible during calcination (Kerr and Fruehan 2004).

11.5.5 Heat transfer in calcination procedure

Each $CaCO_3$ molecule dissociated during the lower limestone cylinder temperature uniformly to below 897 ˚C and the limestone temperature subsequently returns uniformly to the calcination temperature, upon which another $CaCO_3$ molecule dissociates and the process repeats (Kerr and Fruehan 2004).

Conduction in the particle resistance to heat transfer can limit the limestone calcination rate provided the size of the limestone piece is large. If the limestone particles are small enough, the conductive resistance to heat transfer is negligible and the calcination process of small limestone spheres immersed in liquid slag can be broken down into sequential process. Heat is transferred by convection and temperature increases up to 897 ˚C. Then the sphere at the calcination temperature begins to dissociate. Due to the gas halo enveloping the limestone, the ability of convection to transfer heat from slag to limestone subsequently diminishes. As radiation is the mode of heat transfer between surfaces separated by gas at high temperature, the primary mode of heat transfer between the slag and limestone changes from convention to radiation until the calcination is completed. Afterwards, the calcination gas halo collapses and the mode of heat transfer to sphere reverts back to convection to the thermal equilibrium between slag and sphere (Kerr and Fruehan 2004).

The calcination rate of smaller-sized cylinders seems to be controlled by heat transfer to the limestone as opposed to heat transfers though the limestone. The addition of limestone also lowers the local temperature and thus decreases the slag viscosity. A lower slag viscosity increases the foam index. In addition, the process adds the amount of CaO in the slag (Kerr and Fruehan 2004).

The mass spectrometer results in Figure 57 show that the vast majority of the generated gas is CO_2-gas with a small amount of CO-gas present. The measured

amounts of oxygen, hydrogen and nitrogen were also negligible (Kerr and Fruehan 2004).

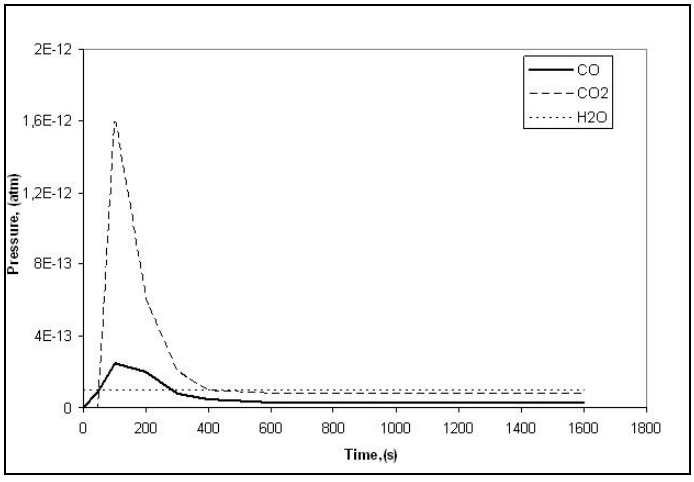

Figure 57. Mass spectrometer results for limestone calcinations (Kerr and Fruehan 2004).

11.5.6 Observed foaming and application to EAF operation

The rate of gas generation is most important to the rate on the foam height. An approximate measurement of the maximum foam height is made during the CVPI experiment. Foam height is observed to be equal in every experiment. The foam height is very large with the larger limestone vessel due to the excessive gas generation rate (Kerr and Fruehan 2004).

Eq. (130) shows the predicted gas generation rate required to produce a desired foam height (H_f) (Kerr and Fruehan 2004):

$$Q_R = \frac{\Sigma H_f}{A_{EAF}} \tag{130}$$

where (A_{EAF}) is the required area of foam and equals the cross-sectional area of the furnace.

Figure 58 shows the carbon content of a hypothetical slag as a constant rate of coke is added to the slag to reduce NiO. The carbon is increased to a steady state value, at which point the coke is provided sufficient area to react with NiO at the same rate at which the carbon is injected. It also shows the similar behaviour for $CaCO_3$ additions. The parameters, such as slag composition, is assumed to be constant. When coke and limestone are injected into the slag, the amount of additives increases until a steady state amount is present (Kerr and Fruehan 2004).

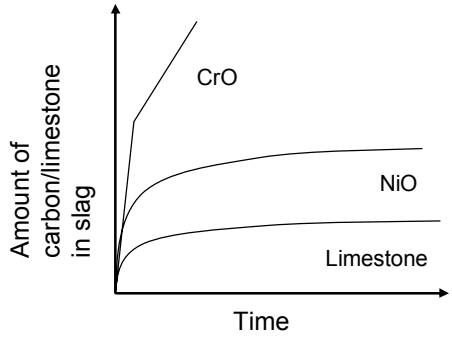

Figure 58. Hypothetical example of wt% of carbon or limestone in a slag (Kerr and Fruehan 2004).

When the steady state condition is achieved, the rate generation from the reaction of carbon with NiO or the dissociation of $CaCO_3$ depends only on the injection rate of these materials. The injection rate of carbon, NiO and limestone is given as follows (Kerr and Fruehan 2004):

$$i = \left(\frac{RTH_f \Sigma}{A_{EAF}} \right) \tag{131}$$

where (R) is the ideal gas constant and (i) is the injection rate [mol/s].

If the reaction rate is slow, an excessively large amount of materials is needed. For example, the reduction of CrO by carbon is exceedingly slow and consequently, excessive amounts of carbon is required for an adequate gas generation rate. However the steady state amount of carbon in the slag may be excessive. The rate of gas generated (Q_R) by NiO reduction is given as (Kerr and Fruehan 2004):

$$Q_R = kA_C RT\left(NiO\%\right) \tag{132}$$

where (A_c) is the carbon area.

The gas generation rate for limestone calcination can be presented when it is controlled by the heat transfer (Kerr and Fruehan 2004):

$$Q = \left(\frac{A_{LS} h_r \left(T_0 - T_x\right)\left(T_0\right)\left(R\right)}{\Delta H} \right) \tag{133}$$

where (ΔH) is the heat of calcination.

It appears that, due to the low NiO slag content, an excessive amount of carbon can be required in the slag to generate gas at a sufficient rate. Limestone and hydrated calcium nitrate appear to be realistic possibilities. The mass spectrometer is used to provide insight in identifying the product gases resulting from reactions (Kerr and Fruehan 2004).

12. Results of model calculation studies

12.1 Results of behaviour of slag foaming with reduction of FeO in molten slags by C

According to Hong et al. (1998), no relation between slag foaming and properties (surface energy, viscosity) could be found in the experimental studies considering slag foaming caused by CO and argon gas injection with FeO-C reaction in alumina crucible and consequent slag foaming height measurements. Neither CO nor argon gas injection is observed to make slag foam in the studied slag system. Slag foaming caused by slag-graphite reaction is dependent mainly on the CO-gas evolution rate (Q_{CO}). However, the withdrawal of the graphite rods from the slag melt causes the reaction to cease, thereby causing the slag foaming to quickly collapse (Hong et al. 1998).

The sulphur addition suppresses slag foaming significantly, but silica has no such an effect on slag foaming, although both sulphur and silica are surface active components in molten slag. Figure 59 shows the typical relation between foaming height and reaction time. The slag height increases with time to the maximum value and then drops. This can be explained by the difference in their effects on the contact angles and surface energies (Hong et al. 1998).

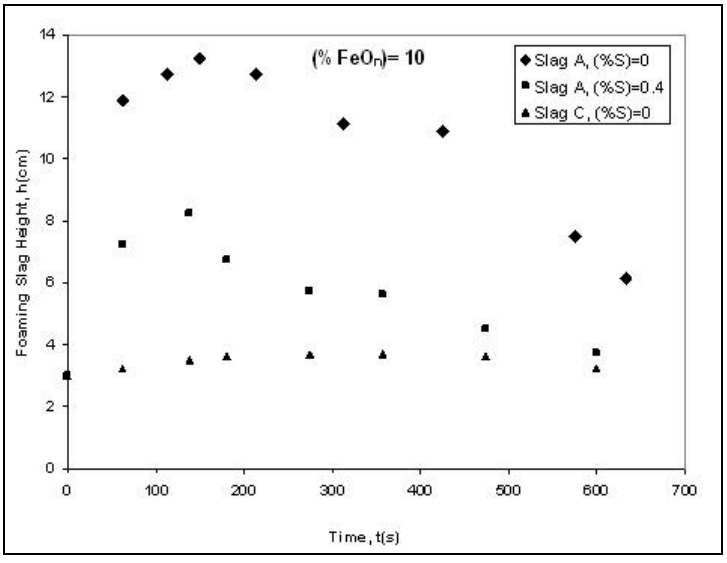

Figure 59. The relation between foaming slag height and time (Hong et al. 1998).

The distribution parameter (α) increased with the increase of sulphur content in Figure 60, whereas the drift flux (Q_d) decreased with increased sulphur content in Figure 61. These can be explained by the decrease in slag surface energy with sulphur addition. (Hong et al. 1998.)

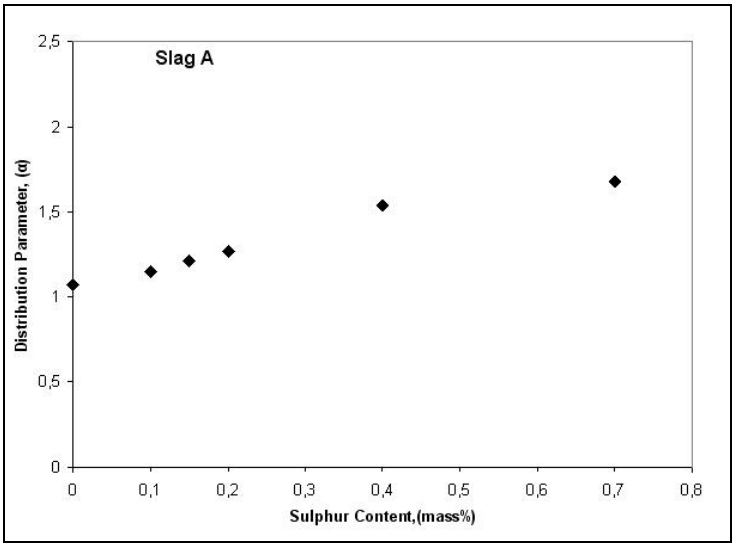

Figure 60. The relation between distribution parameter (α) and sulphur content (Hong et al. 1998).

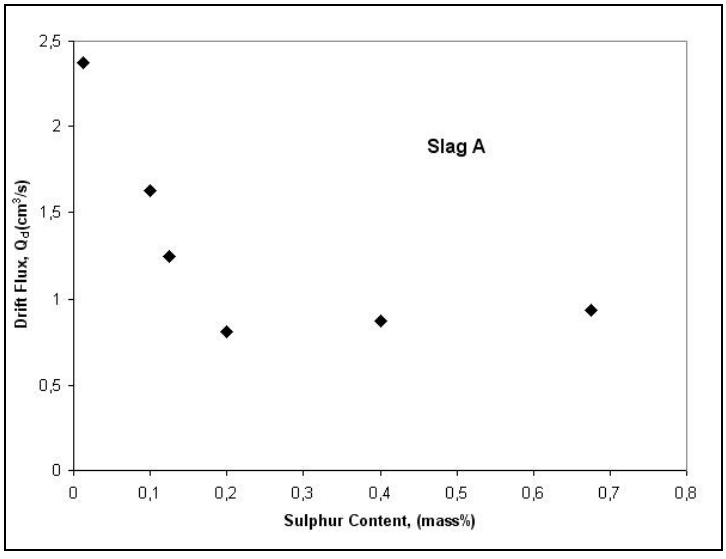

Figure 61. The relation between drift flux (Q_d) and sulphur content (Hong et al. 1998).

12.2 Results of thermodynamic model of EAF process for stainless steel

As described above in Section 9.2, Arnout et al. (2006) have developed an EAF process model for stainless steel production. The model calculates the evolution of temperature and composition of slag and metal phases over time. It calculates the steel composition relatively well. In the slag phase, the formation of excess CO-gas and the fixed oxygen gas balance causes significantly less oxidation of chromium, iron, manganese and silicon. Due to this, the total amount of slag is lower and thus the concentrations of calcium and magnesium are higher, which further increases the basicity compared to the measured value.

Figure 62 shows the temperature evolution in the furnace and the mass of liquid metal. The mass of the total content of the furnace is shown for comparison. Figure 63, however, shows modelled concentrations of the liquid steel phase. The measured (non-reconciled) values of the end composition are indicated on the right axis. According to the simulation, chromium is the first liquid phase to appear. Silicon also melts selectively in the model, but oxidises quickly with added oxygen. Carbon injection mainly increases the carbon content in the metal phase, and leads to the formation of CO-gas, and to a lesser extent reduces the CrO in the slag. The reduction is less than observed, due to a lower level of CrO_x and FeO to start with. In the measured data most of the FeO is reduced during carbon injection and most of CrO_x reduction is established during tapping. The lower values are probably due to the formation of CO-gas and lower oxygen gas input into the model than in reality (Arnout et al. 2006).

In the slag system, only chromium has oxidised before any fluxes. After calcia, chamotte and doloma additions are made, silicon is oxidised by CrO and forms calcium silicates. Alumina from the chamotte forms calcium aluminate. When the temperature reaches 1000 ˚C, aluminates melts and form a liquid slag. After the addition of a second bucket the slag solidifies. As more oxygen is added, chromium oxidises again with the second addition of calcia and doloma, and chromium oxide from the chromites reduces again. The oxidation of silicon compensates for this reduction. The evolution of total slag compositions over time is shown in Figure 64.

The injection of oxygen without carbon oxidises chromium, and carbon injection reduces it slightly. After this, nearly all silicon from the steel is oxidised and there is no room for further reduction of chromium oxide. Then the calcium-aluminate-silicates melt and form a liquid slag (Arnout et al. 2006).

12.2.1 Effect of dynamics and kinetics

The furnace is modelled as a homogenous system; the temperature is the same throughout the entire content. The end temperature level matches the measured end temperature in the transfer ladle as a result of the energy efficiency fitting procedure (Arnout et al. 2006).

The homogeneity of the model causes higher oxidation of the carbon instead of chromium and iron. The slag layer is also in contact with gas phase, as is the steel. The oxygen partial pressure estimated by model can in reality be higher. The temperature of the system is approximated to be homogeneous and the spatial deviations in the equilibrium compositions can be neglected. The constant temperature throughout the furnace reveals the unrealistic homogeneity of the model (Arnout et al. 2006).

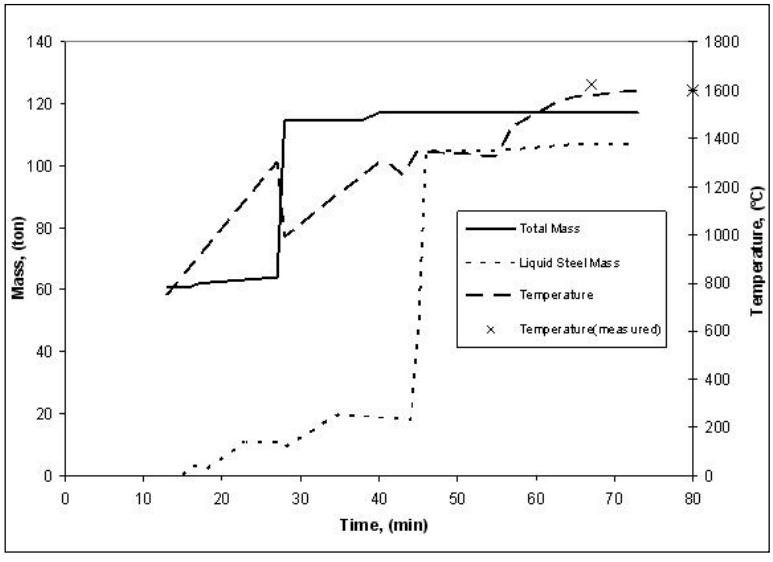

Figure 62. Temperature, total mass and liquid steel mass as a function of time (Arnout et al. 2006).

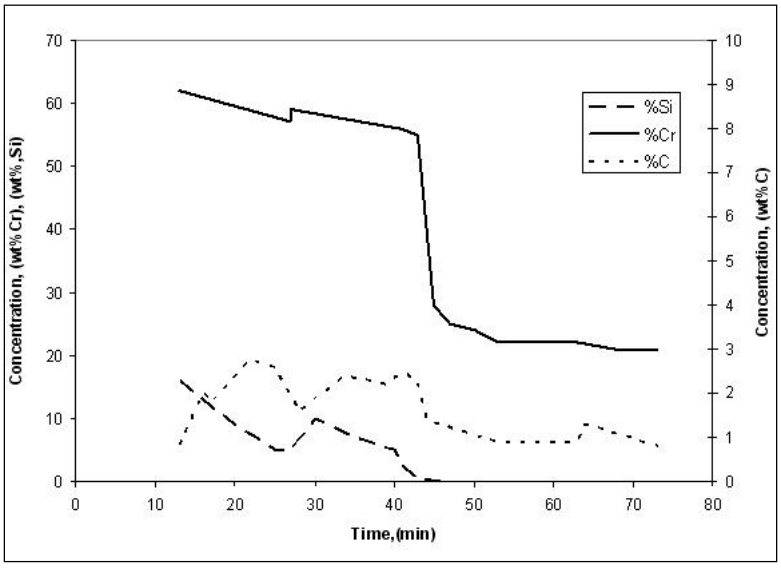

Figure 63. Liquid metal concentration as a function of time (Arnout et al. 2006).

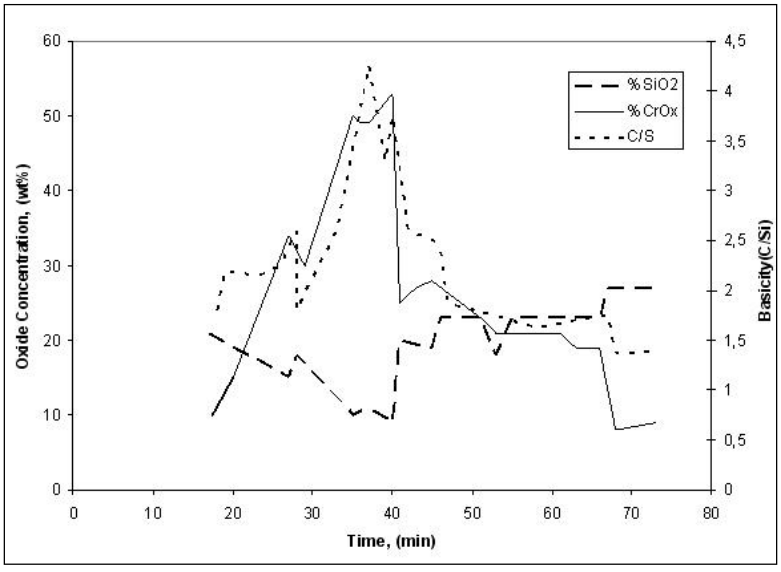

Figure 64. Total slag concentration as a function of time (Arnout et al. 2006).

Figure 65, Figure 66 and Figure 67 show a comparison between industrial slag composition and modelling results for the typical heat. The decrease of basicity and the increase of MgO content are predicted relatively well. In the model, the carbon injection is conducted only one time, instead of long-term injection in reality. Easily reducible elements of chromium, iron and magnesium show low levels in the modelled slags (see Figure 66 and Figure 67). The formation of CO-gas, the increase of carbon levels and the small reduction of chromium are caused by carbon injection. In addition, the oxygen content is lower than in reality and it is distributed homogeneously in the model (Arnout et al. 2006).

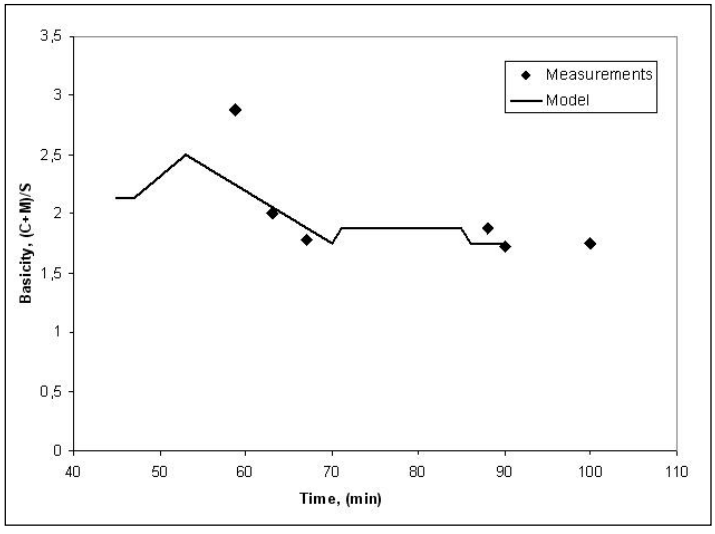

Figure 65. Slag basicity as a function of time (CaO+MgO)/SiO_2 (Arnout et al. 2006).

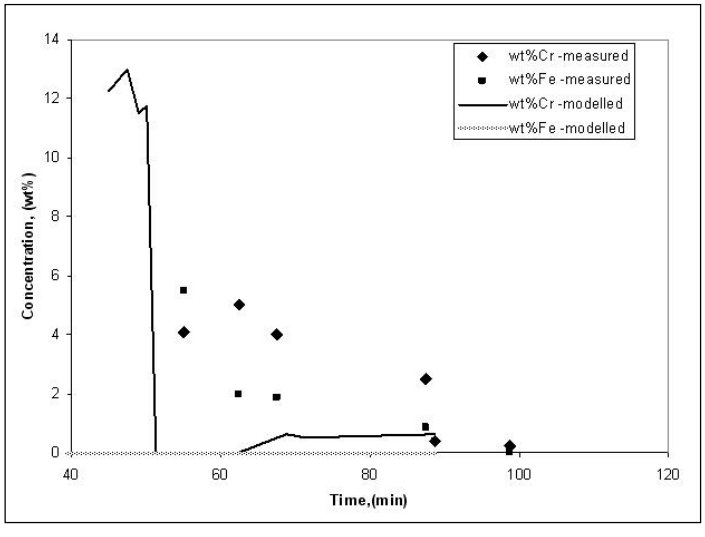

Figure 66. Fe- and Cr-concentrations in the slag as a function of time (Arnout et al. 2006).

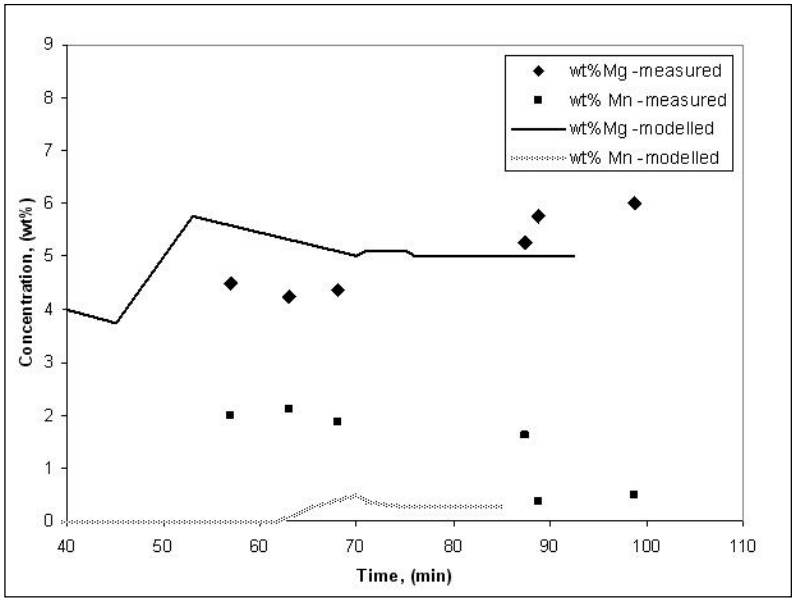

Figure 67. Mn- and Mg-concentrations in the slag as a function of time (Arnout et al. 2006).

In dynamic conditions, the selective melting of chromium and silicon require unphysically large diffusion in the solid steel. In addition, the first liquid slag is Al_2O_3-CaO type and it is unrealistic. In the multi-component slag area, little constitutional data is known (Arnout et al. 2006).

Compared with industrial data, the prediction of the dynamics of the process of the kinetics has to be taken into account explicitly. The kinetics has a significant influence during the following mechanism: during the carbon injection period, carbon and CO-gas are in direct contact with slag, the oxygen reactions from the air are not constant, the oxidation commences at the beginning when the scrap is without slag protection, the slag layer hinders the formation of CO-gas, which is a gradient in the oxygen partial pressure, and slag-steel interfacial reactions are complicated except during tapping (Arnout et al. 2006).

It is possible to partially predict the dynamics with the equilibrium model, but it is strongly controlled by kinetic phenomena. The dynamics of main slag components are relatively in agreement with observations, whereas the model cannot predict the behaviour of chromium, iron and manganese (Arnout et al. 2006).

The measured end compositions of slag and metal were determined by manual sampling from the furnace and XRF method (X-Ray Fluorescence) with high accuracy. In the dynamic evolution experiments, the slag composition is measured using the EDS method (Energy Dispersive Spectroscopy). In order to generate input for the model, reconciliation is performed using the measured slag and steel

composition in the vessel. As a result, mass balance errors during the measured period can have an effect on the dynamic value (Arnout et al. 2006).

12.2.2 Formation of solid compounds

In the early stages of heat, chromium oxide is mainly found in chromate phases ($MgO.Cr_2O_3$ or $CaO.Cr_2O_3$). After ferrosilicon and fluorospar additions, mostly solid CrO is reduced, silicon is oxidised and all the silicates melt into the liquid slag. Some MgO from $MgO.Cr_2O_3$ is also taken into the liquid slag. By using the XRF analysis method a very high accuracy is achieved (Arnout et al. 2006).

The solid phase observed in the slag is a $(Mg,CaO).(Cr,Al,Fe)_2O_3$. However, in the modelled slag the solid phase is pure $MgO\text{-}Cr_2O_3$ for most heats and/or $CaMgSiO_4$ for some. This can be explained by the absence of a solid solution model for this spinel composition in the FactSage database. This can also be explained by the lower CrO content in the slag (Arnout et al. 2006).

12.2.3 Accuracy of simulation

Finally, it can be concluded that the end composition of the metal phase is calculated with relative error from 1% for the main elements to about 20% for the secondary elements. The end composition of the slag phase is calculated with relative errors of 1% for aluminium, calcium and magnesium. In the slag phase for the easily reducible elements iron, chromium, manganese and silicon, a lower oxidation than that measured is reached. It is caused by the production of a higher amount of CO-gas, which is due to the homogeneity of the model without kinetic restrictions. On the whole, the good correspondence for chromium level and lower carbon content in the metal phase of the model can be observed with industrial data (Arnout et al. 2006).

12.3 Results of decarburisation and slag formation model for an electric arc furnace

The model developed by Matsuura et al. (2008) considers the rate phenomena for decarburisation and the carbon-FeO reaction in the slag, the mass balance for each element in the metal, slag and gas phases with the melting behaviour of pig iron scrap and fluxes.

The model can be used to simulate iron yield and carbon loss with the discharged slag. The change of FeO content in slag is affected by the pig iron melting pattern along with the carbon-FeO reaction rate constant and post-combustion ratio. The accurate operation input parameters are needed for the simulation procedure. The simulation results of the melting patterns for pig iron, scrap and post-combustion ratio should be conducted though the comparison of calculation results with real data for many heats. The foaming can be optimised by controlling

the FeO content, slag basicity and CO-gas generation. Nitrogen gas removal can also be improved by changing the operation (Matsuura et al. 2008).

12.3.1 Effect of carbon content

In the study of the change of carbon content in melt as a function of time for each melting pattern it was found that the initial heel is small compared with the amount of charged materials. Therefore, the carbon content in melt changes largely with different melting patterns of pig iron and scrap. With a fast melting rate for pig iron at the early stages of operation, the carbon goes up to 0.7 mass%. The stable carbon profile is seen in all melting patterns after 30 min. Those were 0.1–0.25 mass%, which is higher than the observed carbon content in the furnace of 0.06 mass% (Matsuura et al. 2008).

The change of reaction rate constant (k_{red}) does not affect carbon content in metal considerably, although FeO content changes. The decrease in the rate constant increases the FeO content in the slag. This leads to the increase of FeO and carbon losses. Figure 68 shows the change of the carbon content in the metal. The final carbon content in the metal can increase by 0.005 mass% with the decrease oxygen flow rate (Matsuura et al. 2008).

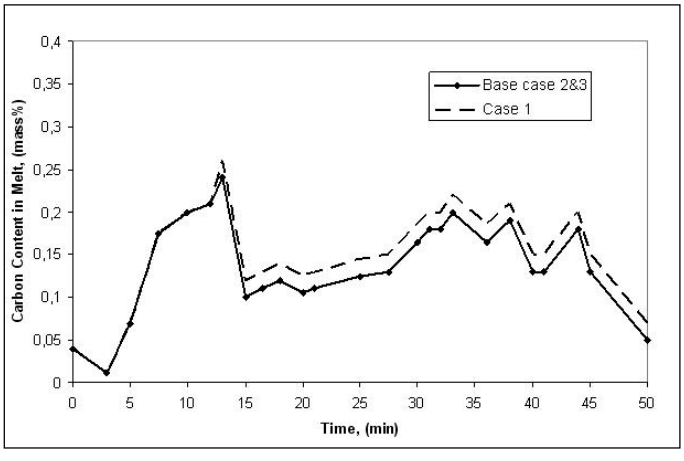

Figure 68. Calculated results of carbon content in metal (Matsuura et al. 2008).

12.3.2 Effect of FeO content

The change of FeO content in slag as a function of time for each melting pattern with analytical results of collected slag samples shows that the minimum FeO content is calculated to occur between 10–20 min. Fast melting of pig iron in the early stage leads to a large decrease in FeO content. Then carbon content in the melt increases and all oxygen injected is consumed by the decarburisation reac-

tion. The scrap impurities and fluxes dissolve continuously and cause the FeO to be diluted. In order to enhance the flux dissolution and maintain the FeO level, the FeO content should be high in the early stage (Matsuura et al. 2008).

The calculated FeO content is higher compared to the analysed results by 5–10 mass%. The high FeO content is due to overestimation of the contribution of the injected oxygen gas from the post-combustion injectors of the reaction and the underestimated post-combustion ratio. Figure 69 shows the change of FeO content in slag as a function of time (Matsuura et al. 2008).

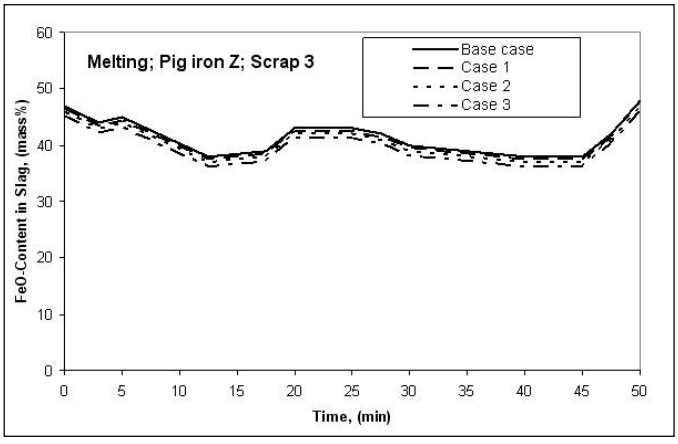

Figure 69. Calculated results of FeO content in slag (Matsuura et al. 2008).

12.3.3 Effect of post-combustion

When the post-combustion ratio is increased to 0.3, the FeO content in the slag decreased, reproducing the composition of the analysed slag very quickly. The FeO content increased later up to 40–45 % due to the termination of pig iron melting. The calculated post-combustion ratio is observed to be overestimated. It is assumed that only 20% of the injected oxygen gas though post-combustion injectors participates in the decarburisation and oxidation reaction occurring in the melt and slag. Figure 70 shows the change of FeO content in the changing post-combustion ratio. The FeO content in slag decreased with increasing post-combustion ratio (Matsuura et al. 2008).

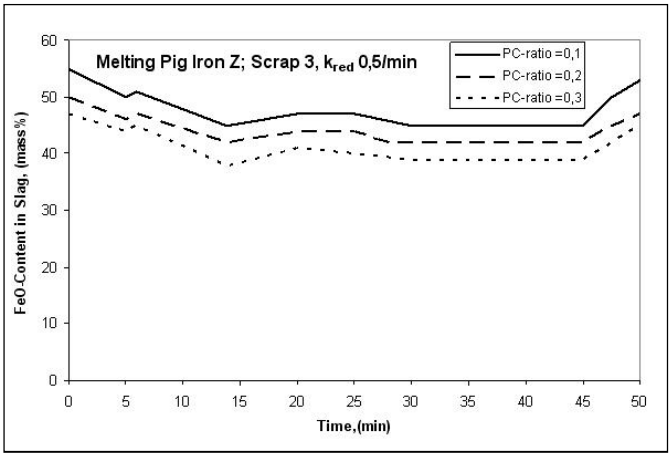

Figure 70. Change of FeO content in slag with changing post-combustion ratio (Matsuura et al. 2008).

12.4 Results of slag foaming in an electric arc furnace

According to Matsuura and Fruehan (2009), the general observations of the calculation results of the model were: the potential foaming is very high when using high amounts of pig iron, carbon and oxygen. The actual foam is simply limited by the height at which the slag is flushed out of the furnace or by the volume of slag. At the end of the process, the foam decays due to lower CO-gas generation.

12.4.1 Slag composition

As opposed to LD and BOF steelmaking, in the EAF the slag composition does not change significantly over time. This can be confirmed through the analysis of slag samples taken during the operation. This is due to the continuous nature of the process in which carbon, CaO and oxygen are continuously injected such that the EAF process is close to a continuously stirred tank reactor with regard to slag composition. Figure 71 and Figure 72 show the slag composition as a function of time calculated by the EAF model (Matsuura and Fruehan 2009).

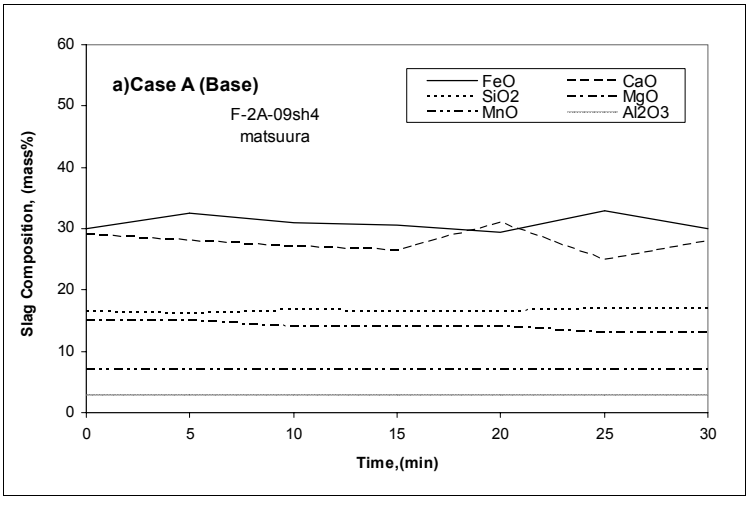

Figure 71. Slag composition as a function of time for Case (A) (Base) (Matsuura and Fruehan 2009).

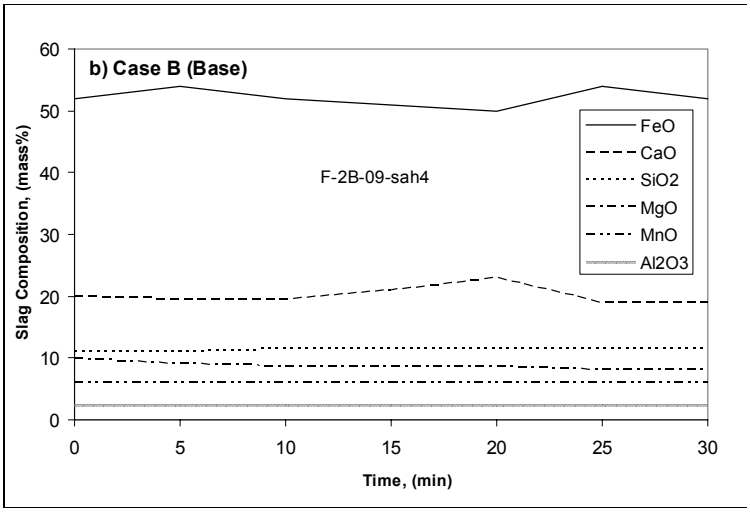

Figure 72. Slag composition as a function of time for Case (B) (Matsuura and Fruehan 2009).

The critical slag component with regard to foaming is FeO. Its content depends on the carbon and oxygen input. The carbon injection and pig iron melting rates roughly matches the oxygen feed rate according to the stoichiometry of Eqs. (1) and (2). The FeO content does not change significantly during the process (Matsuura and Fruehan 2009).

12.4.2 Foam height

The calculated foam height is unrealistically high for the actual furnace operation. In the actual process, as the foam is produced it reaches a certain height and is flushed out of the furnace. In this case, there may not be sufficient slag for the potential foam height computed from the CO-gas rate and the foam index. The slag foam height is only controlled by CO-gas rate early on in the processes and towards the end of the blow when the CO-gas rate is low. During the majority of the process, the foam height is limited. At the end of process the foam decays primarily due to low CO-gas generation rates. In Figures 73-80 the effects of different parameters to the foam height are shown. Finally, Table 14 shows the melting pattern data of heats. (Matsuura and Fruehan 2009.)

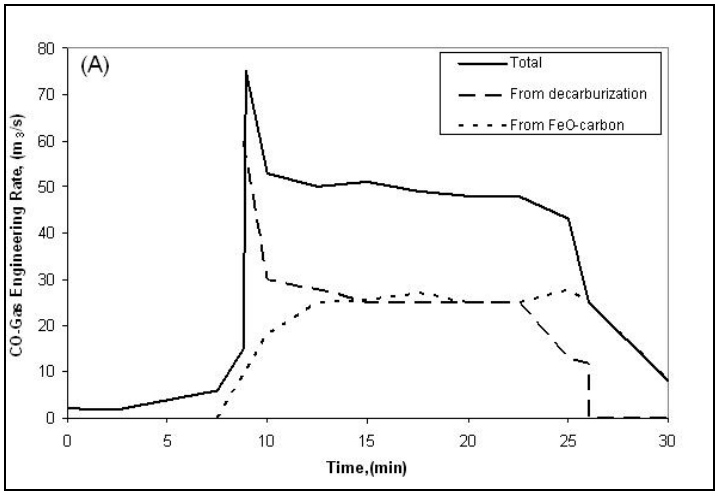

Figure 73. CO-gas generated from decarburisation, the slag-carbon reaction and the total for Case (A) (Matsuura and Fruehan 2009).

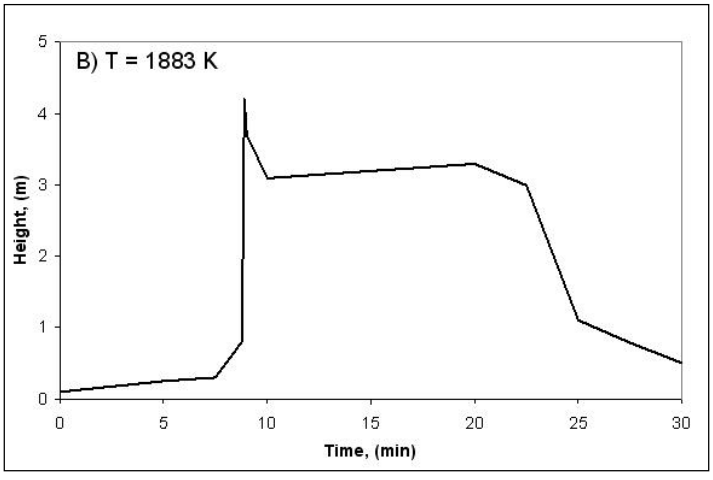

Figure 74. The foam heights for Case (A) with or without considering limitation by amount of slag (Matsuura and Fruehan 2009).

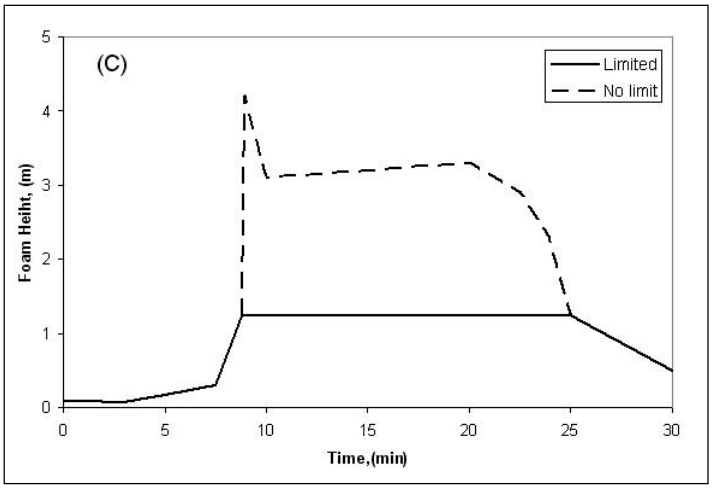

Figure 75. The foam heights considering no limitation from slag volume for case (A) (Matsuura and Fruehan 2009).

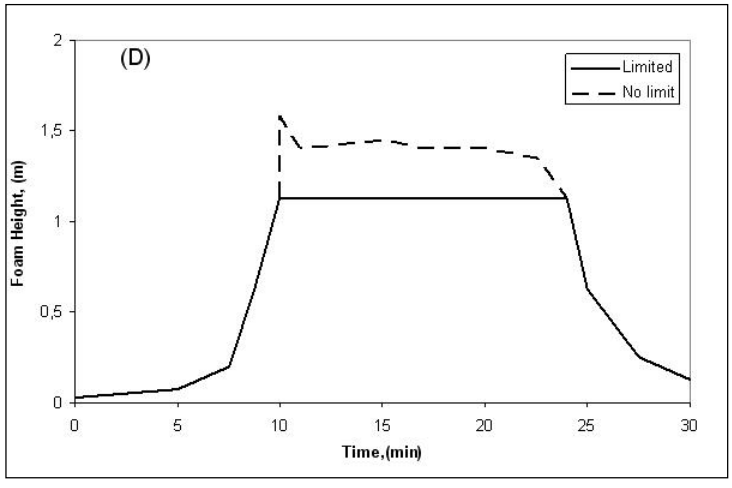

Figure 76. The foam heights for Case (B) in which the amount of pig iron is reduced (Matsuura and Fruehan 2009).

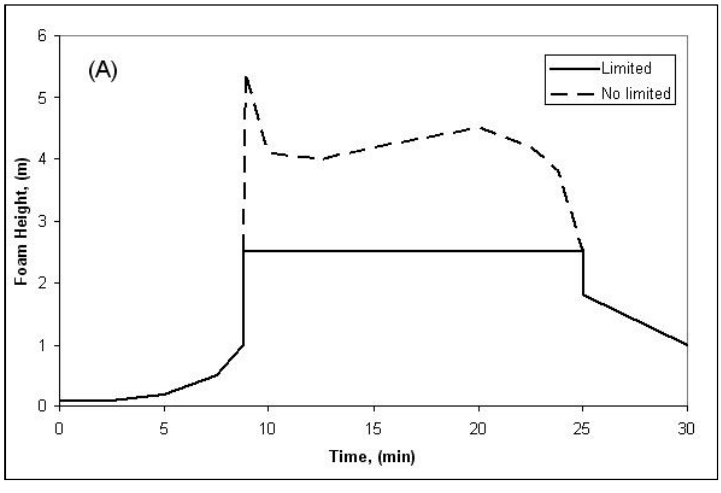

Figure 77. The foam heights for case (C) in which the amount of slag is doubled to 40 t (Matsuura and Fruehan 2009).

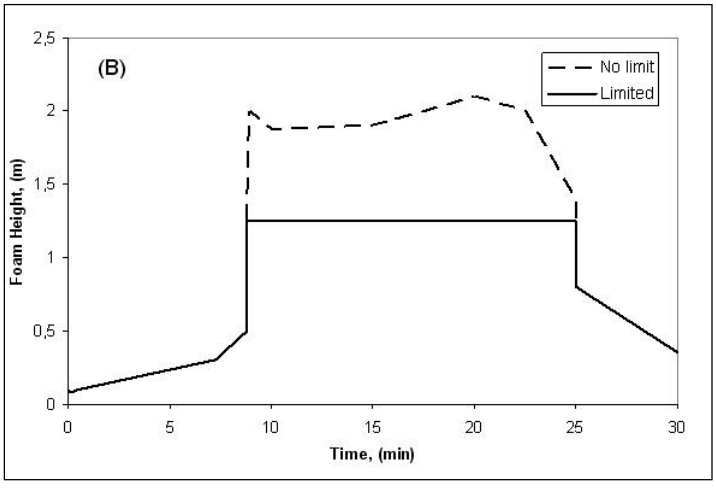

Figure 78. Potential foam heights for Cases (A), (B) and (D) considering the C-FeO reaction only (Matsuura and Fruehan 2009).

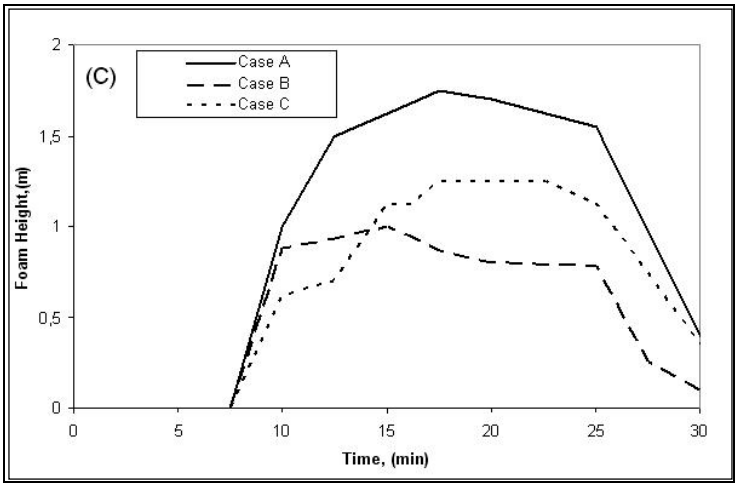

Figure 79. The foam heights for case (D) in which the oxygen gas and carbon are reduced (Matsuura and Fruehan 2009).

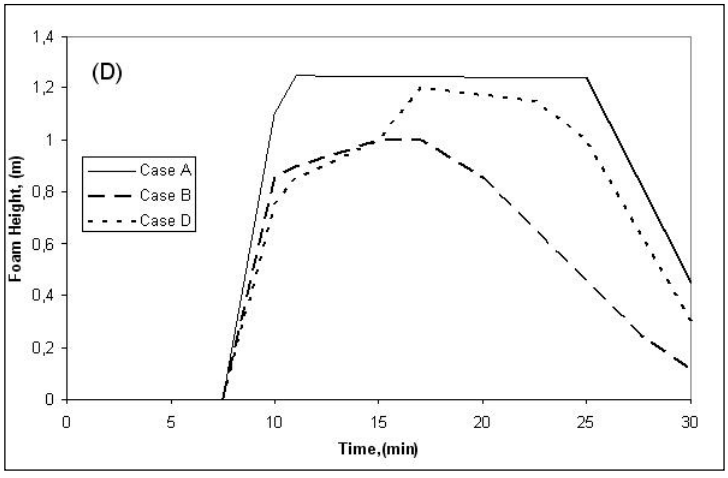

Figure 80. The foam heights for cases (A), (B) and (D) considering the amount of slag and C-FeO reaction only (Matsuura and Fruehan 2009).

Table 14. Melting pattern data of heats (Matsuura and Fruehan 2009).

Pig iron			Scarp		
Code	Melting rate curve	Final value	Code	Melting rate curve	Final value
W	Flat	Lowest	1	Linear	Highest
X	Linear and flat	2nd. Lowest	2	Flat	Lowest
Y	Linear	Highest	3	2-Step and gradual	2nd. Highest
Z	2-Step and gradual	2nd. Highest			

12.4.3 Simulation procedure

The potential foaming is very high with high amounts of pig iron, carbon and oxygen gas and the actual foam is limited by the height at which the slag is flushed out of the furnace or by the volume of slag. At the end of the process, the foam decays due to lower CO-generation and higher FeO contents. In the operations with a lesser amount of pig iron, oxygen and carbon, the foam still reaches the maximum during the middle of heat and is limited by the amount of slag but decays earlier due to lower CO-gas generations (Matsuura and Fruehan 2009).

It is unclear whether the CO-gas generation from decarburisation is as effective as that from the carbon-FeO reaction in slag for producing foam. If the CO-gas from the decarburisation reaction is neglected, the foaming is controlled by the amount of carbon and oxygen injected during the process. If the amount of oxygen is too low, the amount of FeO in the slag decreases and the amount of CO-gas generated decreases. Then carbon is tapped out with slag. If the oxygen gas injection is too high, the FeO content of slag increases, eventually decreasing the foam index and foaming (Matsuura and Fruehan 2009).

13. Summary

Slag foaming has become important in the furnace (EAF). Foaming practices are used to shield the refractory from the arc, the foamed slag stabilises the arc, it shields the metal from the atmosphere and it improves energy efficiency. Foam acts as a thermal insulator between the hot bath and the surroundings, thus reducing the electrical power required to maintain the high operating temperature and limiting electrode consumption. The foaming promotes chromium recovery. This indicates the importance of a well-developed foam to reach low chromium levels. Gas generation is indispensable in order to succeed with a foaming slag practice. In stainless steelmaking, gas is mainly generated by the reduction of CrO and FeO with carbon forming CO-gas (Görnerup and Jacobsson 1998).

The foam index is a parameter that quantifies the ability of slag to generate foam from either an injected gas or a gas that is generated within the slag of metal. The formation of foam is proportional to a gas flow rate and the rupture of foam is proportional to its height. In the ideal slag case, the foaming index is equal to the average foam life. However, the discrepancies in the proportionality constant of foaming index may be due to the accuracy in the estimation of the foaming index on the basis of slag properties as governed by experimental conditions. The foaming index was observed to decrease with decreasing viscosity and increasing surface energy. The increase in injected gas velocity increases foam height. However, the precipitating solid particles increased the foam stability by increasing the viscosity. In the CaO-SiO_2-FeO slags, the foam stability decreases with increasing FeO content and basicity.

In the industrial experiment control method of the slag foaming operations based on the visual observation or noise emitted by EAF vessel, the highest average sound intensity corresponded to the lowest foam level and lowest sound intensity to the highest foam level. The lower Cr_2O_3 content slags were observed to be more foaming. The foaming slags also have a higher initial FeO content and finally a lower content. The foaming is also observed to promote chromium recovery. The foaming index was relatively similar for the slags. This is due to the similarities between viscosity, density and surface energy data, although their compositions were quite different. Considering the nitrogen content in steel, the foamy slag plays an important role for more efficient protection of the melt against the

nitrogen pick-up coming from the atmosphere. The foaming phenomenon of slag was observed to be increased by additives during the steelmaking process.

In the modelling studies, the aim is to understand and predict foaming in EAF steelmaking. In order to achieve this, the foaming characteristics of the slag have to be understood. The slag foaming caused by slag-graphite reaction was observed to be dependent mainly on the CO-gas evolution rate.

A homogenous EAF process for the stainless steel model at a constant temperature calculates the evolution of temperature and the composition of slag and metal phases over time. It calculates the steel composition relatively well. In the slag phase, the formation of excess CO-gas and fixed oxygen gas balance causes the significantly lower oxidation of chromium, iron, manganese and silicon.

The decarburisation and slag formation model considers the rate phenomena for decarburisation and the carbon-FeO reaction in the slag, the mass balance for each element in the metal, and the slag and gas phases along with the melting behaviour of pig iron scrap and fluxes. The model can be used to simulate iron yield and carbon loss with the discharged slag. The foaming can be optimised by controlling the FeO content, slag basicity and CO-gas generation. The change of FeO content in slag is affected by the pig iron melting pattern, along with the carbon-FeO reaction rate constant and post-combustion ratio.

In the foaming of the EAF model, the potential foaming is very high when using high amounts of pig iron, carbon and oxygen. The actual foam is simply limited by the height at which the slag is flushed out of the furnace or by the volume of slag. At the end of the process, the foam decays due to lower CO-gas generation.

References

Arnout, S., Verhaeghe, F., Blainpain, B., Wollants, P., Hendrickx, R., Heylen, G. 2006. A Thermodynamic Model of the EAF Process for Stainless Steel. Steel Research International, 77(2006)5, 317–323.

Bikerman, J.J. 2001. The unit of Foaminess. Transactions of Faraday Society, 38(1938), 634–638. Referred by Pilon, L., Fedorov, A.G., Viskanta, R. Steady-State Thickness of Liquid–Gas Foams. Journal of Colloid and Interfacial Science, 242(2001)2, 425–436

Cooper, C.F., Kitchener, J. A. 1959. The Foaming of Molten Silicates. Journal of the Iron and Steel Institute, London, (1959), 193, 48–55. Referred by Ito, K., Fruehan, R.J. 1989. Study on the Foaming of CaO-SiO_2-FeO Slags: Part I. Foaming Parameters and Experimental Results. Metallurgical and Materials Transactions B, 20B(1989)4, 509–514.

Gunji, K., Dan, T. 1974. Surface Tension of the Molten CaO-SiO_2 Binary and CaO-SiO_2-Al_2O_3 Ternary Systems. Transactions ISIJ, 14(1974)3, 162–169.

Görnerup, M., Jacobsson, H. 1998. Foaming Slag Practice in Electric Stainless Steelmaking. Iron and Steelmaker, 25(1998)5, 59–66.

Hong, L., Hirasawa, M., Sano, M. 1998. Behaviour of Slag Foaming with Reduction of Iron Oxide in Molten Slags by Graphite. ISIJ International, 38(1998)12, 1339–1345

Hrma, J. 1990. Model for a Steady State Foam Blanket. Journal of Colloid and Interfacial Science, 134(1990)1, 161–168.

Ito, K., Fruehan, R.J. 1987. Slag Foaming in Electric Furnace Steelmaking. Proceedings of the Electric Furnace Conference, Vol. 45, (1987). Referred by Marique, C., Nyssen, P., Salamone, P. On-line control of the foamy slag in EAF. Proceedings of the 6th Electric Steelmaking Conference (1999), 154–161.

Ito, K., Fruehan, R. J. 1989a. Study on the Foaming of CaO-SiO_2-FeO Slags: Part I. Foaming Parameters and Experimental Results. Metallurgical and Materials Transactions B, 20B(1989)4, 509–514.

Ito, K., Fruehan, R.F. 1989b. Study on the Foaming of CaO-SiO_2-FeO Slags: Part II. Dimensional Analysis and Foaming in Iron and Steelmaking Processes. Metallurgical and Materials Transactions B, 20B(1989)4, 515–521.

Jiang, R., Fruehan, R.J. 1991. Slag Foaming in Bath Smelting. Metallurgical and Materials Transactions B, 22B(1991)4, 481–489.

Jouhari, A.K. 2000. Foaming During Reduction of Iron Oxide in Molten Slags. Ironmaking and Steelmaking, 27(2000)1, 27–31.

Kerr, J.J., Fruehan, R.J. 2000. ISS 17th, Process Technology Conference Proceedings 2000, 1049–1063. Referred by Vidacak, B., Arvanitidis, I., Jönsson, P.G., Sjöberg, P. Observation on Foaming of EAF in the Production of Stainless Steel, Scandinavian Journal of Metallurgy, 31(2002)5, 321–327.

Kerr, J.J., Fruehan, R.J. 2004. Additions to Generate Foam in Stainless Steelmaking. Metallurgical and Materials Transactions B, 35B(2004)4, 643–650.

Kawai, Y., Mori, K., Shiraishi, H., Yamada, N. 1976. Tetsu-to Hagane, 62(1976)1, 53–61. Referred by Ito, K., Fruehan, R.F. 1989. Study on the Foaming of CaO-SiO_2-FeO Slags: Part II. Dimensional Analysis and Foaming in Iron and Steelmaking Processes. Metallurgical and Materials Transactions B, 20B(1989)4, 515–521.

Lotun, D., Pilon, L. 2005. Physical Modeling of Slag Foaming for Various Operating Conditions and Slag Compositions. ISIJ International, 45(2005)6, 835–840.

Marique, C., Nyssen, P., Salamone, P. 1999. On-line control of the foamy slag in EAF. Proceedings of the 6th Electric Steelmaking Conference (1999), 154–161.

Matsuura, H., Manning, C.P., Fortes, R.A.F.O., Fruehan, R.J. 2008. Development of a Decarburization and Slag Formation Model for the Electric Arc Furnace. ISIJ International, 48(2008)9, 1197–1205.

Matsuura, H., Fruehan, R.J. 2009. Slag Foaming in an Electric Arc Furnace. ISIJ International, 49(2009)10, 1530–1535.

Mills, K.C., Keene, B.J. 1987. Physical Properties of BOS Slags. International Materials Reviews, 32(1987)1, 1–120.

Ozturk, B., Fruehan, R.J. 1995. Effect of Temperature on Slag Foaming, Metallurgical and Materials Transactions B, 26B(1995)5, 1086–1088.

Pretorius, E.B., Nunnington, R.C. 2002. Stainless Steel Slag Fundamentals: from Furnace to Tundish. Iron and Steelmaking, 29(2002)2, 133–139.

Pilon, L., Fedorov, A.G., Viskanta, R. 2001. Steady-State Thickness of Liquid – Gas Foams. Journal of Colloid and Interfacial Science, 242(2001)2, 425–436.

Roscoe, R. 1952. British Journal of Applied Physics, 3(1952)8, 267–269.

Sano, M., Mori, K. 1977. Tetsu-to-Hagane, 63(1977)14, 2308–2315. Referred by Ito, K., Fruehan, R.J. 1989. Study on the Foaming of $CaO\text{-}SiO_2\text{-}FeO$ Slags: Part I. Foaming Parameters and Experimental Results. Metallurgical and Materials Transactions B, 20B(1989)4, 509–514.

Skupien, D., Gaskell, D.R. 2000. The Surface Tension and Foaming Behaviour of Melts in the System $CaO\text{-}FeO\text{-}SiO_2$. Metallurgical and Materials Transactions B, 31B(2000)5, 921–925.

Swisher, J.H., McCabe, C.L. 1964. Cr_2O_3 as a Foaming Agent in $CaO\text{-}SiO_2$ slags. Transactions of the American Institute of Mining. Metallurgical and Petroleum Engineers 230(1964)7, 1669–75. Referred by Ito, K., Fruehan, R.J. 1989. Study on the Foaming of $CaO\text{-}SiO_2\text{-}FeO$ Slags: Part I. Foaming Parameters and Experimental Results. Metallurgical and Materials Transactions B, 20B(1989)4, 509–514.

Urbain, G. 1987. Steel Research, 58(1987)3, 111–116.

Vidacak, B., Arvanitidis, I., Jönnson, P.G., Sjöberg, P. 2002. Obersrvation on Foaming of EAF slags in the Production of Stainless Steel. Scandinavian Journal of Metallurgy, 31(2002)5, 321–327.

Zhang, Y., Fruehan, R.J. 1995a. Effect of the Bubble Size and Chemical Reactions on Slag Foaming. Metallurgical and Materials Transactions B, 26B(1995)4, 803–812.

Zhang, Y., Fruehan, R.J. 1995b. Effect of Carbonaceous Particles on Slag Foaming. Metallurgical and Materials Transactions B, 26B(1995)4, 813–819.

Zhang, Y., Fruehan, R.J. 1995c. Effect of Gas Type and Pressure on Slag Foaming, Metallurgical and Materials Transactions B, 26B(1995)5, 1088–1091. Reference Text

Series title and number
VTT Technology 63

Title	**A compilation of slag foaming phenomenon research** **Theoretical studies, industrial experiments and modelling**
Author(s)	Matti Liukkonen, Karri Penttilä & Pertti Koukkari
Abstract	A literature study was made on the foaming phenomenon in the modern electric arc furnace (EAF) stainless steelmaking process. Slag foaming has become an important feature of the EAF process. The chemical and physical conditions of the slag, which affect the foaming phenomenon of the slag-steel system, appear to be relatively complicated to control in the manufacture of stainless steel. The foaming index is a parameter that quantifies the ability of slag to generate foam from either injected gas or gas that is generated within the slag or metal. In the case of ideal slagging, the foaming index is equal to the average foam life. The foaming index decreases with increasing viscosity and increases with decreasing viscosity. Various techniques based on dimensional analysis of the kinetic properties of the slag have been applied in order to find the relationship describing the foaming index. In industrial experiments, the control methods of the slag foaming operations are based on the visual observation or on noise emitted by the EAF vessel. The lower Cr_2O_3 content slags and large initial FeO content slags are more foaming. The foaming is also observed to promote chromium recovery. The foaming index for the slags is observed to be relatively similar, due to the similarities between viscosity, density and surface energy values, although their compositions are quite different. The foamy slag provides protection for the melt against nitrogen pick-up. The foaming capability of slags can be enhanced by the addition of appropriate materials such as limestone and calcium nitrate. In the modelling studies, the aim is to understand and predict foaming in EAF steelmaking. The slag foaming caused by slag-graphite reaction is dependent mainly on the CO-gas evolution rate. Decarburisation and slag formation models consider the rate phenomena for decarburisation and the carbon-FeO reaction in the slag, and the mass balance for each phase with the melting behaviour of pig iron scrap and fluxes. A recent thermodynamic model of the EAF process for stainless steel calculates the evolution of temperature and the composition of slag and metal phases with time. In the slag foaming in the EAF model the potential foaming is very high when using high amounts of input materials. The actual foam is limited by the height at which the slag is flushed out or by the volume of slag. At the end of the process the foam decays due to lower CO-gas generation.
ISBN, ISSN	ISBN 978-951-38-7897-9 (URL: http://www.vtt.fi/publications/index.jsp) ISSN 2242-122X (URL: http://www.vtt.fi/publications/index.jsp)
Date	November 2012
Language	English
Pages	128 p.
Keywords	Electric arc furnace, EAF, stainless steel, slag foaming, gas generation, foam index, foam life, foaming, surface energy, viscosity, interface, basicity, temperature, gas velocity, bubble size, dimensional analysis, carbon, CO-gas, CaO-SiO_2-FeO, Cr_2O_3, modelling, reconciliation, mass balance, reaction rate, kinetics, dynamics, Fact, Fortran, Chemapp
Publisher	VTT Technical Research Centre of Finland P.O. Box 1000, FI-02044 VTT, Finland, Tel. 020 722 111

VTT Technical Research Centre of Finland is a globally networked multitechnological contract research organization. VTT provides high-end technology solutions, research and innovation services. We enhance our customers' competitiveness, thereby creating prerequisites for society's sustainable development, employment, and wellbeing.

Turnover: EUR 300 million
Personnel: 3,200

VTT publications

VTT employees publish their research results in Finnish and foreign scientific journals, trade periodicals and publication series, in books, in conference papers, in patents and in VTT's own publication series. The VTT publication series are VTT Visions, VTT Science, VTT Technology and VTT Research Highlights. About 100 high-quality scientific and professional publications are released in these series each year. All the publications are released in electronic format and most of them also in print.

VTT Visions

This series contains future visions and foresights on technological, societal and business topics that VTT considers important. It is aimed primarily at decision-makers and experts in companies and in public administration.

VTT Science

This series showcases VTT's scientific expertise and features doctoral dissertations and other peer-reviewed publications. It is aimed primarily at researchers and the scientific community.

VTT Technology

This series features the outcomes of public research projects, technology and market reviews, literature reviews, manuals and papers from conferences organised by VTT. It is aimed at professionals, developers and practical users.

VTT Research Highlights

This series presents summaries of recent research results, solutions and impacts in selected VTT research areas. Its target group consists of customers, decision-makers and collaborators.

A compilation of slag foaming phenomenon research

Theoretical studies, industrial experiments and modelling

A literature study was made on the foaming phenomenon in the modern electric arc furnace (EAF)- stainless steelmaking process. Slag foaming has become an important feature of the EAF-process. The chemical and physical conditions of the slag, which affect the foaming phenomenon of the slag-steel system, appear to be relatively complicated to control in the manufacture of stainless steel. The foaming index is a parameter that quantifies the ability of slag to generate foam from either injected gas or gas that is generated within the slag or metal. In the case of ideal slagging, the foaming index is equal to the average foam life. The foaming index decreases with increasing viscosity and increases with decreasing viscosity. Various techniques based on dimensional analysis of the kinetic properties of the slag have been applied in order to find the relationship describing the foaming index. In the industrial experiments, the control methods of the slag foaming operations are based on the visual observation or on noise emitted by the EAF-vessel. The lower Cr_2O_3-content slags and large initial FeO-content slags are more foaming. The foaming is also observed to promote chromium recovery.

ISBN 978-951-38-7897-9 (URL: http://www.vtt.fi/publications/index.jsp)
ISSN 2242-122X (URL: http://www.vtt.fi/publications/index.jsp)